Finite Element Analysis of Post-buckled Composite Structures

Kayla Wielgus

A thesis
submitted in partial fulfillment of the
requirements for the degree of

Master of Science in Civil Engineering

University of Washington

2020

Committee:

Richard Wiebe

Paolo Calvi

Michael Motley

Program Authorized to Offer Degree:
Civil and Environmental Engineering

University of Washington

Abstract

Finite Element Analysis of
Post-buckled Composite Structures

Kayla Wielgus

Chair of the Supervisory Committee:
Richard Wiebe
Department of Civil and Environmental Engineering

During high-speed flight, an aircraft may experience high stress gradients as a result of high-frequency aerodynamic interactions. Exterior composite panels on an aircraft are also susceptible to buckling due to thermally-induced axial loads. These exterior post-buckled panels are prone to snap-though behaviours resulting in large deformation responses coupled with high internal stresses. This phenomenon may lead to reduced structural integrity, resulting in a reduced life-cycle.

Previous work investigated snap-through of a laminated composite plate specimen. A composite plate was mechanically buckled and subjected to dynamic loading via a shaker system. The post-buckled plate's snap-through displacement responses were analyzed. Later, numerical models of the plate specimen were created using in-house finite element codes to analyze the stress fields. The models concluded that post-buckled plates experiencing snap-through may result in larger amplitude stresses and reduced fatigue life.

This thesis serves to advance this previous work and the understanding of post-buckled plate snap-through behavior using commercial finite element software. Finite element models generated in Abaqus/CAE are used to study these structural components. As preliminary work, an Abaqus plate model of the experimental composite plate specimen from previous work is created. The Abaqus model is subjected to dynamic loading resulting in snap-through behaviors. The snap-through results are compared with previous experimental and

numerical results mentioned above. The Abaqus finite element models matched the expected results of the previous experimental and numerical work very closely, validating the Abaqus model.

The relationship between static and dynamic analysis of snap-through responses is then explored within this work to further develop an understanding of the effect of snap-through on fatigue life. An important, previously unexplored, aspect of this work is the comparison of dynamic stresses to the stresses in the static equilibrium configurations. Within this thesis laminated composite plates undergoing snap-through are modeled using Abaqus both statically and dynamically. The stress results are compared between static and dynamic simulations to determine the efficacy of utilizing static analyses, which are computationally efficient, to predict dynamic stresses.

Finally, fatigue methods are analyzed for the applications of composite plates undergoing snap-through responses. As composite panels experience periodic snap-through stresses may increase significantly. Plate life will be evaluated using a method involving constant fatigue life diagrams to characterize fatigue life of plates along the entire plate surface.

TABLE OF CONTENTS

Page

List of Figures iii

Chapter 1: Introduction 1
1.1 Motivation 1
1.2 Thesis Overview 2

Chapter 2: Background 4
2.1 Chapter Overview 4
2.2 Post-buckled Plates and Snap-through Responses 4
2.3 Laminated Composites 9
2.4 Methods of Fatigue Analysis 12
2.5 Introduction to Finite Elements and Abaqus/CAE 14

Chapter 3: Theory and Modeling 16
3.1 Chapter Overview 16
3.2 Plate Theory 16
3.3 Modeling plates in Abaqus/CAE 26
3.4 Chapter Conclusion 37

Chapter 4: Model Validation of Linear and Nonlinear Problems 38
4.1 Chapter Overview 38
4.2 Linear Model Validation: Scenario 1 Isotropic Plate Thickness Study 39
4.3 Linear Model Validation: Scenario 2 Cylindrical Bending 44
4.4 Nonlinear Model Validation Using the Snap-through Boundary 49
4.5 Chapter Conclusion 63

Chapter 5: Stress Field Characterization and Exploration of Static Reduction . . . 65

5.1 Chapter Overview 65
5.2 Static Snap-through Modeling 66
5.3 Static Snap-through Results 68
5.4 Dynamic Snap-through Modeling 75
5.5 Dynamic Snap-through Results 77
5.6 Comparison of Stresses Under Static and Dynamic Response 83
5.7 Chapter Conclusion 92

Chapter 6: Fatigue Framework 94
6.1 Chapter Overview 94
6.2 Fatigue Characterization 95
6.3 Fatigue Mapping 98
6.4 Chapter Conclusion 105

Chapter 7: Thesis Conclusion 106
7.1 Summary of Work 106
7.2 Future Work 107

Bibliography 109

Appendix A: Additional stress field results for post-buckled plate used in validating snap-through boundary 111

Appendix B: Effects of increasing forcing amplitude in dynamic snap-through: stress results comparison between static and dynamic analysis 116
B.1 40g-130Hz dynamic snap-through 116
B.2 48g-130Hz dynamic snap-through 118
B.3 56g-130Hz dynamic snap-through 120
B.4 64g-130Hz dynamic snap-through 121
B.5 72g, 80g, and 88g-130Hz dynamic snap-through 122

LIST OF FIGURES

Figure Number		Page
2.1	Snap-through of structure under axial load.	5
2.2	Dynamic responses of a post-buckled plate a) single-well displacement response d) single-well phase projection, b) c-snap displacement response e) c-snap phase projection, c) p-snap displacement response f) p-snap phase projection	6
2.3	Figure reproduced from [5].	6
2.4	Harmonic forcing parameter snap-through boundary map. Figure reproduced from [5].	8
2.5	Boeing 787 materials. Courtesy of Boeing [2]	10
2.6	Laminated composite layup with a) single direction plies, b) mulitdirectional plies	11
2.7	Modes of failure, recreated from [14]	12
2.8	Stress history with simple σ_a and σ_m calculations from maximum and minimum stress value	13
2.9	A simple recreation of a constant fatigue life diagram for mode I failure of a carbon/epoxy laminate from work of Kawai and Koizumi [4]	13
3.1	Coordinate system for Classical Laminate Theory reproduced from [7]	17
3.2	Local and global laminate coordinate systems, local coordinate system appears in red with 1-2-3 axes labels, with "1" defined as aligned with the fiber direction	20
3.3	z measurements from the reference plane for a 4-ply laminate, reproduced from [12]	22
3.4	Abaqus modeling of a) flat plate model b) composite layup of flat plate using $[45]_4$ orientation angles created in the "Property" module	29
3.5	Abaqus plate model with a) small imperfection applied using transverse pressure load and boundary conditions b) axial load applied as a shell edge load with boundary conditions	31
3.6	Abaqus buckled plate as a result of applied axial loading	32

3.7 Abaqus plate model with a) varying dynamic pressure loading with fixed boundary conditions, b) input amplitude for varying dynamic pressure load (50 Hz frequency) 34
3.8 Abaqus plate model configuration during dynamic harmonic forcing over time 34
4.1 Boundary conditions and loading for plate thickness parametric study models (plan view) 40
4.2 Deflected plate models with 20mm x 5 mm x 0.1 mm (h x b x t) dimensions, a) analytical model using Kirchhoff plate theory and Mathematica, b) finite element model using Abaqus 41
4.3 3D percent error surface of midnode displacements corresponding to varying thickness-to-length (t/h) and thickness-to-width (t/b) ratios. Black points depict error plot results. The meshed surface is created by interpolating between all points. 42
4.4 2D percent error of midnode displacements corresponding to varying thickness-to-length (t/h). Plate width is denoted as b (in inches). 42
4.5 Cylindrical bending test geometry, boundary conditions, and loading (plan view) 45
4.6 Abaqus model composite laminae ply orientation. 45
4.7 Midsection displacement results location. 46
4.8 Cylindrical bending results across midsection, a) transverse displacement, b) axial stress σ_{xx}, c) transverse shear force along the plate width. See Figure 4.7 for plate location of these results. 47
4.9 Experimental composite plate shaker setup. Reproduced from Kim [5] 49
4.10 Harmonic forcing parameter snap-through boundary map. Reproduced from [5] 51
4.11 Dynamic model plate dimensions and boundary conditions 52
4.12 Experimental post-buckled plate specimen prior to dynamic analysis a) 3D shape b) asymmetric shape along the y-axis. Figure reproduced from Kim [5] 52
4.13 Modeling asymmetric plate buckling 53
4.14 Abaqus asymmetric post-buckled shape 54
4.15 In-plane axial stress field σ_{xx} at top surface (z = h/2) for a) in-house post-buckled plate model b) Abaqus post-buckled plate model 56
4.16 Transverse shear stress field σ_{xx} at midplane for a) in-house post-buckled plate model b) Abaqus post-buckled plate model 57
4.17 Responses for post-buckled plate dynamically excited at 7g-60Hz a) single-well displacement response b) single-well velocity vs. displacement phase projection 60

4.18 Responses for post-buckled plate dynamically excited at 7g-70Hz a) p-snap displacement response b) p-snap velocity vs. displacement phase projection . 60
4.19 Responses for post-buckled plate dynamically excited at 7g-90Hz a) c-snap displacement response b) c-snap velocity vs. displacement phase projection . 61
4.20 Displacement response for post-buckled plate dynamically excited at 7g-80Hz. Response begins with c-snap and switches to p-snap at around 0.5 seconds. . 62
4.21 Abaqus simulations plotted with the HFP map. Green circle markers depict Abaqus simulations that matched the expected response type. All Abaqus results aligned to the predicted HFP map response. 63

5.1 Buckled rises with equivalent given names and center node displacements . . 67
5.2 Displacement example of 3B buckled plate undergoing snap-through from uniform pressure loading during a static analysis 68
5.3 Midnode location on Abaqus plate model. 69
5.4 1B force-displacement curve with displacement measured at the plate midnode. 1-3 markings report plate configurations at specified locations along the curve. 69
5.5 Force-displacement curves for varying buckled rises 1B-6B 71
5.6 Maximum tensile (a) and compressive (b) in-plane axial stresses σ_{xx} at plate midplane for static snap-through of 5B structure 71
5.7 Force-displacement curves and center node axial stresses for varying buckled rises 1B-6B 73
5.8 Maximum transverse shear stresses τ_{xz} at plate midplane for static snap-through of 5B structure 74
5.9 Transverse shear stresses at different locations (both nodes and elements) along the 5B plate throughout increments of static snap-through simulation . 75
5.10 Center node displacements for a) 4B structure, 120Hz-18g forcing, b) 5B structure, 130Hz-32g forcing 77
5.11 Center node displacements for 5B structure, subjected to 130Hz forcing frequency, with varying forcing amplitudes 32g-88g 78
5.12 Force-displacement results for 5B structure for a) many cycles, 130Hz-32g, b) one cycle, 130Hz-32g, c) one cycle, 130Hz-(32g-88g). 78
5.13 Maximum tensile (a) and compressive (b) in-plane axial stresses σ_{xx} at plate midplane for dynamic snap-through of 5B structure subjected to 32g-130Hz forcing 80
5.14 Midnode displacements and axial stress at the mid node for 5B structure, subjected to 32g-130Hz forcing for a) many snap-through cycles, b) single cycle 80

5.15 Maximum transverse shear stresses τ_{xz} at plate midplane for dynamic snap-through of 5B structure subjected to 32g-130Hz forcing 81
5.16 Midnode displacements and transverse shear stress at the midplane for 5B structure, dynamic analysis subjected to 32g-130Hz for a) many snap-through cycles, b) single cycle 82
5.17 Maximum compressive axial stresses throughout entire time history for a) 5B 32g-130Hz dynamic contour, b) 5B static contour 83
5.18 Maximum tensile axial stresses throughout entire time history for a) 5B 32g-130Hz dynamic contour, b) 5B static contour 84
5.19 Center node displacements and axial stress at the mid node for 5B structure, a) dynamic analysis at 32g-130Hz harmonic loading, b) static analysis 85
5.20 Maximum magnitudes of transverse shear stresses throughout entire time history for a) 5B 32g-130Hz loading dynamic analysis, b) static analysis 87
5.21 Midnode displacements and transverse shear stress τ_{xz} at the midplane for 5B structure, a) dynamic analysis at 32g-130Hz harmonic loading, b) static analysis 87
5.22 Midnode displacements and location (d) shear stress for 5B structure, a) dynamic analysis at 32g-130Hz harmonic loading, b) static analysis 88
5.23 Applied loading versus transverse shear stress for 32g-130Hz dynamic loading and static loading, a) at the mid node b) at location (d) 89
5.24 Center node displacements and axial stress for 5B structure with varying amplitudes, a) 32g-88g loading dynamic analysis, b) static analysis 91
5.25 Midnode displacements and transverse shear stress for 5B structure with varying amplitudes, a) 32g-88g loading dynamic analysis, b) static analysis . . . 92
6.1 a) Required periodic snap-through loading for static and dynamic analyses with varying plate thickness, b) Mode 1 frequencies and periodic snap-through forcing frequencies for varying plate thickness 97
6.2 CFL diagram for $[45/90/-45/0]_{2S}$ laminate, mode one failure, recreated from [4] 99
6.3 Axial stress σ_{xx} history for arbitrary point along surface of 3mm thick plate from 165g-280Hz dynamic loading 100
6.4 Alternating and mean stress per element for 3mm thick plate with 165g-280Hz dynamic loading 101
6.5 CFL diagram with stress results for 3mm thick plate with 165g-280Hz dynamic loading 102
6.6 Fatigue life plot results for 3mm thick plate with 165g-280Hz dynamic loading 102

6.7 CFL diagram with axial stress results for varying plate thicknesses 104
6.8 Fatigue life plot results for 5mm thick plate with 200g-300Hz dynamic loading 104

A.1 In-plane axial stress field σ_{xx} at bottom surface (z = -h/2) for a) in-house post-buckled plate model b) Abaqus post-buckled plate model 112
A.2 In-plane axial stress field σ_{yy} at top surface (z = h/2) for a) in-house post-buckled plate model b) Abaqus post-buckled plate model 113
A.3 In-plane axial stress field σ_{yy} at bottom surface (z = -h/2) for a) in-house post-buckled plate model b) Abaqus post-buckled plate model 114
A.4 Transverse shear stress field τ_{yz} at midplane (z = 0) for a) in-house post-buckled plate model b) Abaqus post-buckled plate model 115

B.1 Maximum in-plane axial stress σ_{xx} at midplane a) tensile, dynamic snap-through 40g-130Hz forcing, b) tensile, static snap-through, c) compressive, dynamic snap-through 40g-130Hz forcing, d) compressive, static snap-through 117
B.2 Maximum magnitude of transverse shear stress τ_{xz} at midplane a) dynamic snap-through 40g-130Hz forcing, b) static snap-through 117
B.3 Maximum in-plane axial stress σ_{xx} at midplane a) tensile, dynamic snap-through 48g-130Hz forcing, b) tensile, static snap-through, c) compressive, dynamic snap-through 48g-130Hz forcing, d) compressive, static snap-through 119
B.4 Maximum magnitude of transverse shear stress τ_{xz} at midplane a) dynamic snap-through 48g-130Hz forcing, b) static snap-through 119
B.5 Maximum in-plane axial stress σ_{xx} at midplane a) tensile, dynamic snap-through 56g-130Hz forcing, b) tensile, static snap-through, c) compressive, dynamic snap-through 56g-130Hz forcing, d) compressive, static snap-through 120
B.6 Maximum magnitude of transverse shear stress τ_{xz} at midplane a) dynamic snap-through 56g-130Hz forcing, b) static snap-through 121
B.7 Maximum in-plane axial stress σ_{xx} at midplane a) tensile, dynamic snap-through 64g-130Hz forcing, b) tensile, static snap-through, c) compressive, dynamic snap-through 64g-130Hz forcing, d) compressive, static snap-through 122
B.8 Maximum magnitude of transverse shear stress τ_{xz} at midplane a) dynamic snap-through 64g-130Hz forcing, b) static snap-through 122
B.9 Maximum in-plane axial stress σ_{xx} at midplane a) tensile, dynamic snap-through 72g-130Hz forcing, b) tensile, static snap-through, c) compressive, dynamic snap-through 72g-130Hz forcing, d) compressive, static snap-through 124
B.10 Maximum magnitude of transverse shear stress τ_{xz} at midplane a) dynamic snap-through 72g-130Hz forcing, b) static snap-through 124

B.11 Maximum in-plane axial stress σ_{xx} at midplane a) tensile, dynamic snap-through 80g-130Hz forcing, b) tensile, static snap-through, c) compressive, dynamic snap-through 80g-130Hz forcing, d) compressive, static snap-through 125
B.12 Maximum magnitude of transverse shear stress τ_{xz} at midplane a) dynamic snap-through 80g-130Hz forcing, b) static snap-through 125
B.13 Maximum in-plane axial stress σ_{xx} at midplane a) tensile, dynamic snap-through 88g-130Hz forcing, b) tensile, static snap-through, c) compressive, dynamic snap-through 88g-130Hz forcing, d) compressive, static snap-through 126
B.14 Maximum magnitude of transverse shear stress τ_{xz} at midplane a) dynamic snap-through 88g-130Hz forcing, b) static snap-through 126

ACKNOWLEDGMENTS

I wish to express sincere appreciation to University of Washington, where I had the opportunity to work with Professor Richard Wiebe and Dr. Han-Gyu Kim studying post-buckled plate behavior attributed to aerospace structures.

Specifically, I would like to thank Dr. Richard Wiebe for being a kind, patient, and brilliant advisor. Throughout my thesis, Professor Wiebe showed joy and sincere interest in our work, resembling a true researcher at heart. Professor Wiebe has not only been my advisor, but has become an influence on learning to embrace my own curiosity.

I'd also like to thank my fellow graduate students for supporting me throughout time at University of Washington. I owe my thanks to them for their help during coursework.

DEDICATION

Behind this thesis lies not only a great effort, but those that supported me throughout my time in graduate school. I dedicate this to my family for their endless support. Special gratitude to my father who inspired me to become the engineer I am today and to my mother who always believed in me.

Chapter 1
INTRODUCTION

1.1 Motivation

1.1.1 Overview

In today's aerospace industry, the use of composite panels is nearly inevitable as composites provide high strength at a light weight, and can be easily customised to achieve specific mechanical properties [1]. Incidentally, composite panels are often utilized to construct an aircraft's wing, fuselage, or tail due to their effectiveness [16]. High-speed flight conditions are of particular interest in this thesis. Constrained composite panels along an aircraft's surface experience large thermal stresses during high-speed flight [5].

Under dynamic loading post-buckled composite panels can exhibit snap-through behaviours, resulting in larger deformations which may reduce the life-cycle of the panels significantly. Snap-through is a complex phenomenon to model due to the large deformations involved, which lead to nonlinearities in the underlying governing equations. Additionally, variations in forcing amplitude and frequency can alter the plate responses significantly. Various characteristic response types occur, which may be large or small amplitude displacements and stresses. As frequency or amplitude changes a response type may transition from a small amplitude response to a large amplitude response. The ability to model the complicated behaviour of snap-through is desirable as it serves as a model validation while also providing insight on this complex phenomenon. To validate existing models of snap-through, finite element methods (FEM) are often utilized to approximate the expected solution given a structure's geometry, material properties, and loading. A portion of this work will explore validating an in-house finite element code and experimental data for a snap-through boundary problem of a post-buckled composite plate utilizing Abaqus/CAE finite element

software. After validation, variations of the Abaqus model will be used to explore dynamic snap-through behaviours further.

1.1.2 Objectives

To author's knowledge no work has been done to compare snap-through of plates both statically and dynamically. Specifically, no studies have analyzed the potential of using static stresses to predict dynamic stresses and fatigue life. Currently, dynamic analyses are used to model snap-through with dynamic loading. These dynamic analyses require great computational expense and time in order to run the simulations. The static analysis equivalent, however, is much faster and less complex. A portion of this work will address comparing the static and dynamic analyses of post-buckled composite plates undergoing snap-through to determine the efficacy of using static analyses to predict the dynamic analyses results. The stress results between both methods will serve as the indicator of validity of using static analysis to predict stresses experienced during dynamic response.

As snap-through of post-buckled panels potentially increases internal stresses greatly, fatigue failure of aerospace structures is a primary concern to ensure safety and an effective lifespan of an aircraft. After analyzing the stresses associated with snap-through, a fatigue method involving constant fatigue life (CFL) diagrams for composites will be explored. CFL diagrams are created from experimental test data and provide an estimated fatigue life given a mean and alternating stress. Exploring this method will provide insight on the benefits and limitations of determining fatigue life for composite panels and provide fatigue life information for possible future experimental work.

1.2 Thesis Overview

The following chapters will explore the objectives provided here further and will build on the ideas previously mentioned here. Chapter 2 provides relevant background information important for understanding studies investigated later in this work.

In Chapter 3, theory behind classical laminate plate theory is discussed along with theoretical approximation methods. Additionally, a parametric study on Abaqus finite element plate modeling is explored using varying thickness-to-length ratios for plate models. This study was used to evaluate the accuracy of Abaqus comparing with analytical values.

Chapter 4 introduces a cylindrical bending plate problem with analytical and Abaqus finite element solutions. This section served as a validation for modeling composite plates undergoing a uniform pressure load. Displacement, axial stress, and shear stress results are compared to validate the Abaqus model. Following this section, a previous study on dynamic snap-through of post-buckled plates in harmonic forcing parameter space is validated using Abaqus models. This section explores the effects of loading parameters on snap-through behavior and supports previous work which used an in-house finite element code.

In Chapter 5, static and dynamic models are created in Abaqus to assess stress results of periodic snap-through. Differences between static and dynamic results are analyzed and discussed for axial and shear stress.

Chapter 6 characterizes fatigue life for composite plate models undergoing snap-through responses. The fatigue life is mapped along every location on the plate surface using a constant fatigue life (CFL) diagram method. Using similar stress contour plots introduced in Chapter 5, fatigue life information can be plotted along the plate to provide an easy method of observing fatigue data.

Chapter 2
BACKGROUND

2.1 Chapter Overview

The previous chapter provided motivations behind this thesis along with a brief introduction to the topics of this work. This chapter will explore these topics more thoroughly and will provide relevant background information important for understanding the remaining portion of this thesis. First, snap-through of post-buckled plates will be introduced and explained. Laminated composites will then be discussed because these materials will be used within the entirety of this work. Methods of fatigue analysis are also discussed to explain how snap-through analysis results will be analyzed later. Lastly, finite element analysis (FEA) is introduced as a method of solving snap-through problems and investigating the topics of this work.

2.2 Post-buckled Plates and Snap-through Responses

Structural skin on aircraft is prone to buckling during flight as high thermal and mechanical axial loading is applied to the aircraft. This axial loading may cause the constrained panels to buckle. Post-buckled structures such as the panels along an aircraft's exterior are susceptible to snap-through, a phenomenon consisting of dynamic nonlinear deformations. Figure 2.1 depicts two related buckling phenomena. First, an axial load is applied to a structure resulting in Euler buckling. Then, transverse loading on the post-buckled structure causes snap-through buckling. Snap-through occurs when the structure snaps from one state of equilibrium to another at the same loading, resulting in a large deformation within a short period of time. This is shown in the figure, where the displacement of the mid point may jump from a negative to a positive displacement value from small perturbation in transverse

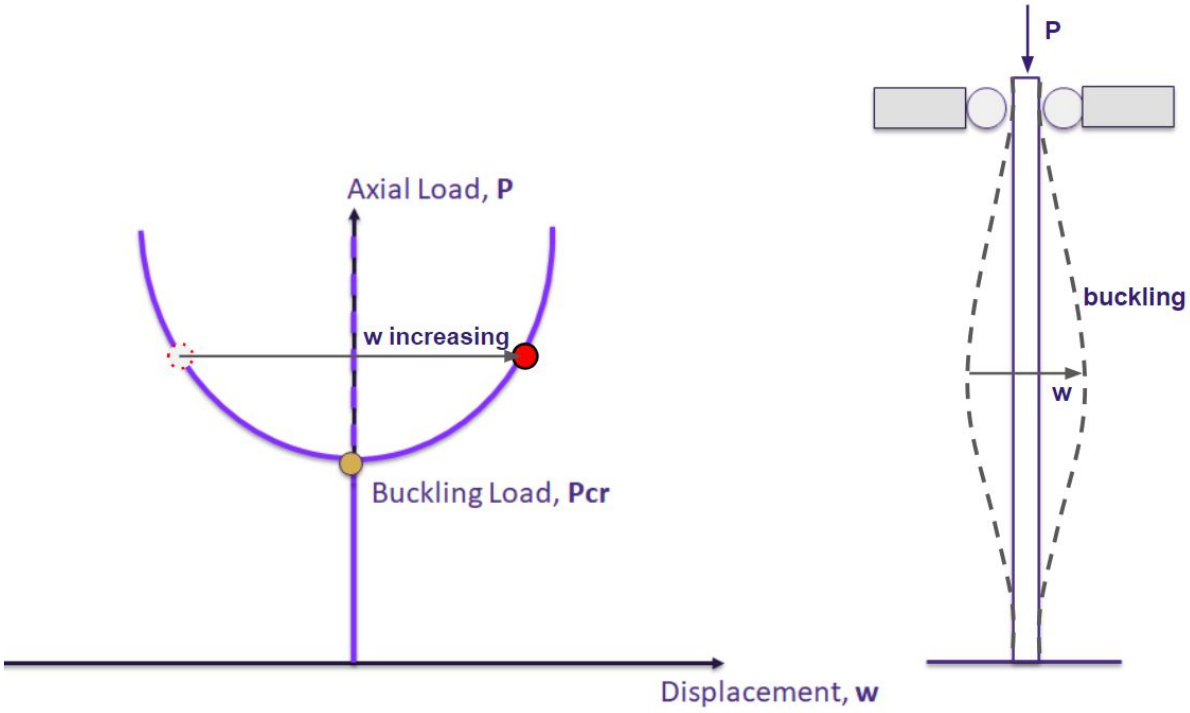

Figure 2.1: Snap-through of structure under axial load.

loading. These snap-through instances can be chaotic responses, where the structure can jump from one stable equilibrium position to another, but are irregular (and unpredictable). A structure will present varying behaviors given the forcing and initial conditions. Three main types of responses are common: single-well, chaotic snap-through (c-snap), and periodic snap-through (p-snap) [5]. These three types of responses may be characterized through phase projections, which are an informative way to display nonlinear responses. Graphing a structure's momentum versus position creates a phase projection plot. Figure 2.2 provides examples of midnode displacements and phase projections of the three snap-through responses for a plate under dynamic loading. This figure will be explained further shortly.

Post-buckled structures are bi-stable, meaning they possess two static stable equilibria. These two stable equilbria are represented by local minima in the potential energy, as illustrated in Figure 2.3. Observing Figure 2.3, it can be interpreted that with low energy input,

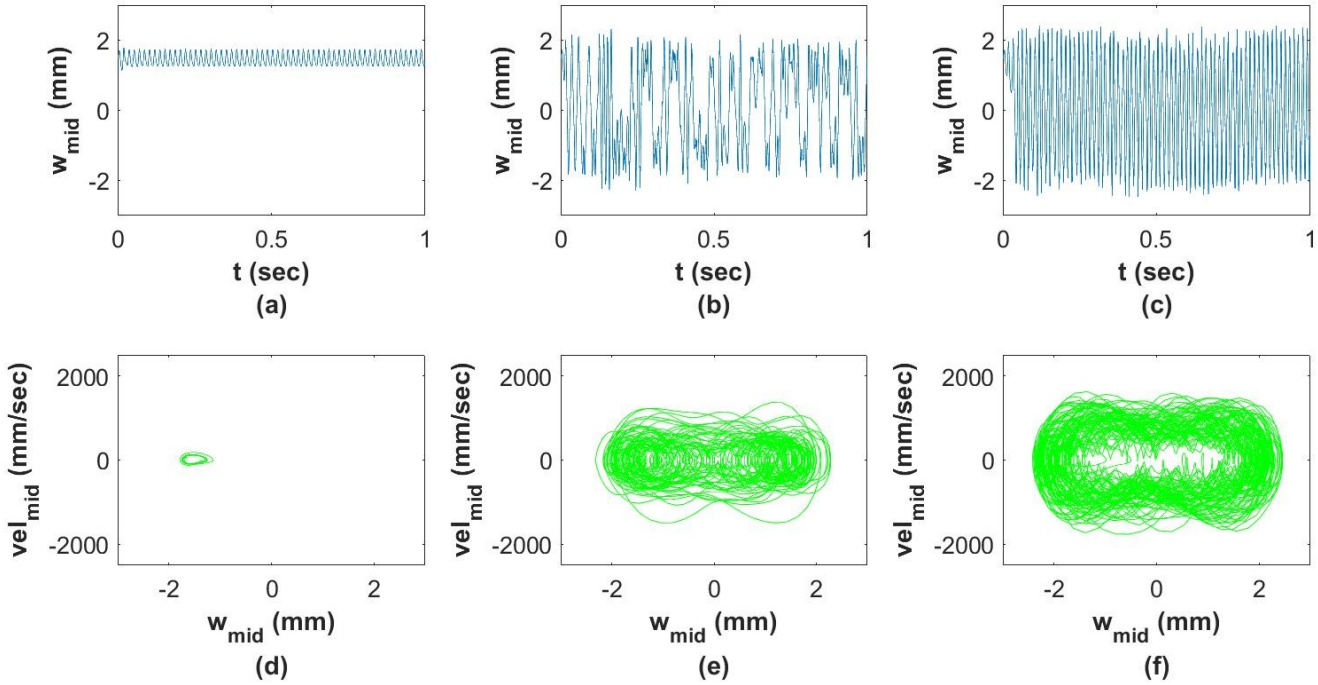

Figure 2.2: Dynamic responses of a post-buckled plate a) single-well displacement response d) single-well phase projection, b) c-snap displacement response e) c-snap phase projection, c) p-snap displacement response f) p-snap phase projection

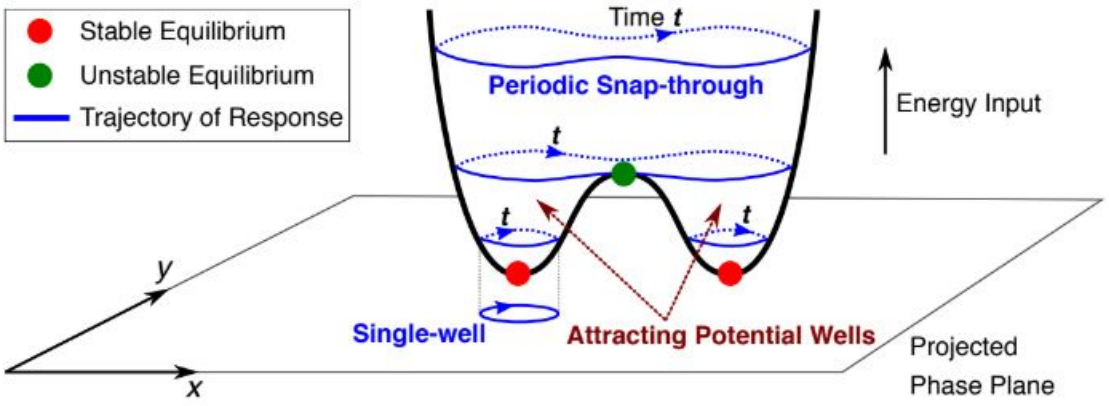

Figure 2.3: Figure reproduced from [5].

the response of the bi-stable structure will lie within one of the two attracting potential wells. This is the single-well case, where the phase projection will appear as a simple elliptical shape around a single point, as shown in Figure 2.2d. Increasing the energy input tends to adjust the single-well response into a more chaotic response, identified as the c-snap response. This higher-energy response consists of the structure oscillating in a more unpredictable manner from one stable equilibria to another. This is shown in Figure 2.2b, where the midnode displacement of a plate jumps irregularly from positive to negative values. The phase projection of this response will show the structure switching between the two potential wells in a frenzied manner, shown in Figure 2.2e. Finally, with enough energy input the structure will reach periodic snap-though, or p-snap. At this stage, the structure bounces from one potential well to another in a more consistent manner. The phase projection now appears as a single ellipse, however, is slightly less orderly when compared to the single-well phase projection, while more orderly when compared to the c-snap response. Figure 2.2f portrays an example of a phase projection for a p-snap response.

Previous work by Kim and Wiebe [5] found that given a structure, the type of snap-through response may be predicted given the forcing amplitude and excitation frequency. From this work, a harmonic forcing parameter (HFP) map was created for a composite post-buckled plate using experimental and finite element model data. Figure 2.4 displays this HFP map. This figure provides information regarding forcing frequency and amplitude and connects which snap-through response is associated to the specific forcing. In the figure, the legend provides information on the experimental boundary. The experimental boundary is depicted by a range of colors to show where on the HFP map snap-through responses were found with the experimental specimen. Based on the experimental boundary, snap-through is mainly found between the excitation frequencies of 60-150Hz. The legend in Figure 2.4 also mentions simulation results. These simulation results are plotted along many different frequency and amplitude loadings and are depicted by different markers. The markers are plotted within HFP space and denote which snap-through type was found using the in-house finite element model. Looking at the figure, mainly single-well responses are found for a

majority of the excitation parameters. However, at specific frequencies between about 60-140Hz and amplitudes between about 2-7g, chaotic and periodic snap-through are found for the finite element model simulation. This HFP map will be explored and used to validate a dynamic finite element model developed later within this work.

The different snap-through response types discussed here and mapped within HFP space exhibit varying deflection responses as well as varying stress responses. Previous dynamic simulations have shown that larger stress fields are expected from periodic snap-through [5].

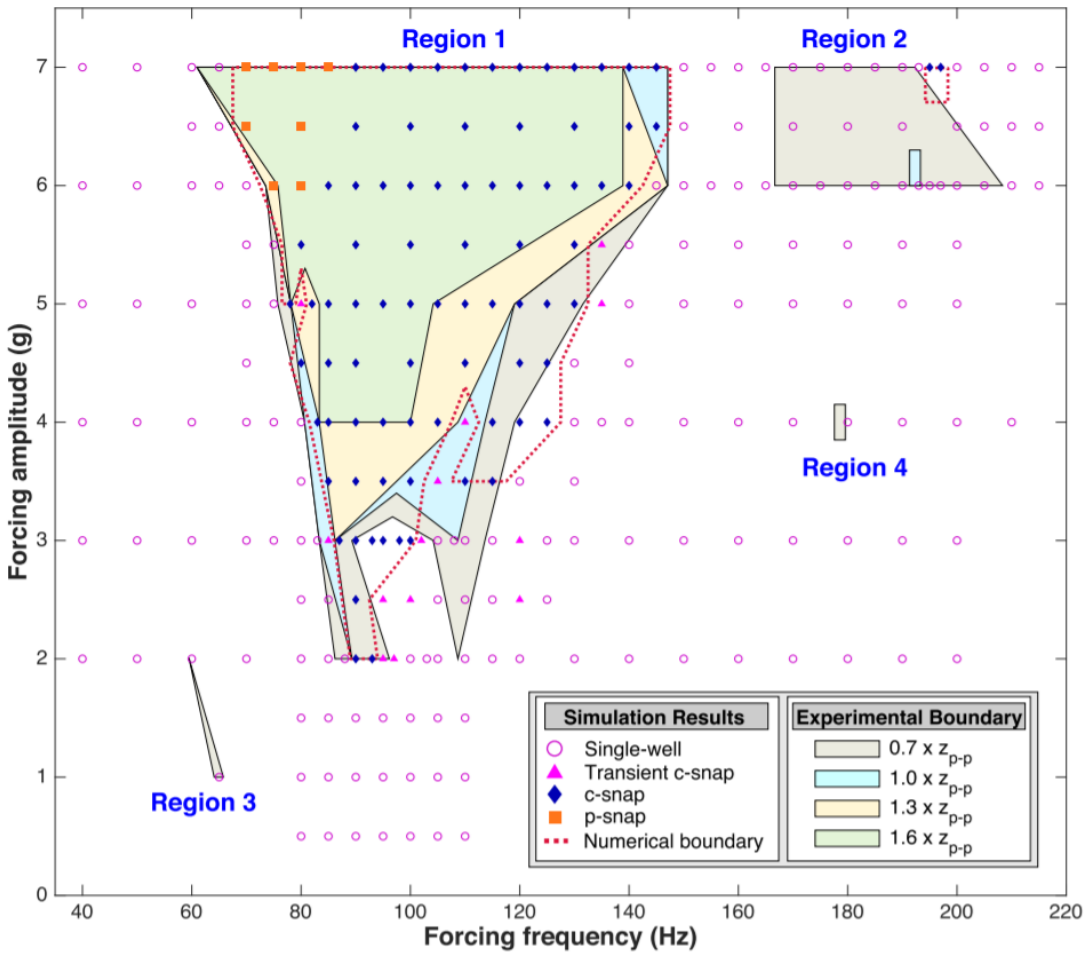

Figure 2.4: Harmonic forcing parameter snap-through boundary map. Figure reproduced from [5].

Chaotic snap-though yields large stress fields compared to single-well responses, however, they are smaller than periodic snap-through. These varying stress responses are worth noting as they can directly influence fatigue life of the panels. This suggests that given a snap-through response type, the composite panels may possess a significantly different life expectancy.

The snap-through responses discussed in this section have previously been explored using dynamic analysis. One issue with dynamic analyses of snap-through is computational expense. In addition to the larger computation time, dynamic analyses produce a greater set of data as results are evaluated over time histories, often consisting of exceptionally large quantities of time steps. For this reason, dynamic analyses can quickly become very complex both spatially and temporally, producing large sets of data with substantial amounts of run time devoted to each dynamic simulation. Generally, dynamic analysis may be desired, as the inertial effects and time dependencies are considered.

Formerly the relationship between static and dynamic stress values has not been carefully quantified. Thus, this thesis will investigate snap-through responses for both dynamic and static analyses in addition to exploring snap-through. This relationship between static and dynamic results will later be studied for the specific phenomenon of snap-through of post-buckled composite plates.

2.3 Laminated Composites

Composite materials are frequently a crucial aspect of the design process in the aerospace industry. Composites offer high strength, low weight, good fatigue and corrosion resistance, which are all desirable characteristics with regard to the design of aircraft [7]. Due to this quality, composites not only are significant to aerospace structures but are invaluable in automotive and civil engineering applications as well.

The use of composites can be illustrated by the Boeing 787, shown in Figure 2.5. According to Boeing, about half of the airframe now consists of advanced composites which reduces the weight by 20 percent [2]. Boeing reports that utilizing composites over aluminum in

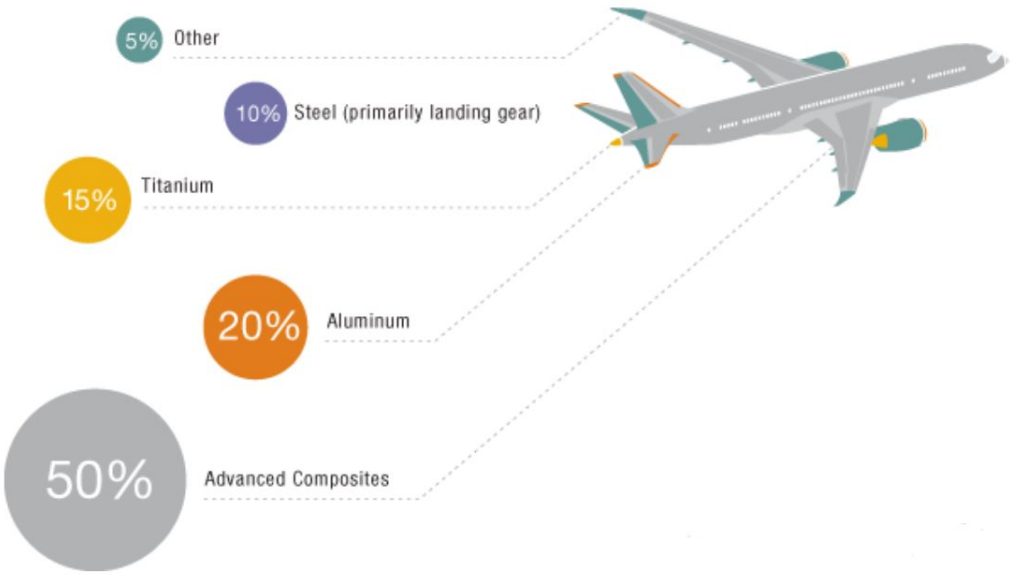

Figure 2.5: Boeing 787 materials. Courtesy of Boeing [2]

the fuselage minimizes the occurrences of needed maintenance for fatigue compared to when using aluminum. Along with strength and weight reduction benefits, composites also offer manufacturing benefits such as formability for design of unique structural shapes. Other aircraft besides the Boeing's 787, such as the Northrop Grumman's B-2 stealth bomber, use primarily composite materials for exterior structures for benefits of formability and even radar-absorption [3].

At the micromechanics level, composite materials are composed of a fiber and matrix material. The fiber material is composed of small strands of strong and stiff materials such as graphite or boron. The matrix material of composites is more ductile, and bonds the fibers together and offers a mean of transferring load from one fiber to another [7]. Composite structures are often fabricated as laminates, which are created from a stack of individual laminae, or plies, each consisting of both matrix and fiber materials. A common type of laminate is one created from unidirectional fiber plies. For each lamina, the small fibers are formed parallel in one direction. Each ply can be stacked in different fiber orientations to

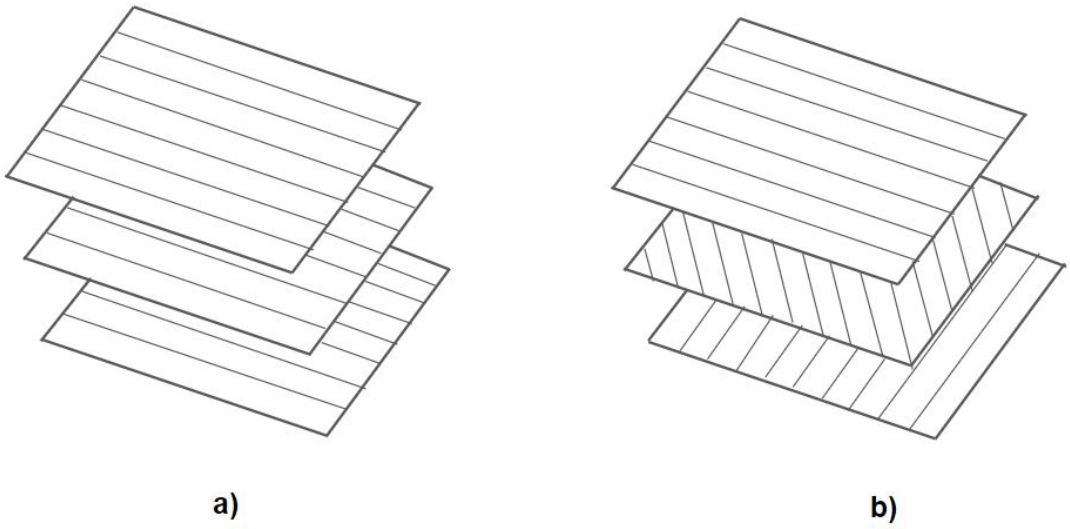

Figure 2.6: Laminated composite layup with a) single direction plies, b) mulitdirectional plies

create a laminate composed of plies all orientated in different directions. The orientations of the laminae within the composite will determine how the laminate responds to applied forces and moments. Essentially, different laminates made of the same materials but with different ply orientations will experience different strains and stresses given similar loading. This tailoring of composites gives engineers the ability to design composite structures in an effective manner given the loading conditions. This work will later focus on unidirectional fiber composites, consisting of laminates composed of fibers all oriented in a single direction within each individual ply, along with multidirectional composites, with plies oriented in different directions. These two composite laminate layups are illustrated in Figure 2.6. Although this work focuses on unidirectional and multidirectional plies, not all laminated composites are composed of plies where the fibers are oriented parallel to eachother in each ply. It should be noted that other composite types exist, including woven fabric, chopped fiber composites, and braided composites [7].

2.4 Methods of Fatigue Analysis

As aircraft undergo repetitive loads over time, fatigue becomes a concern. Characterizing fatigue is often deemed a challenge for composite structures as large sets of experimental data are required for identifying lifetime. Additionally, composite structures such as aircraft or wind turbines experience varying loading consisting of altering forcing frequencies, amplitudes, and sometimes difficult to predict stresses as a result.

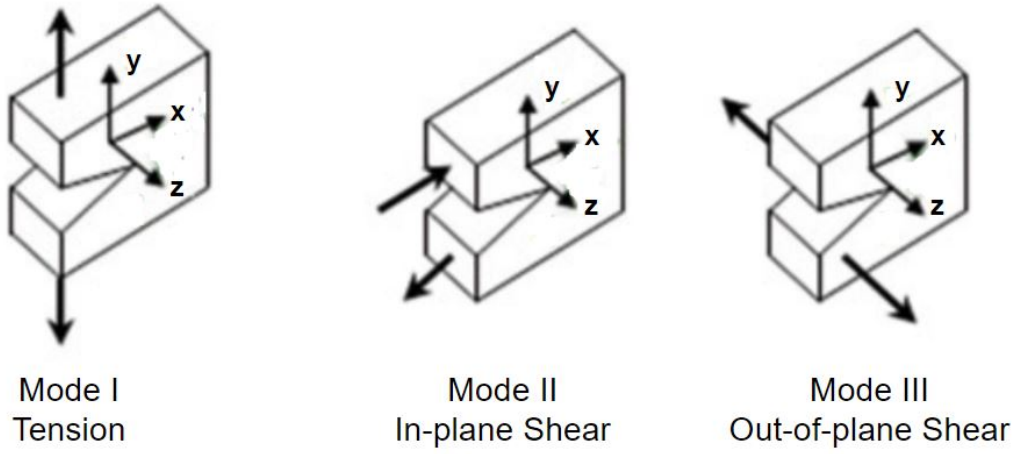

Figure 2.7: Modes of failure, recreated from [14]

Mechanical failure from fatigue may occur from different failure modes. These failure modes dictate crack growth directions during fracture and occur as loading causes surface crack displacements [14]. Figure 2.7 provides examples of three key failure modes: tension, in-plane shear, and out-of-plane shear. Mode I failure can occur when axial loading to a body is significant and causes a tension fracture. Here the crack surfaces are pulled apart. The remaining failure modes II and III are related to shear failure. These failure modes may result when a body experiences large shear stresses and the crack surfaces slide past one another rather than being pulled apart. Each failure mode is significant, however, this section will discuss fatigue life caused by axial failure related to mode I.

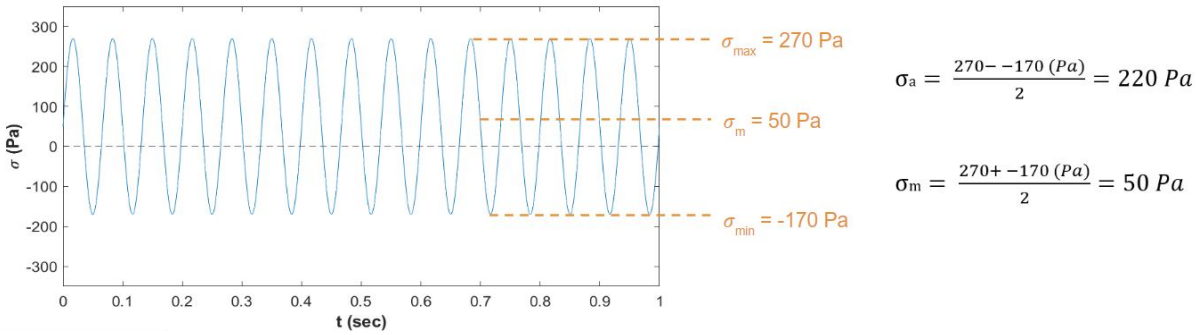

Figure 2.8: Stress history with simple σ_a and σ_m calculations from maximum and minimum stress value

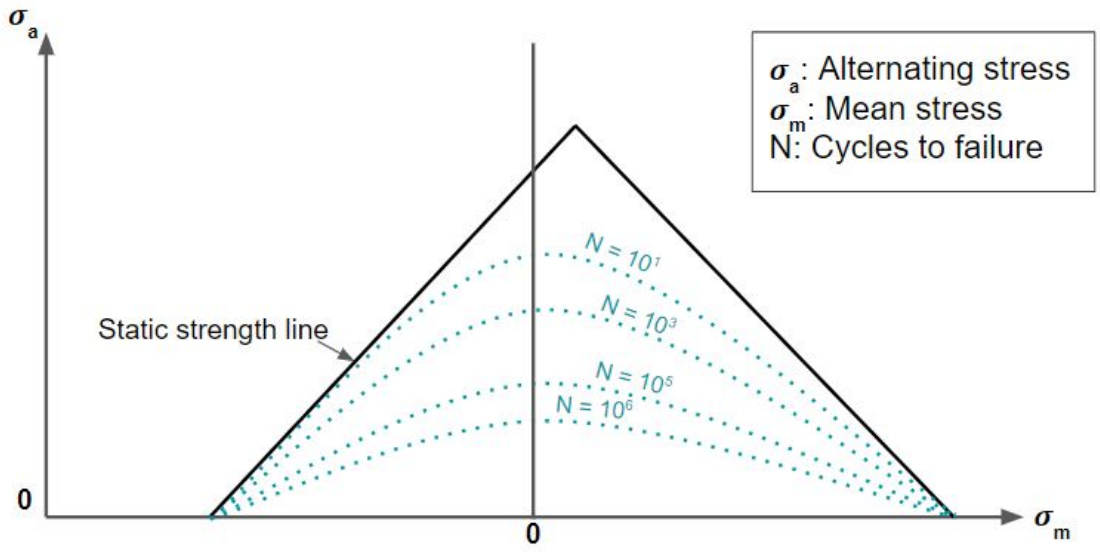

Figure 2.9: A simple recreation of a constant fatigue life diagram for mode I failure of a carbon/epoxy laminate from work of Kawai and Koizumi [4]

One method of characterizing fatigue life for composite materials consists of a diagram-based fatigue life prediction called constant fatigue life (CFL) diagram method [4]. A previous study developed the CFL diagram for multidirectional carbon fiber laminates with varying composite lay-ups [4]. This study focuses on the idea that fatigue stresses can be

broken down into alternating stress σ_a and mean stress components σ_m, then using these stress values, the fatigue life may be predicted from a predetermined CFL diagram created through experimental data. These stress components are found as:

$$\sigma_a = \frac{\sigma_{max} - \sigma_{min}}{2}, \qquad \sigma_m = \frac{\sigma_{max} + \sigma_{min}}{2} \tag{2.1}$$

Examples of a stress time history and the simple calculations to find σ_a and σ_m are found in Figure 2.8. Ultimately, the CFL diagram is created by observing mode I failure from static compression and tension tests along with numerous constant amplitude fatigue tests to a specific composite material and lay-up. Following these tests, alternating stress is plotted against mean stress for varying constant values of life [4]. This creates a triangular shaped plot, as shown in Figure 2.9, with a generally increasing fatigue life as the alternating stress decreases. Likewise, mean stress also contributes to fatigue life, as generally the fatigue life tends to decrease with increasing magnitudes of mean stress. The CFL diagram appears asymmetric, this is stated to be attributed to the difference in the laminate's compressive and tensile strengths [15]. Each CFL diagram created correlates to one mode of failure and separate diagrams would be required to predict the life of axial stress and shear stress.

With a known stress field, the CFL diagram may be utilized to predict fatigue life. This work will explore the stress field for post-buckled plates experiencing high-frequency dynamic loading. Stress values will then be used to determine fatigue life along all points of the plate. Fatigue is of interest within this work as post-buckled plates may experience higher mean stress values compared to flat plates. An increase in mean stress can ultimately lower the fatigue life which can be observed from the CFL diagram method.

2.5 Introduction to Finite Elements and Abaqus/CAE

In order to tackle the topics mentioned above in this work, finite element analysis will be used. In structural analysis, finite element methods (FEM) is a common numerical method for approximating the solution of a given boundary-value problem. Using FEM allows for a field of stress or displacement to be approximated over a domain, which is a valuable tool, as

stress is a crucial design parameter for aerospace engineering along with other engineering fields.

Specifically, Abaqus/CAE is a popular commercial finite element analysis software which allows a user to solve boundary-value problems given a specified structure and loading. For this work, Abaqus will be utilized to model composite post-buckled plates using shell elements. Finite element modeling will weigh heavily into this work, as displacements and stresses will be explored given varying static and dynamic loading conditions of composite plates undergoing snap-through. Stresses will be analyzed closely, as these parameters will be highly influential in fatigue and lifetime analysis of the structures. the following chapter will provide a detailed description of modeling the topics discussed in this chapter (i.e. modeling laminated composites, buckling, snap-through).

Chapter 3
THEORY AND MODELING

3.1 Chapter Overview

Introduced in the previous chapter, laminated composites are an essential topic within this work as they are often the material of choice for aerospace panels. This chapter outlines the basic theories for solving problems involving laminated composites. Before investigating the problems such as snap-through of composite plates discussed in the previous chapter, the behavior of laminated composites should first be discussed and understood. This chapter will discuss Classical Laminate Theory (CLT), a tool used to predict the behavior of laminated composites under given load conditions. As a foundation of CLT, Kirchhoff-Love Plate Theory will be discussed, a mathematical model used as a foundation for solving plate problems.

Following the introduction of these theories, this chapter will discuss modeling plate problems using Abaqus/CAE. This thesis will focus heavily on using this finite element software to model problems of snap-through of buckled composite panels. Thus, the process of modeling a post-buckled laminated composite plate will be presented in this chapter as it serves as a foundation for the remainder of this thesis. Additionally, the process of creating both dynamic and static snap-through plate models will also be discussed as these finite element models will later prove to be significant to this work.

3.2 Plate Theory

3.2.1 Thin Laminates and Kirchhoff-Love Plate Theory

Kirchhoff-Love or Kirchhoff plate theory is an accepted method for determining thin plate deformations and stresses. The theory is often referred to as an extension of Euler-Bernoulli

beam theory, which assumes that normals to the plate midplane remain straight and perpendicular following deformation. To solve for stresses and deformations of thin composite plates, laminate plate theory is used. Strains are assumed to vary linearly through the thickness of the plate and out-of-plane shear deformations are assumed to be negligible. Additionally, plane-stress conditions are applied as out-of-plane stresses are small compared to in-plane stresses [7].

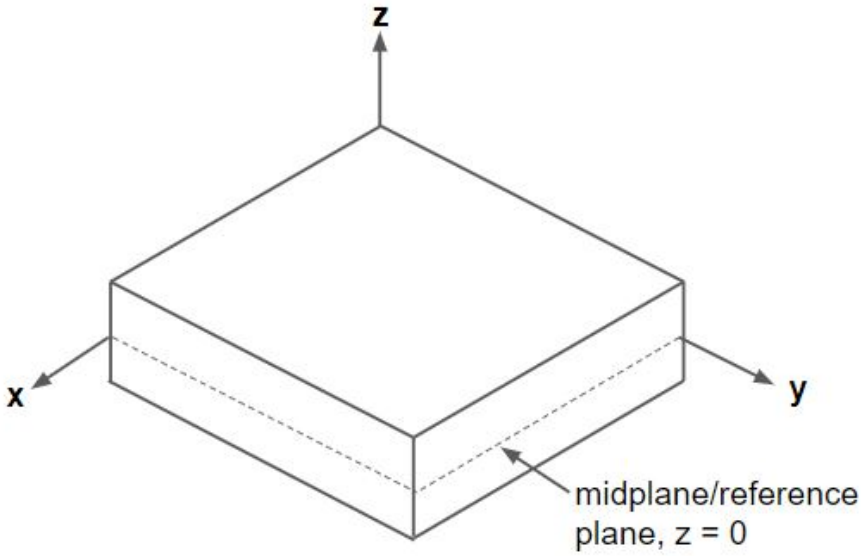

Figure 3.1: Coordinate system for Classical Laminate Theory reproduced from [7]

According to Classical Laminate Theory, when solving for strain and stress within composites the reference plane is defined as the midplane of the plate [7]. Figure 3.1 shows this reference plane and the global coordinate system associated with this theory. Prior to calculating the strain through the entire thickness of the plate, the strains are first calculated at the plate midplane. From Kollar and Springer [7], plate midplane strains are denoted by the superscript o and are evaluated as shown in Equation 3.1. Variables u and v signify the deformations in the x and y directions respectively.

$$\epsilon_x^o = \frac{\partial u^o}{\partial x} \qquad \epsilon_y^o = \frac{\partial v^o}{\partial y} \qquad \gamma_{xy}^o = \frac{\partial u^o}{\partial y} + \frac{\partial v^o}{\partial x} \tag{3.1}$$

Additionally, the angles of rotation of the normals to the plate midplane χ_{xz} and χ_{yz} are evaluated as provided in Equation 3.2, where w^0 is the transverse deflection along the plate midplane.

$$\chi_{xz} = \frac{\partial w^o}{\partial x} \qquad \chi_{yz} = \frac{\partial w^o}{\partial y} \tag{3.2}$$

Displacements in the x and y directions can be calculated as u and v by combining Equations 3.1 and 3.2. This results in the expressions provided by Equation 3.3. Using z the expressions can be evaluated at any location through the thickness of the plate.

$$u = u^o - z\chi_{xz} = u^o - z\frac{\partial w^o}{\partial x} \qquad v = v^o - z\chi_{yz} = v^o - z\frac{\partial w^o}{\partial y} \tag{3.3}$$

Looking back at Equation 3.1, the strains at the midplane are calculated as partial derivatives of the displacements. Incorporating this knowledge with Equation 3.3, the normal and shear strains at locations anywhere throughout the thickness of the plate can be calculated with Equations 3.4 and 3.5. Finding the strains at any location in the plate thickness is accomplished by simply varying z within these equations.

$$\epsilon_x = \frac{\partial u^o}{\partial x} - z\frac{\partial^2 w^o}{\partial x^2} \qquad \epsilon_y = \frac{\partial v^o}{\partial y} - z\frac{\partial^2 w^o}{\partial y^2} \tag{3.4}$$

$$\gamma_{xy} = \frac{\partial u^o}{\partial y} + \frac{\partial v^o}{\partial x} - z\frac{2\partial^2 w^o}{\partial x \partial y} \tag{3.5}$$

Equations 3.4 and 3.5 can be written similarly in matrix form for ease of simplification [7]. The variables κ signify the midplane curvatures of the plate.

$$\begin{Bmatrix} \epsilon_x \\ \epsilon_y \\ \gamma_{xy} \end{Bmatrix} = \begin{Bmatrix} \epsilon_x^o \\ \epsilon_y^o \\ \gamma_{xy}^o \end{Bmatrix} + z \begin{Bmatrix} \kappa_x \\ \kappa_y \\ \kappa_{xy} \end{Bmatrix} \tag{3.6}$$

$$\begin{Bmatrix} \kappa_x \\ \kappa_y \\ \kappa_{xy} \end{Bmatrix} = \begin{Bmatrix} -\frac{\partial^2 w^o}{\partial x^2} \\ -\frac{\partial^2 w^o}{\partial y^2} \\ -\frac{2\partial^2 w^o}{\partial x \partial y} \end{Bmatrix} \tag{3.7}$$

Equation 3.7 displays the midplane curvatures of the plate which are substituted into Equation 3.6 to solve for the normal and shear strain values. Again, the strains may be evaluated at any location along the plate thickness by varying z, with $z = 0$ being at the plate midplane.

Forces and moments applied to the plate may be expressed using integration over the plate thickness, where h_{bot} and h_{top} refer to the plate bottom and top measured from the midplane respectively. Variables N and M refer to resultant force and moments applied along the plate length and are reported in units of per unit length. An expression for evaluating force and moments is provided in Equation 3.8. Note that the equations for calculating forces and moments are nearly identical and both include stress, however, the moment expressions also include the variable z.

$$\begin{Bmatrix} N_x \\ N_y \\ N_{xy} \\ M_x \\ M_y \\ M_{xy} \end{Bmatrix} = \int_{-h_{bot}}^{h_{top}} \begin{Bmatrix} \sigma_x dz \\ \sigma_y dz \\ \tau_{xy} dz \\ z\sigma_x dz \\ z\sigma_y dz \\ z\tau_{xy} dz \end{Bmatrix} \tag{3.8}$$

In order to evaluate the expressions provided by Equation 3.8, the normal and shear stresses σ_x, σ_y, and τ_{xy} must be calculated. To calculate these stresses, the stiffness matrix for the each ply within the laminate must be defined. The stiffness matrix for each ply may be denoted as $[Q]_{local}$ using a local coordinate system. The "local" notation exists as each ply may be oriented at a different angle within the laminate. At the local coordinate system, the x-axis is aligned to the fiber direction of the ply. Figure 3.2 illustrates the local

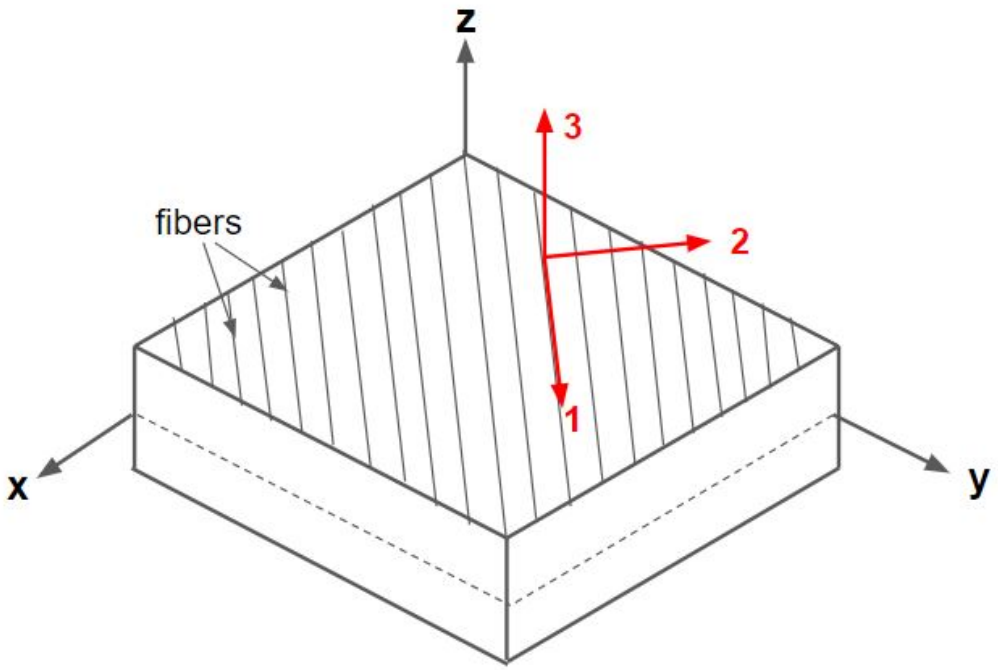

Figure 3.2: Local and global laminate coordinate systems, local coordinate system appears in red with 1-2-3 axes labels, with "1" defined as aligned with the fiber direction

and global coordinate systems discussed here. The local stiffness matrix for a transversely isotropic material which applies to all plies is displayed in Equation 3.9, where E, G, and v are Young's modulus, shear modulus and Poisson's ratio respectively in the fiber and matrix directions [7].

$$[Q]_{local} = \begin{bmatrix} \frac{E_1}{D} & \frac{v_{12}E_2}{D} & 0 \\ \frac{v_{12}E_2}{D} & \frac{E_2}{D} & 0 \\ 0 & 0 & G_{12} \end{bmatrix} \qquad where \quad D = 1 - \frac{E_2}{E_1}v_{12}^2 \tag{3.9}$$

To align the local stiffness matrix of a ply to global coordinates, the local stiffness matrix must be multiplied by a rotational matrix which is dependent on the ply angle orientation, where the angle is denoted by θ. This must be done to each ply's stiffness matrix to be sure

that all stiffness matrices follow the same, global coordinate system. The global stiffness matrix may be calculated using the local stiffness matrix as shown in Equation 3.10.

$$[Q]_{global} = [R]_1^{-1}\ [Q]_{local}\ [R]_2 \tag{3.10}$$

$$[R]_1 = \begin{bmatrix} cos^2\theta & sin^2\theta & 2cos\theta sin\theta \\ sin^2\theta & cos^2\theta & -2cos\theta sin\theta \\ -cos\theta sin\theta & cos\theta sin\theta & cos^2\theta - sin^2\theta \end{bmatrix} \tag{3.11}$$

$$[R]_2 = \begin{bmatrix} cos^2\theta & sin^2\theta & cos\theta sin\theta \\ sin^2\theta & cos^2\theta & -cos\theta sin\theta \\ -2cos\theta sin\theta & 2cos\theta sin\theta & cos^2\theta - sin^2\theta \end{bmatrix} \tag{3.12}$$

Using Equations 3.9, 3.11, and 3.12, the global stiffness may be calculated with Equation 3.10 [7]. Again, each ply orientation requires its own global stiffness matrix calculation as each ply may be oriented at a different angle. With the global stiffness defined, the stresses throughout the laminate may be calculated with Equation 3.13.

$$\begin{Bmatrix} \sigma_x \\ \sigma_y \\ \tau_{xy} \end{Bmatrix} = [Q]_{global} \begin{Bmatrix} \epsilon_x \\ \epsilon_y \\ \gamma_{xy} \end{Bmatrix} \tag{3.13}$$

By combining the Equation 3.13 into Equation 3.8, a general expression for the forces and moments applied to the plate may be evaluated [7].

$$\begin{Bmatrix} N_x \\ N_y \\ N_{xy} \end{Bmatrix} = \int_{-h_{bot}}^{h_{top}} \left\{ [Q]_{global} \begin{Bmatrix} \epsilon_x^o \\ \epsilon_y^o \\ \gamma_{xy}^o \end{Bmatrix} + z[Q]_{global} \begin{Bmatrix} \kappa_x^o \\ \kappa_y^o \\ \kappa_{xy}^o \end{Bmatrix} \right\} dz \tag{3.14}$$

$$\begin{Bmatrix} M_x \\ M_y \\ M_{xy} \end{Bmatrix} = \int_{-h_{bot}}^{h_{top}} \left\{ z[Q]_{global} \begin{Bmatrix} \epsilon_x^o \\ \epsilon_y^o \\ \gamma_{xy}^o \end{Bmatrix} + z^2[Q]_{global} \begin{Bmatrix} \kappa_x^o \\ \kappa_y^o \\ \kappa_{xy}^o \end{Bmatrix} \right\} dz \tag{3.15}$$

Using Equations 3.14 and 3.15, strains may be evaluated at any location through plate thickness. Components of Equations 3.14 and 3.15 are defined as the the stiffness matrices of the laminate, denoted as the $[A]$, $[B]$, and $[D]$ matrices [7]. These matrices are used to describe in-plane stiffness, out-of-plane in-plane coupling stiffness, and bending stiffness respectively. Equation 3.16 offers a method of summations to calculate each of these stiffnesses, where k refers to each ply and z is the distance to each respective ply from the midplane. Figure 3.3 depicts these variables with a 4-ply laminate.

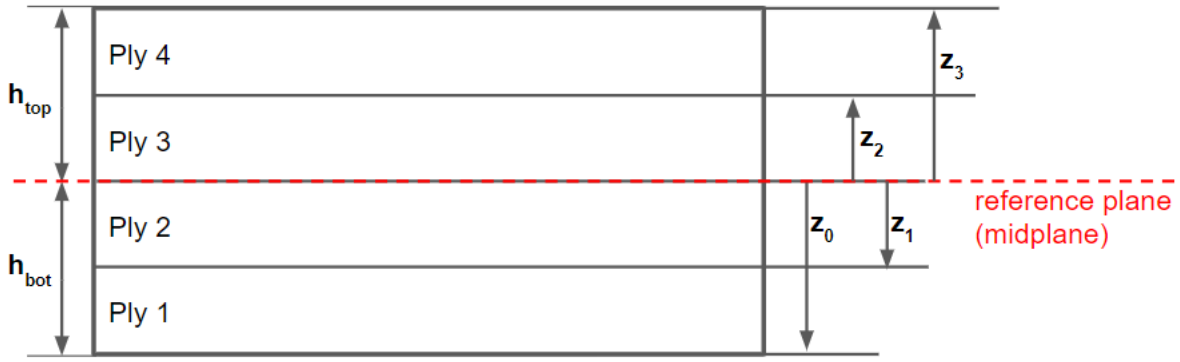

Figure 3.3: z measurements from the reference plane for a 4-ply laminate, reproduced from [12]

$$
\begin{aligned}
A_{ij} &= \sum_{k=1}^{K} (Q_{global\ ij})_k\ (z_k - z_{k-1}) \\
B_{ij} &= \sum_{k=1}^{K} \frac{1}{2}\ (Q_{global\ ij})_k\ (z_k^2 - z_{k-1}^2) \\
D_{ij} &= \sum_{k=1}^{K} \frac{1}{3}\ (Q_{global\ ij})_k\ (z_k^3 - z_{k-1}^3)
\end{aligned}
\tag{3.16}
$$

Finally, the forces and moments applied to the laminate may be expressed in matrix form through the stiffness matrices previously defined. See Equation 3.17 for this expression [12].

$$\begin{Bmatrix} N_x \\ N_y \\ N_{xy} \\ M_x \\ M_y \\ M_{xy} \end{Bmatrix} = \begin{bmatrix} A_{11} & A_{12} & A_{16} & B_{11} & B_{12} & B_{16} \\ A_{12} & A_{22} & A_{26} & B_{12} & B_{22} & B_{26} \\ A_{16} & A_{26} & A_{66} & B_{16} & B_{26} & B_{66} \\ B_{11} & B_{12} & B_{16} & D_{11} & D_{12} & D_{16} \\ B_{12} & B_{22} & B_{26} & D_{12} & D_{22} & D_{26} \\ B_{16} & B_{26} & B_{66} & D_{16} & D_{26} & D_{66} \end{bmatrix} \begin{Bmatrix} \epsilon_x^o \\ \epsilon_y^o \\ \gamma_{xy}^o \\ \kappa_x \\ \kappa_y \\ \kappa_{xy} \end{Bmatrix} \tag{3.17}$$

With the final expression provided in Equation 3.17, the strains and curvatures at the midplane may be calculated using the known stiffness matrix and known applied forces and moments. After determining the midplane strains, the strain at any location within the laminate thickness can then be evaluated by varying z from Equation 3.6 which was previously defined within this section. Likewise, the stresses at any location within the laminate thickness may be computed utilizing Equation 3.13. The ability to calculate these values in this simple form is derived from the Kirchhoff theory and Classical Laminate Theory.

Kirchhoff plate theory was discussed within this section, however, Abaqus FEA utilizes the Reissner-Mindlin plate theory as plate thickness increases. Similar to Timoshenko beam theory, this plate theory is an extension of Kirchhoff plate theory, however, assumes that lines perpendicular to the plate midplane do not remain orthogonal and takes into account shear deformation.

Later the accuracy of thin plate theory will be explored and compared with Reissner-Mindlin theory. Therefore, the following section discusses how Fourier series may be used to closely approximate plate deflection for a simple case.

3.2.2 Static Analysis with Fourier Series

After understanding the theory and behavior of thin laminated plates, components of Fourier series may be used to closely calculate the displacement of composite plates undergoing uniform pressure loading. Utilizing this analytical approach simplifies calculations for various cases of plate problems and avoids the need for complex algorithms. This section will focus on

the deflection of simply-supported plates with symmetrical composite layups. To begin, an expression is selected to express the plate deflection while adhering to the given boundary conditions. In the case of a fully simply-supported plate, the deflection expressions must allow for zero displacement at all plate edges.

To start, the applied load is described using Fourier components [11]. This load can be calculated as shown in Equation 3.18. The indices are depicted as m and n, where increasing these number of terms increases accuracy of the analytical approximation. Additionally, q_0 represents the load magnitude and h and b are the plate length and width.

$$q(x,y) = q_0 = \sum_{n=1}^{\infty}\sum_{m=1}^{\infty} e_{mn} sin(\frac{m\pi y}{h}) sin(\frac{n\pi x}{b}) \tag{3.18}$$

$$e_{mn} = \frac{4}{hb}\int_0^h \int_0^b q_0 sin(\frac{n\pi x}{b}) sin(\frac{m\pi y}{h}) dxdy \tag{3.19}$$

The Fourier coefficient, e_{mn} from Equation 3.19 may be further evaluated as it is a definite integral, simplifying to the equation provided in Equation 3.20. This equation applies for when m or n are odd, and $e_{mn} = 0$ when m or n are even due to the sinusoidal terms involved in the Fourier coefficient.

$$e_{mn} = \frac{16 q_0}{mn\pi^2} \tag{3.20}$$

Displacement can spatially be described from Equation 3.21.

$$w(x,y) = \sum_{n=1}^{\infty}\sum_{m=1}^{\infty} d_{mn} sin(\frac{m\pi y}{h}) sin(\frac{n\pi x}{b}) \tag{3.21}$$

$$d_{mn} = \frac{e_{mn}}{D[(\frac{n\pi}{b})^4 + 2(\frac{n\pi}{b})^2(\frac{m\pi}{h})^2 + (\frac{m\pi}{h})^4]} \tag{3.22}$$

$$D = \frac{Et^3}{12(1-v^2)} \tag{3.23}$$

Combining Equations 3.22 and 3.23 results in the simplified Equation 3.24 to calculate deflection for a simply-supported, uniformly-loaded rectangular plate.

$$w(x,y) = \frac{\sum_{n=1}^{\infty}\sum_{m=1}^{\infty} 16q_0 sin(\frac{m\pi y}{h})sin(\frac{n\pi x}{b})}{mn\pi^2 D[(\frac{n\pi}{b})^4 + 2(\frac{n\pi}{b})^2(\frac{m\pi}{h})^2 + (\frac{m\pi}{h})^4]} \tag{3.24}$$

In a later section, a parametric study with varying plate dimensions will be conducted using Equation 3.24 to determine plate deflection given constant uniform loading. This study will explore the theory behind plate modeling in Abaqus while using this convenient analytical tool to calculate and compare plate deflection results to the finite element models. These analytical plate deflections will be compared with Abaqus deflection results to determine the accuracy of Abaqus given varying plate dimensions. With a basic understanding of the theories behind plates, the next section of this chapter will discuss how to model plates in Abaqus

3.3 Modeling plates in Abaqus/CAE

The theories discussed earlier in this chapter serve as a baseline for understanding the theory behind Abaqus/CAE when solving plate boundary value problems. Within this work, Abaqus is utilized for all finite element modeling as it is an easily accessible and powerful finite element tool. Later in this work, both static and dynamic analyses of plates will be employed to study the responses of post-buckled plates experiencing snap-through behaviors. To model these problems, Abaqus shell elements will be used.

Shell elements are used to model plates as the thickness is significantly smaller compared to the other dimensions. Specifically, Abaqus' conventional shell elements are used throughout this thesis. Conventional shell elements consist of both rotational and displacement degrees of freedom allowing for three-dimensional analysis [8]. All plates modeled within this work are composed of 4-node, fully integrated shell elements, identified as S4 elements in the Abaqus user interface. This specific element type uses thick shell theory known as Reissner-Mindlin when plate models approach large thicknesses, and defaults to Kirchhoff shell theory which was previously discussed in this chapter as plate model thickness decreases [8]. In general, plates are considered to be thick when the plate thickness-to-length ratio exceeds 1/15. For our cases, plate thickness relative to the other characteristic dimensions remains small, allowing Abaqus to utilize Kirchhoff shell theory.

This section will discuss how the modeling process in Abaqus for varying thin plate problems that will be later explored in this thesis. First, a description of the Abaqus modules is provided, Then, four key modeling processes are discussed that will be essential to the work later in this thesis. The Abaqus modeling problems which will be presented include (1) creating a flat laminated composite plate (2) creating a buckled plate (3) creating a dynamic snap-through plate model (4) creating a static snap-through plate model. These models will be frequently used throughout this work in various studies throughout the succeeding chapters, so it is of importance to discuss these here.

3.3.1 Abaqus/CAE Modules

Prior to discussing the modeling problems, it is important to understand the modules in Abaqus. Abaqus is divided into modules to provide a user-friendly environment for the modeling process. These modules will be mentioned throughout this work, so it is important to understand the modeling setup of Abaqus prior to investigating the topics previously discussed in this chapter. Here, a brief description of the modules will be provided, however, a detailed description of each module is provided in the Abaqus User's Manual [9]. To begin, the geometry of the structure of interest must be defined. In Abaqus, the "Part" module allows the user to create the structure using design tools. For the case within this work, the part will be defined as a deformable shell.

After creating a part geometry, the material properties are assigned to the part using the "Property" module. Because this work focuses on laminated composites, the properties will be elastic and will be entered as "Lamina" types since the composites here are transversely isotropic. Aside from this, Abaqus allows many other entries of material properties types, including "Isotropic", "Engineering Constants", and "Orthotropic" to name a few. The "Property" module also allows users to define a composite layup consisting of plies made from materials of their choice. Here Abaqus allows users to assign ply orientation angles and ply thickness.

The "Assembly" module is used to assign a global coordinate system to the parts created. When a part is created in the "Part" module, it consists of its own local coordinate system. Adding multiple parts together is allowed in the "Assembly" module, where a global coordinate system will be defined. This work will focus on a single part per simulation, so this module seems less significant as multiple parts will not be combined here.

The "Step" module defines the analysis type of interest for the model. A simulation may consist of one or more analysis steps depending on the desired loading and boundary conditions. Defining several steps allows you to change loading, boundary conditions, or type of analysis performed during the simulation. Examples of types of analysis steps include

static analysis, dynamic implicit analysis, heat transfer procedure, and Riks static analysis steps. Because Abaqus allows the change of analysis types by implementing several steps in the order of the user's choice, it offers great flexibility in performing analysis. This flexibility to tailor the analysis type will be utilized significantly in this thesis.

The "Load" module provides tools for users to define loading to the parts they have created. Boundary conditions are also defined within this section. A load and boundary condition are assigned to each step that has been created. Depending on the step type and load parameters, Abaqus will solve the boundary value problem accordingly. For instance, an applied pressure load which is assigned to a static general analysis step will solve the problem statically, however the same load assigned to a dynamic implicit analysis step will solve the problem including inertial terms. Again, this flexibility in load assignment and analysis options allows ease in customization of analysis which is ideal for this work.

The "Mesh" module allows users to create meshes on parts to a mesh resolution of the user's choice. Meshes may be controlled to different sizes and shapes depending on what is desired in analysis. Additionally, element types may be defined, allowing the user to pick which finite element type will be used in solving the problem. Understanding the basic purposes of these modules discussed here is essential for understanding modeling processes which will be discussed next.

3.3.2 Creating a Flat Laminated Composite Plate Using Abaqus/CAE

This section outlines the modules involved in the modeling process using Abaqus/CAE to create laminated composite plates. Specifically, the modeling process of creating a post-buckled plate will be discussed here as this modeling process will be used throughout the thesis for several studies.

Part

The first step to the modeling process in Abaqus involves creating a part. Although there are several ways to create a composite part, this work will model laminated composites

using conventional shell elements. Another way to model composites is using continuum shell elements, however, this requires greater computational expense. Conventional shell elements will be utilized within this thesis it offers sufficient accuracy for the scope of this work. To create the plate using shell elements in the "Part" module, the part was selected as a "Deformable" with a "3D" modeling space and to be modeled as a "Shell" feature. After these options are selected, the plate is drawn as a simple rectangle by entering the desired length and width dimensions. Plate thickness will be defined later in the "Property" module when defining the composite layup.

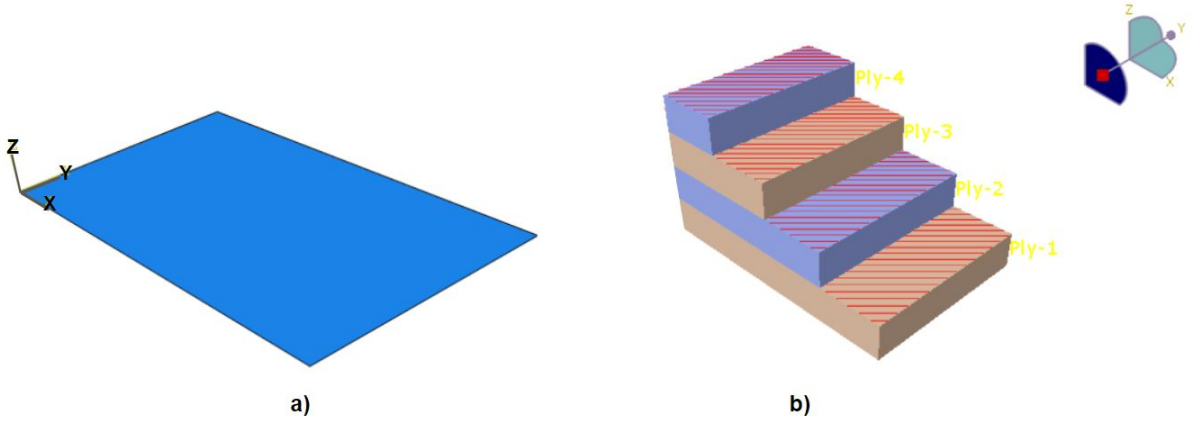

Figure 3.4: Abaqus modeling of a) flat plate model b) composite layup of flat plate using $[45]_4$ orientation angles created in the "Property" module

Property

After the part is created, the desired material properties are entered into the "Property" module. Laminate properties are entered by selecting "Mechanical", then "Elastic", followed by "Lamina". Note that the "Lamina" was selected as the properties for laminated composites will be transversely isotropic. Instead of "Lamina", "Orthotropic" or "Engineering Constants" could also have been selected, however, the former method will be used in this thesis. Here the Young's moduli, Shear moduli, and Poisson's ratio are entered. Addi-

tional material properties required for dynamic analysis are also added into the "Property" module section. Material damping is added by selecting "Mechanical" then "Damping" and adding the correct alpha and beta values to Rayleigh damping. The composite material density is added by selecting "General" then "Density". The material is then saved within the "Property" module and will be used in the next step as it is assigned to each ply in the layup.

The composite layup is also defined within the "Property" module in Abaqus. To create the composite layup, "Create Composite Layup" is selected using a "Conventional Shell" and the "initial ply count" number is entered depending on the desired number of plies. Within the "Edit Composite Layup" window, the ply material (previously defined above), individual ply thicknesses, and orientation angles are input. This input allows the user to define different ply thicknesses and orientation angles for each individual ply if so desired. Additional, a different material could be assigned to each individual ply, however, the scope of this work will focus on using the same material for all plies. Figure 3.4 shows an example of a flat rectangular plate model with a laminated composite layup of $[45]_4$ as an example for a result of completing the "Property" module and defining a layup.

Mesh

The "Mesh" module discretizes the part and defines the plate mesh and element types. For the purpose of this thesis, "S4" shell element type will be selected. These elements are 4-node, fully integrated shell elements. This element type was selected to match previous finite element work by Kim [5] which this thesis will expand on later. Plate dimensions will vary throughout this work, so plate mesh size will be specified later depending on the plate dimensions in each study.

3.3.3 Creating a Buckled Plate Using Abaqus/CAE

This thesis heavily focuses on the behavior of post-buckled laminated composite plates. Thus, it is important to first model a buckled plate. The process of buckling a plate requires the

primary steps of first (1) creating a flat plate model and (2) applying an axial load to one edge of the flat plate sufficient to cause buckling. The steps to create a flat plate in Abaqus are presented above in Section 3.3.2. The remaining process to apply an axial load to buckle the plate is provided below in the following sections.

Step

The "Step" module in Abaqus allows the user to select an analysis type for the loading which will be assigned to the model later. In the process of axially buckling a plate, a "Static, General" step is selected. Nonlinear is set to "on" as the plate may experience large displacements during the buckling process.

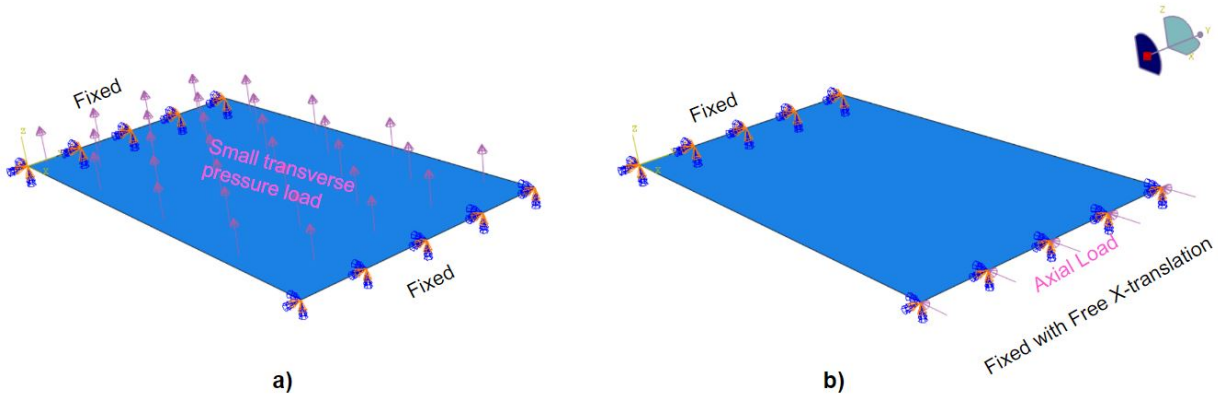

Figure 3.5: Abaqus plate model with a) small imperfection applied using transverse pressure load and boundary conditions b) axial load applied as a shell edge load with boundary conditions

Load

The "Load" module defines loading and boundary conditions to be used during the analysis. In order to buckle the flat plate, a small transverse load will need to be first applied (prior to the axial load) in order to create a small imperfection in the plate geometry. This will allow the plate to buckle once the axial load is applied as a completely perfect plate will

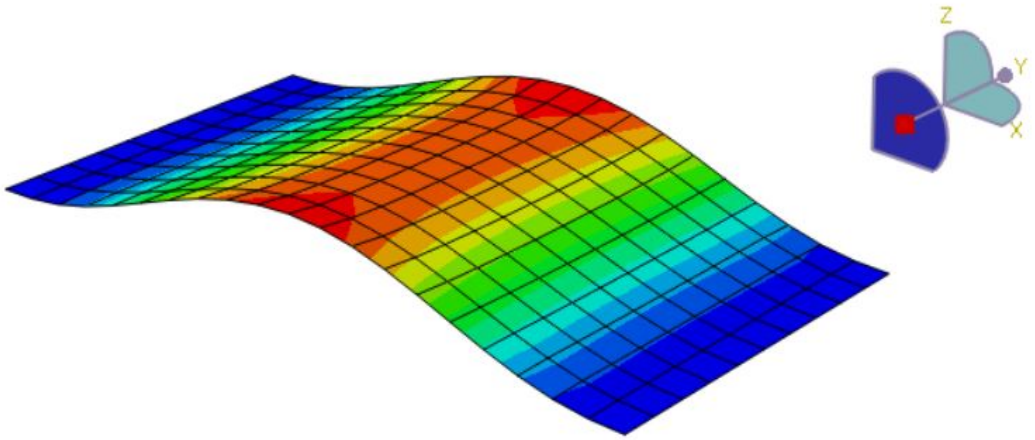

Figure 3.6: Abaqus buckled plate as a result of applied axial loading

not buckle. Prior to assigning loading, the boundary conditions are set to fixed-fixed on two parallel edges, leaving the remaining two edges completely free. At this point, the small transverse load discussed earlier is applied using a "Static, General" step. Figure 3.5a displays the boundary conditions and loading to create a small imperfection in the plate's configuration. Following this, the axial load will need to be applied. Before applying this load, the boundary conditions must be modified slightly on the plate edge where loading will be assigned. The right plate edge boundary condition is changed to allow free translation in the x-direction. Figure 3.5b displays the boundary conditions and loading for this step. The axial load is then applied uniformly as a "Shell edge load" with the desired magnitude. This is equivalent to a uniform distributed load. This axial loading and the small imperfection result in transverse buckling of the plate out-of-plane into the positive z-direction. Figure 3.6 portrays the result in Abaqus of a laminated composite plate buckled through axial loading.

3.3.4 Creating a Dynamic Snap-through Plate Model

Throughout this thesis, the need for dynamic snap-through plate models is frequent. This section will discuss the general process for creating a model for a plate that undergoes

harmonic loading over time. The reason for requiring this model type will be discussed in a later chapter, however, it is important to first understand how this is modeled. In order to create a dynamic snap-through model, first a post-buckled plate model must be created. After the buckled plate model is produced, a dynamic analysis is performed on the plate with sinusoidal loading by adding additional analysis steps within the "Step" module. The process to create a post-buckled plate has been provided in the previous section. This section will introduce how to take this post-buckled plate model and perform a dynamic snap-through analysis on the plate with pressure loading that varies harmonically over time.

Step

Beginning with a buckled plate model, a dynamic analysis is defined within the "Step" module in Abaqus. The process to create a buckled plate is described previously in Section 3.3.2. To create a dynamic analysis in the "Step" module, a "Dynamic, Implicit" analysis type is defined. In the "Edit Step" window under the "Basic" tab, nonlinear is set to "on" to allow for nonlinear analysis as snap-through contains nonlinear behaviors and large deformations. Under the "Incrementation" tab, the incrementation type is set to "automatic" and the maximum increment step size is set to 0.00015. This defined dynamic analysis step will be assigned to the dynamic loading defined in the following section.

Load

The "Load" module is where the dynamic harmonic loading will be assigned to the buckled plate model. Boundary conditions are applied within this module by creating a new boundary condition in the "Boundary Conditions Manager" window. Within this window the dynamic, implicit step (created above) is selected so that Abaqus will use these boundary conditions in this dynamic analysis step. The boundary condition is listed under "Mechanical" and "Symmetry/Encastre" is selected within the window. Next, the two parallel shorter edges are selected and "Encastre" is selected. This will assign these two plate edges a clamped-clamped boundary condition, while the remaining two unselected plate edges will remain to

be free edges. Following the assignment of the boundary conditions, the load information is

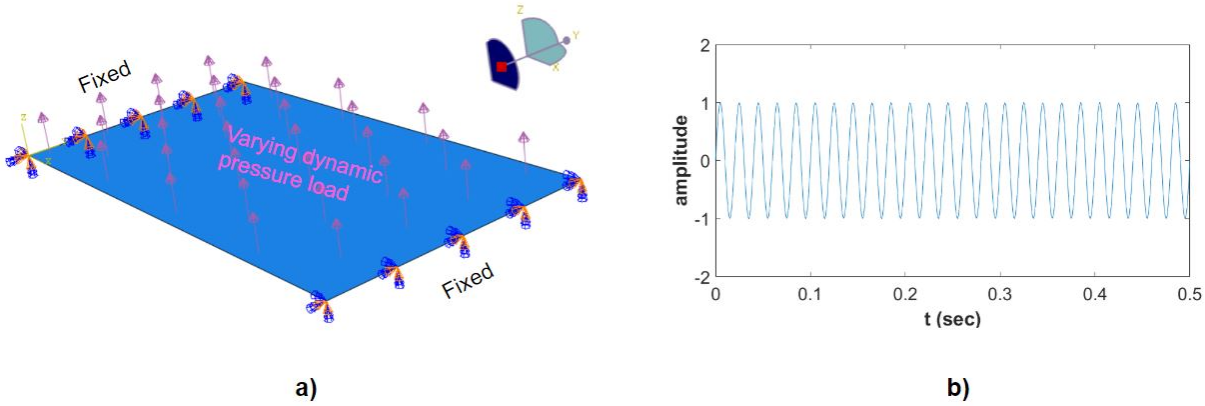

Figure 3.7: Abaqus plate model with a) varying dynamic pressure loading with fixed boundary conditions, b) input amplitude for varying dynamic pressure load (50 Hz frequency)

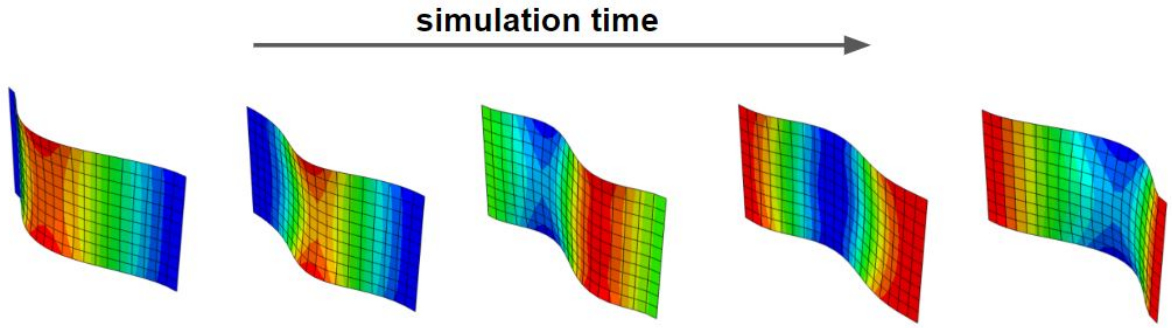

Figure 3.8: Abaqus plate model configuration during dynamic harmonic forcing over time

added for the dynamic analysis step in the "Load" module. A new load is created in the "Load Manager" window. The dynamic, implicit step is selected and the load is created by selecting "Mechanical" category load and "Pressure" as a load type. The top plate surface is selected for the pressure location, triggering the "Edit Load" window to appear. The "Edit Load" window allows the user to modify the pressure load amplitude and forcing frequency. To

assign the load forcing amplitude, the desired load amplitude is entered in the "Magnitude" box. Assigning a harmonic forcing is slightly more involved. First, a changing amplitude is created by clicking the "Create amplitude" icon within the "Edit Load" window. The forcing frequencies were entered by selecting "Tabular". Forcing amplitude changes over time depending on the forcing frequency. This information is entered using data values for both time and amplitude. "Amplitude" is defined as a sinusoidal function provided in Equation 3.25, where t is time in seconds and f is forcing frequency provided in Hertz.

$$a(t) = sin(2\ \pi\ f\ t) \tag{3.25}$$

Using Equation 3.25, amplitude data can be created and then entered into the "Tabular" amplitude window. This sinusoidal changing amplitude entry will tell Abaqus to vary the load magnitude over time using these values, simulating the harmonic pressure loading that is desired. For instance, if a magnitude of 1 MPa is entered as the pressure load, assigning the sinusoidal changing amplitude to this load will result in this 1 MPa load varying from 1 MPa to 0 MPa sinusoidally over time depending on the frequency of the sine data. Figure 3.7 shows the model boundary conditions and loading for dynamic snap-through. Notice the transverse pressure load shown in Figure 3.7a varies depending on the input forcing amplitude shown in Figure 3.7b. This input amplitude is a plot of the Equation 3.25 using a forcing frequency f of 50 Hz for example. Creating a dynamic snap-through plate model will result in the plate oscillating from a positive to a negative displacement over time. Figure 3.8 provides an example of a plate's deflection over time during a dynamic simulation with harmonic forcing for one half cycle.

3.3.5 Creating a Static Snap-through Plate Model

The need for creating a static snap-through model will not be required until a later chapter. However, the process to model a static snap-through of a plate will still be discussed here in this section and will be referred to later. A static version of dynamic snap-through may be created by buckling a post-buckled plate by means of applying a transverse pressure load

that is sufficient in magnitude to cause out-of-plane buckling. A static analysis in Abaqus is used here. Similar to creating a dynamic snap-through model, the static snap-through model must also start with a post-buckled plate model. See the Section 3.3.2 for instructions on creating the buckled plate which will be needed for the static snap-through model. After creating the buckled plate model, the following sections describe the next steps for creating the static snap-through model.

Step

Starting with a buckled plate model, a new static analysis is defined within the "Step" module in Abaqus. The static analysis step is added by creating a new step as a "Static, Riks" step. Riks method is recommended for unstable collapse of structures along with nonlinear behaviors such as snap-through [9]. This analysis type uses the Arc Length method to solve for nonlinear problems. Under the "Basic" tab in the "Edit Step" window, nonlinear is turned on to account for large deformations often associated with snap-through. Under the "Incrementation" tab, incrementation type is set to automatic. The intial arc length increment is set to 5E-5, with a maximum arc length increment size of 1E-4. This static analysis step will be implemented into the model in the next section.

Load

The "Load" module is where the static pressure loading will be defined. First, the boundary conditions that are desired for the static analysis are defined. A new boundary condition is created in the "Boundary Conditions Manager" window. Within this window the static, Riks step that was created previously is selected, assigning these boundary conditions to the correct analysis step. The boundary condition is listed under "Mechanical" and "Symmetry/Encastre" is selected within the window. Next, the two parallel shorter edges are selected and "Encastre" is selected. This will assign these two plate edges a clamped-clamped boundary condition, while the remaining two unselected plate edges will remain to be free edges.

These boundary conditions are identical to the boundary conditions for creating a dynamic plate snap-through analysis shown in Figure 3.7a from the previous section.

After the boundary conditions are applied, the static pressure load is assigned to the model. This is accomplished by creating a load in the "Load Manager". In the "Edit Load" window, the static, Riks step is selected and the "Mechanical" load category is selected along with "Pressure" being selected under the load type. The top surface of the plate is selected as the region for the pressure load, and the desired magnitude of the load is entered in the "Magnitude" text box. Abaqus uses modified Riks method to solve this static problem, and as a result will use proportional loading of the entered magnitude to solve for the load-displacement response [9]. This completes the steps for creating a static snap-through model.

3.4 Chapter Conclusion

This chapter focused on plate theories and Abaqus/CAE modeling which will be relevant to the remainder of this thesis. To begin, Classical Laminate Plate theory was introduced, along with Kirchhoff plate theory, two important theories for understanding the behavior of laminated composite plates. Following the introduction of these theories, Abaqus plate modeling was discussed. Four modeling processes are considered: (1) creating a composite laminated plate (2) buckling a laminated plate (3) performing a dynamic snap-through analysis on a buckled plate and (4) performing a static snap-through analysis on a buckled plate. These modeling processes will prove to be important in the following chapters, as snap-through of post-buckled composite plates is investigated further.

Chapter 4

MODEL VALIDATION OF LINEAR AND NONLINEAR PROBLEMS

4.1 Chapter Overview

As discussed in previous chapters, laminated composite panels along an aircraft can experience aerodynamic heating during flight causing high axial loading. These panels can buckle as thermally-induced axial loading and stresses increase. With transverse pressure loading the post-buckled panels then may experience large deformations resulting in dynamic snap-through and increasing stresses, which may decrease the fatigue life. Previous work by Kim focused on this phenomenon of snap-through with experimental work and numerical modeling [5]. It was found that snap-through response types may be characterized by three different dynamic responses: (1) single-well (2) chaotic snap-through (3) periodic snap-through. Using experimental and in-house finite element codes, Kim's work determined that these three response types are dependent on the load parameters of forcing amplitude and forcing frequency. A snap-through boundary was developed within harmonic forcing parameter space following these results, providing a tool to predict snap-through responses for laminated composite plates depending on loading parameters. The primary focus of this chapter is to develop the snap-through boundaries using Abaqus. The snap-through boundaries will be compared with results from Kim's research to validate the models used herein.

The previous chapter introduced plate theories and finite element modeling processes essential to the topics presented in this thesis. This chapter will focus on using these understandings and Abaqus/CAE modeling processes to model post-buckled laminated composite plates, and ultimately reproducing the snap-through boundary introduced above. There are three key validation exercises in this chapter. First, a statics validation for flat, isotropic

plates against an analytical solution was conducted using Abaqus. This involved a plate thickness parametric study with varying plate dimensions. This study explored plate theory discussed previously in Chapter 3 and leads to a better understanding of modeling thin plates in Abaqus. Next, a static validation using the cylindrical bending problem was conducted. This problem was investigated to validate modeling laminated composite plates using static analysis in Abaqus. Then, the primary portion of this chapter involved a nonlinear dynamics validation using experimental and in-house finite element model results from Kim's research. With this, the snap-through boundary was reproduced in Abaqus, ultimately validating the Abaqus post-buckled dynamic plate models. This chapter is of great importance as it will validate the Abaqus laminated composite plate models which will be used in later chapters for further studies on snap-through.

4.2 Linear Model Validation: Scenario 1 Isotropic Plate Thickness Study

4.2.1 Introduction and Modeling

Prior to investigating snap-through, a parametric plate study was performed to explore the plate theory behind Abaqus finite element software. An added purpose of this study was to validate modeling simple isotropic thin plates in Abaqus prior to advancing to modeling laminated composite plates in a later section. In this study plate length, width, and thickness were varied and the maximum deflection results were compared using the analytical method and the Abaqus results. The percent error between the Abaqus displacement results and displacements calculated using Kirchhoff theory were compared to investigate the theory behind Abaqus. Abaqus is capable of using Reissner-Mindlin plate theory. Thus, it is expected that the Kirchhoff displacement results should deviate from the Abaqus results at certain plate dimensions. This will be observed later in this section. To begin, numerous plate models were created with varying dimensions to test the thickness-to-length ratio influence on deflection calculations. Plate thickness was varied from 0.1 mm to 5 mm and plate lengths and widths were varied 2 mm to 40 mm. The plate was modeled as an isotropic material with

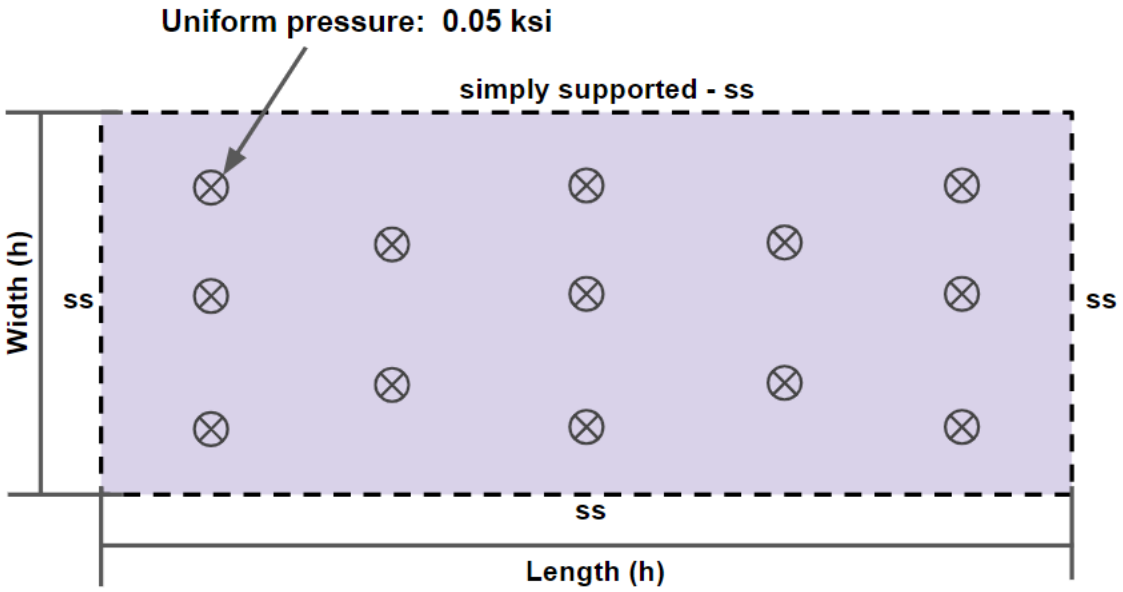

Figure 4.1: Boundary conditions and loading for plate thickness parametric study models (plan view)

Young's modulus of 29000 ksi and a Poission's ratio of 0.3. Plates were simply supported on all edges for boundary conditions. A static, uniform pressure load of 0.05 ksi was applied to each plate model. Figure 4.1 provides these boundary conditions and loading for the plate models in this section. The detailed modeling process for modeling plates in Abaqus is provided in Chapter 3.

4.2.2 Plate Thickness Parametric Study Results

The deflections at the midnode for each plate were calculated using Equation 3.24 from Chapter 3 for each varying thickness-to-length ratio. Then, these calculated deflections were compared with the deflections output from the Abaqus finite element models. Figure 4.2 shows an example of both the analytical and finite element model for one plate with a length, width, and thickness of 20 mm, 5 mm, and 0.1 mm respectively.

The plate models shown in Figure 4.2 both possess a thickness-to-length ratio of 1/200.

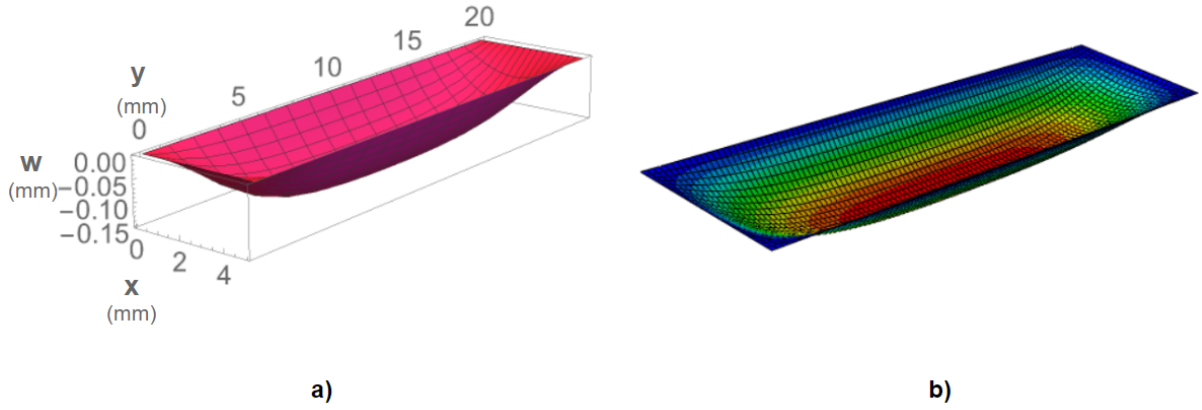

Figure 4.2: Deflected plate models with 20mm x 5 mm x 0.1 mm (h x b x t) dimensions, a) analytical model using Kirchhoff plate theory and Mathematica, b) finite element model using Abaqus

When comparing the midnode displacements of the analytical model with the Abaqus model, the displacements are 0.1508 mm and 0.1505 mm respectively. The small error between these methods is approximately 0.16%. However, as the thickness-to-length ratio increases this error also increases since Abaqus calculates the displacements utilizing Reissner-Mindlin plate theory. The analytical method used here strictly uses Kirchhoff plate theory, therefore, an increase in error is expected. For instance, when this same plate's thickness is increased from 0.1 mm to 2 mm, the thickness-to-length ratio increases to 1/10. At this high ratio the Kirchhoff plate theory approximation is no longer as accurate, causing the analytical approximation for the midnode displacement to be inaccurate. At these plate dimensions the midnode displacement is calculated analytically and using Abaqus as 1.88E-05 mm and 2.76E-05 mm respectively. Comparing these two displacement values yields an error of 46.5%. This high error is expected as the thickness-to-length ratio increased enough to where Abaqus' approximations remain valid, while the analytical method utilizing Kirchhoff theory begins to lose accuracy.

Many plate models with varying dimensions and thickness-to-length ratios were evaluated

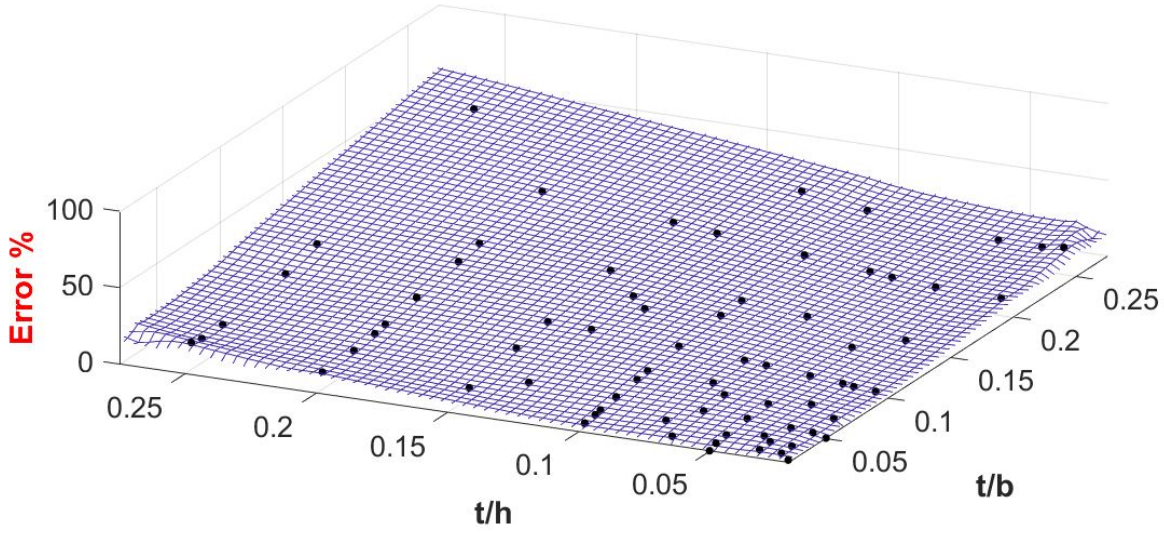

Figure 4.3: 3D percent error surface of midnode displacements corresponding to varying thickness-to-length (t/h) and thickness-to-width (t/b) ratios. Black points depict error plot results. The meshed surface is created by interpolating between all points.

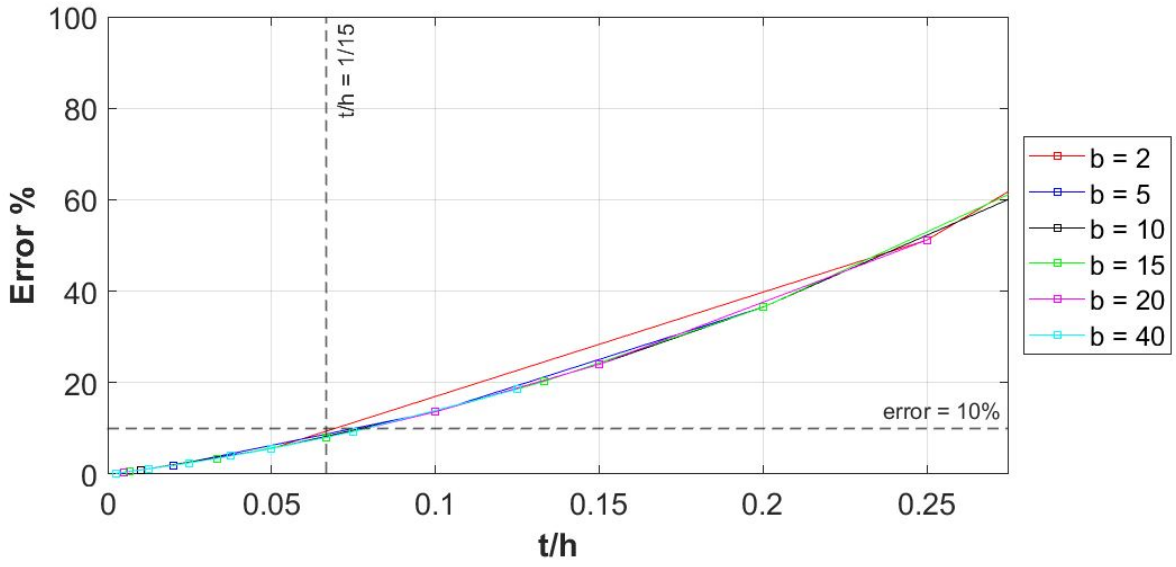

Figure 4.4: 2D percent error of midnode displacements corresponding to varying thickness-to-length (t/h). Plate width is denoted as b (in inches).

similarly. The error between the analytical method and Abaqus midnode displacement results were documented and the percent error between these values was plotted in 3D space. Figure 4.3 depicts the error for these displacement results. The figure shows that increasing the thickness ratios results in an increased error. The midnode displacement results compared in the percent error are the analytical approximation and the Abaqus model results. Again, an increased error is expected between these results because as plate thickness increases, the analytical equation no longer is accurate while Abaqus remains accurate. This is due to the difference in theories between the two solving methods: Abaqus has the ability to use Reissner-Mindlin (thick) plate theory, while the analytical equation used in this study uses Kirchhoff (thin) plate theory. Thus, at larger plate thicknesses the analytical equation is no longer correct. Figure 4.4 provides another visual of the percent error plot as a 2D cross-section of the 3D surface plot. The figure shows that increasing the thickness ratio past $t/h = 1/15$ results in an error greater than 10%. Note that this error refers only to the error in the midnode displacement. This error may vary in other quantities such as stress.

4.2.3 Parametric Plate Study Discussion

Midnode displacement error increased with increasing thickness-to-length ratios when comparing the analytical approximation results to the Abaqus model results. This result was expected because the equation utilizes Kirchhoff (thin) plate theory while Abaqus uses Reissner-Mindlin (thick) plate theory. Thus, the analytical approximation method was not accurate for thick plates which caused the increased error. This parametric study served as an exercise to investigate the plate theory behind Abaqus/CAE. Additionally, this study validated modeling isotropic plates in Abaqus since the thin plate displacements matched the calculated displacement results. The next section will advance to modeling laminated composite plates for a cylindrical bending problem.

4.3 Linear Model Validation: Scenario 2 Cylindrical Bending

4.3.1 Introduction and Modeling

After exploring the plate theory behind Abaqus in the previous section, a cylindrical bending problem was investigated. The cylindrical bending problem involved creating a laminated composite plate model under a static, uniform pressure loading in Abaqus. In a later section of this chapter, a similar composite plate will be modeled to investigate snap-through using dynamic analysis. Thus, this section will serve as a form of validation for the laminated composite plate model with a static analysis before advancing to dynamic analyses that are implemented later.

The Abaqus finite element plate model was created to reproduce a previous model created using an in-house finite element code by Kim [5]. The in-house model used bilinear interpolation functions with 4-node, fully integrated elements to model a long, rectangular plate. In Abaqus, an identical model was created using 4-node, fully integrated shell elements. Full-integration and reduced-integration 4-node shell elements were tested, along with 8-node reduced-integration shell elements to be compared with the analytical results. Both the in-house model and the Abaqus model used the same plate dimensions, material properties, and loading. The rectangular plate of interest is illustrated in Figure 4.5. A detailed description of how a laminated composite plate is modeled in Abaqus is provided in Chapter 3 Section 3.3.2. The plate was modeled with a length along the x-axis of 635.0 mm, and a width along the y-axis of 228.6 mm. The plate was a 4-ply laminae with a total thickness of 0.72 mm. Each ply was 0.18 mm thick and oriented at 45 degrees from the x-axis ($[45]_4$ composite layup). The ply stack orientation is depicted in Figure 4.6.

The plies were modeled as plain-weave prepreg, T800H-6K/3900-2, which contains the material properties provided in Table 4.1. The plate edges parallel to the x-axis were clamped on both edges (resisting rotation and translation) while the plate edges parallel to the y-axis were left free to deform, as shown in Figure 4.5. Both the in-house and Abaqus model adopted an element size of 11.43 x 12.70 mm to create a 1000 element, 1071 node mesh.

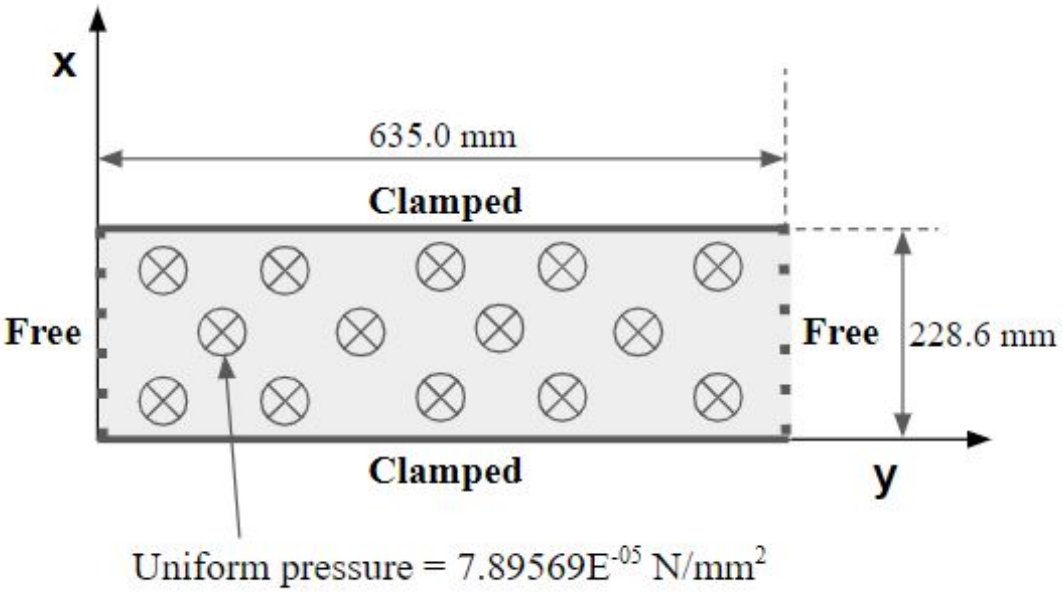

Figure 4.5: Cylindrical bending test geometry, boundary conditions, and loading (plan view)

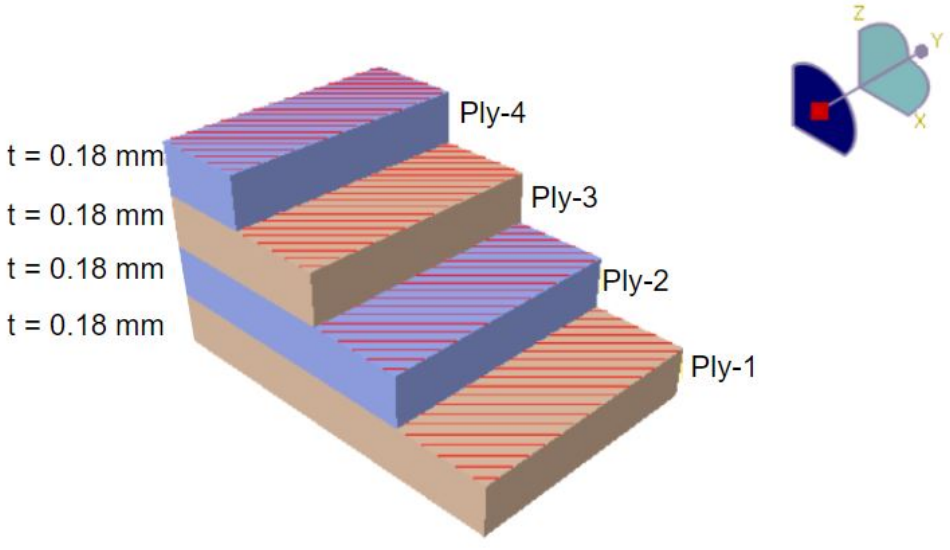

Figure 4.6: Abaqus model composite laminae ply orientation.

Table 4.1: T800H-6K/3900-2 Material Properties

Property	Value	units
E1/E2	75900	Pa
v12	0.037	
G12	3960	Pa
G13/G23	3320.6	Pa

This mesh resolution was chosen as it is used in the later dynamic analyses and allows for lower computational time while retaining accuracy, as well as also matching Kim's in-house finite element model's mesh size. The rectangular plate was subjected to a static, uniform pressure of 7.89569E-05 MPa causing the plate to deform into a cylindrical shape. A linear static analysis was performed in Abaqus, as no large deformations were expected. For the detailed steps of modeling a laminated composite in Abaqus, see Chapter 3 Section 3.3.2.

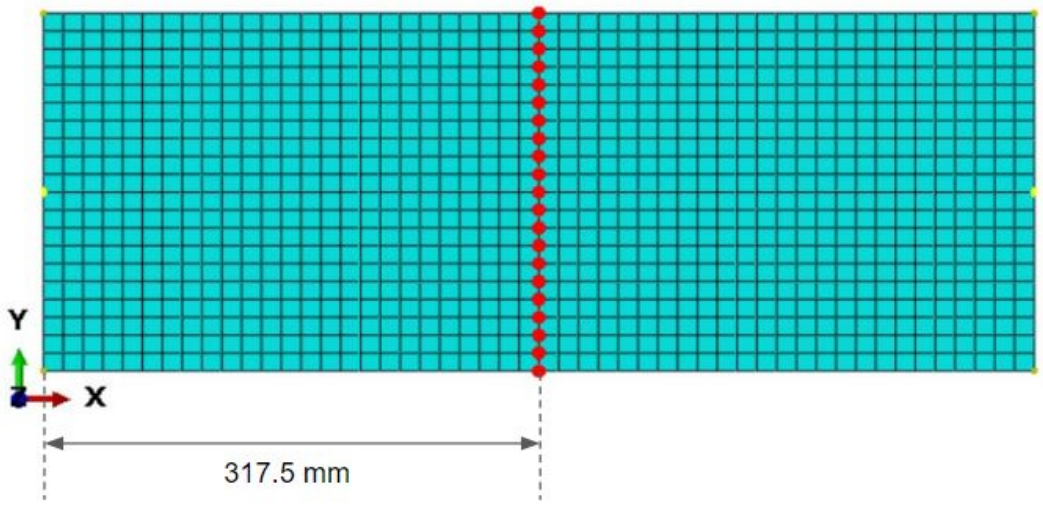

Figure 4.7: Midsection displacement results location.

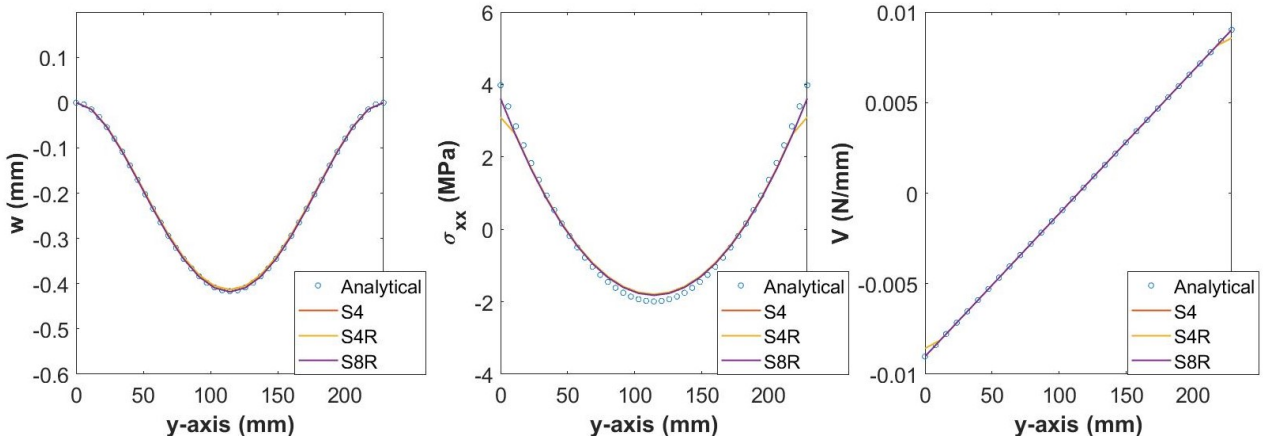

Figure 4.8: Cylindrical bending results across midsection, a) transverse displacement, b) axial stress σ_{xx}, c) transverse shear force along the plate width. See Figure 4.7 for plate location of these results.

4.3.2 Cylindrical Bending Results

After modeling the rectangular plate in Abaqus the displacement results were first compared with the analytical predicted results. The displacements are reported at the midsection of the plates, at x = 317.5 mm, as illustrated by Figure 4.7. Along this section of the plate, the Abaqus transverse displacements for 4-node full-integration (S4), 4-node reduced-integration (S4R), and 8-node reduced-integration (S8R) shell elements were compared with the analytical transverse displacements. These results are found in Figure 4.8a, where the displacements of all element types are proven to match with the analytical displacement very closely. The in-plane normal stress, σ_{xx}, was also plotted along the midsection of the plate for all cases. Figure 4.8c depicts these results, where all Abaqus element types appear to match the expected result quite closely. It should be noted that element types S4 and S4R exhibit a small inaccuracy in the stress results at the clamped boundary conditions while S8R elements match more closely. The transverse shear force along the plate width Abaqus results also appear to match the analytical values closely for all element types. Again, the 4-node element types exhibit a small inaccuracy in the shear force results at the clamped

boundary. Overall, the laminated composite plate created in Abaqus yields the expected results for a clamped plate under a static, uniform pressure load. This validates the Abaqus static analysis plate model.

4.3.3 Cylindrical Bending Static Analysis Discussion

Exploring the cylindrical bending problem allowed for verification in Abaqus modeling of laminated composites using static analysis. Agreement between analytical and finite element results validates the Abaqus composite plate model. Altering shell element types from 4-node full integration and reduced integration, to 8-node elements showed small improvements in results, primarily at the plate edges for stress calculations. Although various element types were explored, the remaining portions of this work will utilize S4 element types (4-node shells) to match Kim's previous in-house finite element code for comparison purposes. Additionally, error near supports found in the cylindrical bending problem results for stress motivated the decision to omit analysis of stresses near supports in the remaining portion of this thesis. The next section will advance to analyzing laminated composite plates using dynamic analysis to investigate snap-through.

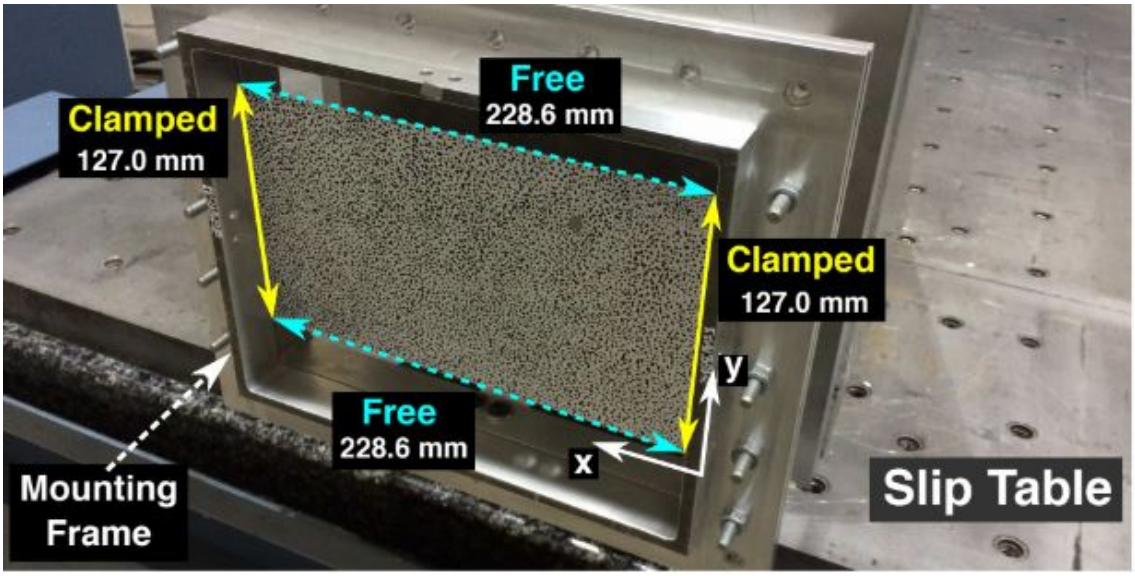

Figure 4.9: Experimental composite plate shaker setup. Reproduced from Kim [5]

4.4 Nonlinear Model Validation Using the Snap-through Boundary

4.4.1 Introduction

The previous section validated an Abaqus laminated composite plate model using a static analysis of a cylindrical bending problem. This section, a study of dynamic snap-through of composite plates is considered. This section will validate an Abaqus dynamic model by reproducing the results of an in-house finite element dynamic model that was based on an experiment. Previous work identified different dynamic snap-through behaviors with changing the dynamic forcing parameters (amplitude and frequency) on a post-buckled composite plate. Kim's previous research included experimental work of mechanically buckling a laminated composite plate and subjecting the buckled plate to dynamic loading. This was accomplished by subjecting the plate specimen to various accelerations using a shaker system while monitoring the plate displacements using digital image correlation (DIC) cameras [5]. For visualization the composite plate, boundary conditions, and shaker setup from the prior experimental work are provided in Figure 4.9. It was found that altering the forc-

ing amplitude and frequency of the shaker varied the snap-through response types from (1) single-well (2) chaotic snap-through and (3) periodic snap-through. These response types are discussed thoroughly in Chapter 2 Section 2.2. Following this experimental work, Kim developed an in-house finite element code to numerically model the plate behavior and compare the results with the experimental work. From both the experimental and the in-house finite element results, the three different snap-through behaviors were identified in harmonic forcing parameter (HFP) space, where the snap-through type can be predicted based on the forcing amplitude and frequency experienced by the plate. Forcing amplitude is measured in multiples of acceleration due to gravity, i.e., g-level.

Figure 4.10 displays the HFP map generated by Han-Gyu Kim in previous work [5]. This figure will be briefly discussed here, for a more detailed discussion see Chapter 2 Section 2.2. Based on the marker shapes, the three types of snap-through are identified in frequency-amplitude space. Along certain frequencies and high amplitudes the plate is shown to exhibit periodic or chaotic snap-through. These snap-through responses can transition into single-well responses with small alterations in frequency or amplitude and is characterized by small displacements where the plate does not exhibit dynamic snap-through. This section will focus on validating, first, the static buckled shapes, then the dynamic response of the Abaqus model.

4.4.2 Post-buckled Plate Modeling

In order to reproduce the snap-through boundary discussed above, a post-buckled plate was first created in Abaqus to match Kim's in-house finite element model [5]. Following the same material properties and ply layup as previously mentioned in Section 4.3.1 of this chapter, a 228.6 mm x 127.0 mm composite plate was constructed identical Kim's experimental model. The plate consists of two parallel fully clamped edges and two parallel free edges to match the experimental test setup, as shown in Figure 4.11. Again, the plate of interest is modeled as a $[45]_4$ composite, with equal thickness plies totaling to a plate thickness of 0.72 mm. The detailed process for modeling a laminated composite in Abaqus is provided in Chapter

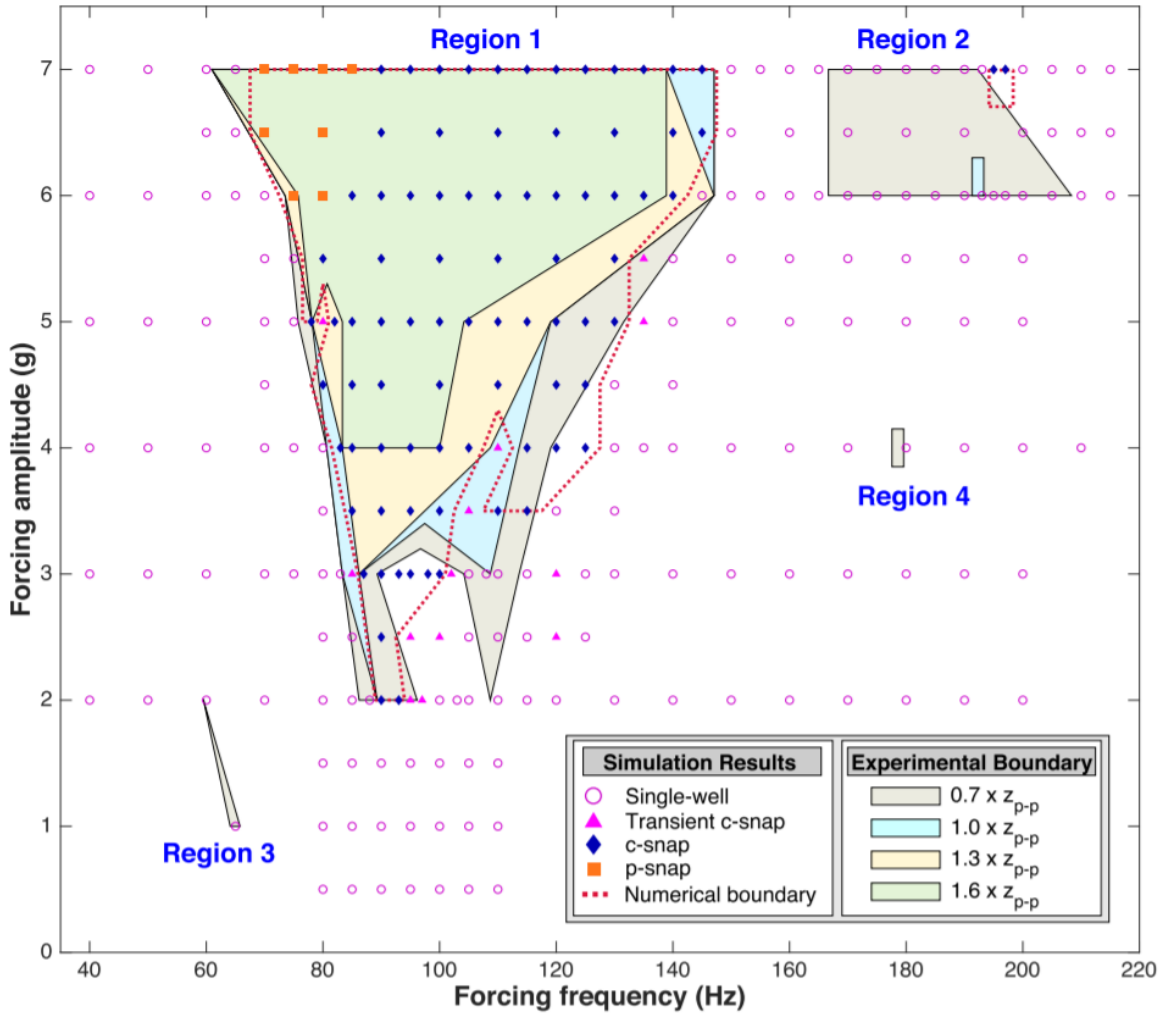

Figure 4.10: Harmonic forcing parameter snap-through boundary map. Reproduced from [5]

3 Section 3.3.2.

The plate model contained a mesh consisting of fully integrated, 4-node shell elements (S4 elements) sized at 11.43 mm x 12.70 mm. This totalled to a mesh containing 200 elements and 231 nodes. This mesh was chosen to match the mesh resolution of previous work, as well as to reduce computational time since finer meshes would result in greater computational expense later during the dynamic analyses. This mesh size was tested for accuracy in the

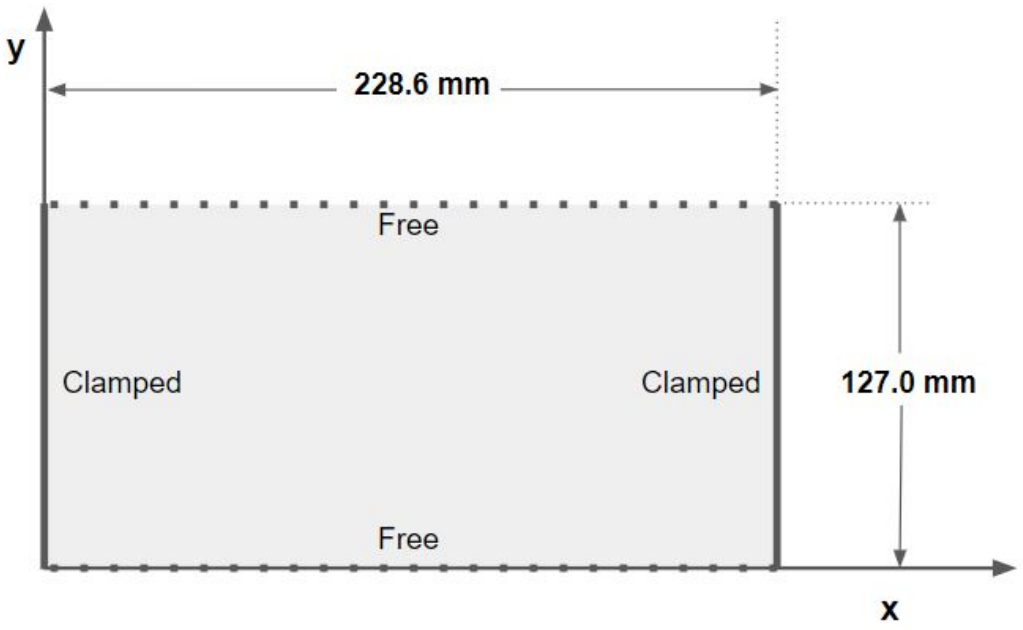

Figure 4.11: Dynamic model plate dimensions and boundary conditions

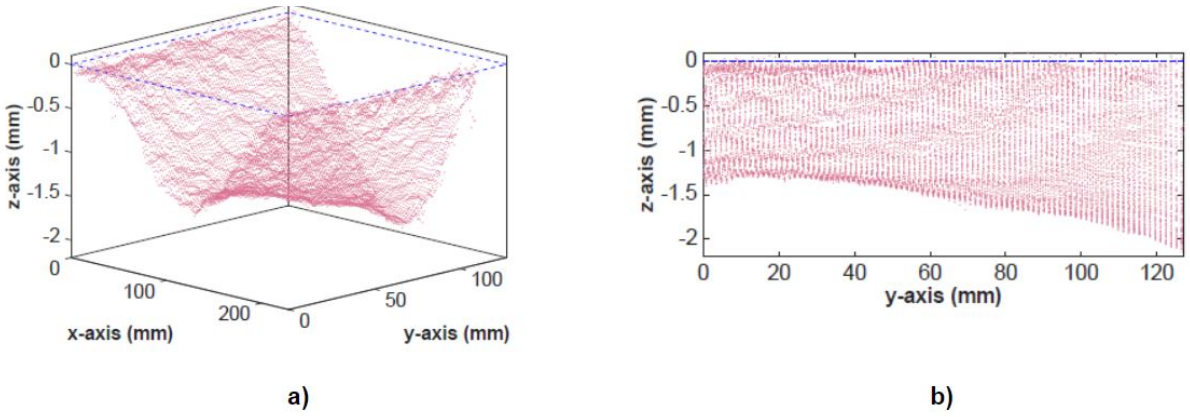

Figure 4.12: Experimental post-buckled plate specimen prior to dynamic analysis a) 3D shape b) asymmetric shape along the y-axis. Figure reproduced from Kim [5]

previous section as it was used in the cylindrical bending problem static analysis and yielded results close to the analytical approximation. The next modeling step involved buckling the composite plate. A detailed description of the modeling process to create a post-buckled composite plate is provided in Chapter 3 Section 3.3.2. However, specific values for loading will be given here. First, the buckling load of the plate was determined using Abaqus. The buckling load was then applied as a shell edge load, and was found as 852.39 N/m. This is close to the value of 852.9 N/m reported in [5]. The composite plate in Kim's work was asymmetrically buckled as shown in Figure 4.12b, where DIC was used to determine the buckled shape of the experimental specimen prior to dynamic forcing. Thus, to match Kim's experimental work and finite element model, the Abaqus plate model was buckled asymmetrically. First, the buckling load of 852.39 N/m was applied uniformly as a static shell edge load to the right edge of the plate. The left plate edge remained fully fixed. To achieve the asymmetric buckled shape, the plate was further buckled with a fixed asymmetric horizontal displacement of the right plate edge, as shown in Figure 4.13. This nonuniform displacement was set larger near the top edge of the plate to create the desired asymmetric buckled shape.

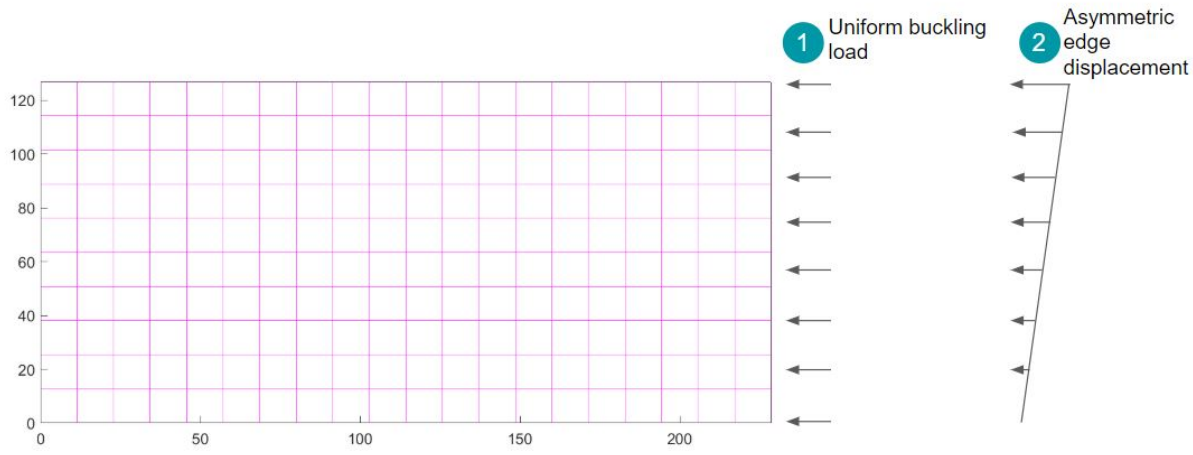

Figure 4.13: Modeling asymmetric plate buckling

The Abaqus plate was buckled to match Kim's model from previous work and possessed a maximum buckled rise of just over 2 mm. Because the objective was to validate the new model using the previously validated model in [6], the post-buckled shape generated using Abaqus was compared to the previous model's buckled shape prior to running any dynamic simulations on the plate. The final Abaqus post-buckled shape is portrayed by Figure 4.14.

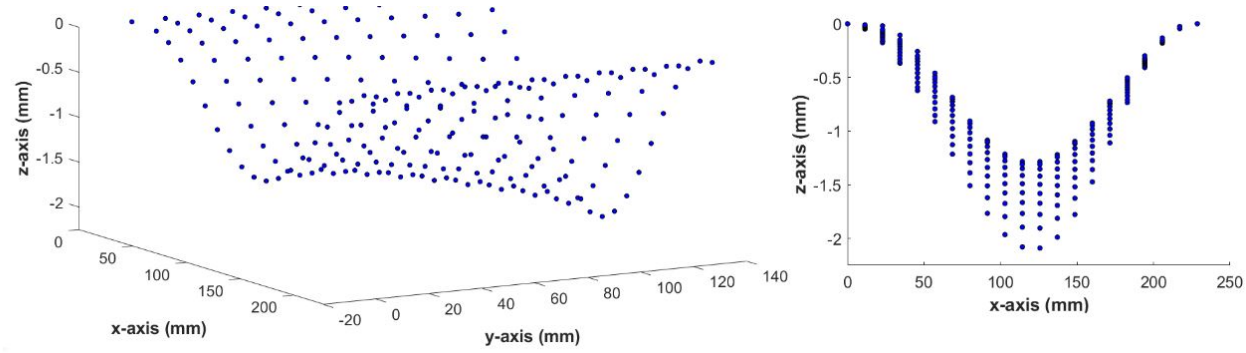

Figure 4.14: Abaqus asymmetric post-buckled shape

To further validate the Abaqus post-buckled plate model, a frequency analysis was performed. The first four mode shapes and natural frequencies of the Abaqus model were compared with the previous in-house model's modes. Results are provided in Table 4.2, showing the natural frequencies closely match for both models with minimum difference in values. The experimental specimen's frequency results are also provided in this table, where "NM" indicates "not measured".

Table 4.2: Abaqus Natural Frequency Comparison

Mode	Experimental (Hz)	In-house model (Hz)	Abaqus (Hz)	Difference
1	113	103.50	103.58	0.08%
2	NM	134.41	134.97	0.42%
3	NM	192.26	193.14	0.46%
4	NM	278.80	279.76	0.34%

Stresses were also compared between the in-house and Abaqus post-buckled plate models. Stress components compared included axial and shear stresses σ_{xx}, σ_{yy}, τ_{xz}, and τ_{yz}. Axial stresses were evaluated at the top and bottom plies, while shear stresses were evaluated at the plate midplane. All stress values were evaluated at the centroid of each element within the plate's mesh and stress fields near the boundaries were disregarded. First, Figure 4.15 shows the axial stresses σ_{xx} at the top of the surface ply for the in-house model and the Abaqus model. As shown in this figure, the in-house and Abaqus models have very close axial stress fields where maximum axial stresses are found at the plate midspan and the boundaries.

Figure 4.16 depicts the transverse shear stress τ_{xz} for the in-house and Abaqus post-buckled plate models. Shear stress is provided along the plate midplane. Again, the results for the in-house and Abaqus models match closely. Maximum stress values for transverse shear stress are shown to occur along the free boundary where $y = 127.0mm$ as this is the location of the maximum buckled depth. Remaining stress fields are provided in Appendix A for reference.

Comparing the buckled shapes, natural frequencies, and stress fields for the in-house finite element model and the Abaqus model showed that both models match very closely. This verified that the Abaqus model is an accurate representation of the experimental plate specimen as well as the in-house model. After confirming this the dynamic analysis is considered

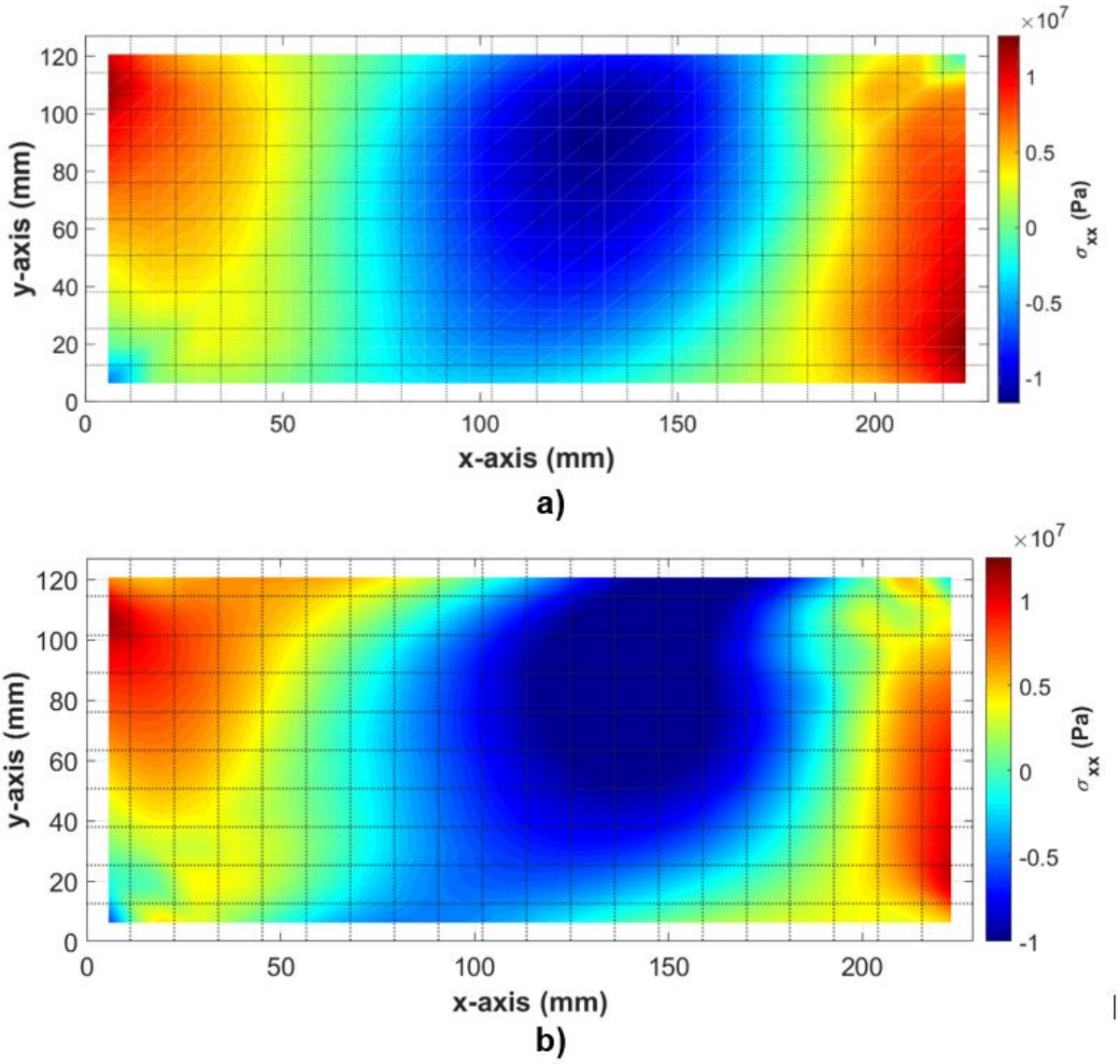

Figure 4.15: In-plane axial stress field σ_{xx} at top surface (z = h/2) for a) in-house post-buckled plate model b) Abaqus post-buckled plate model

in the next section.

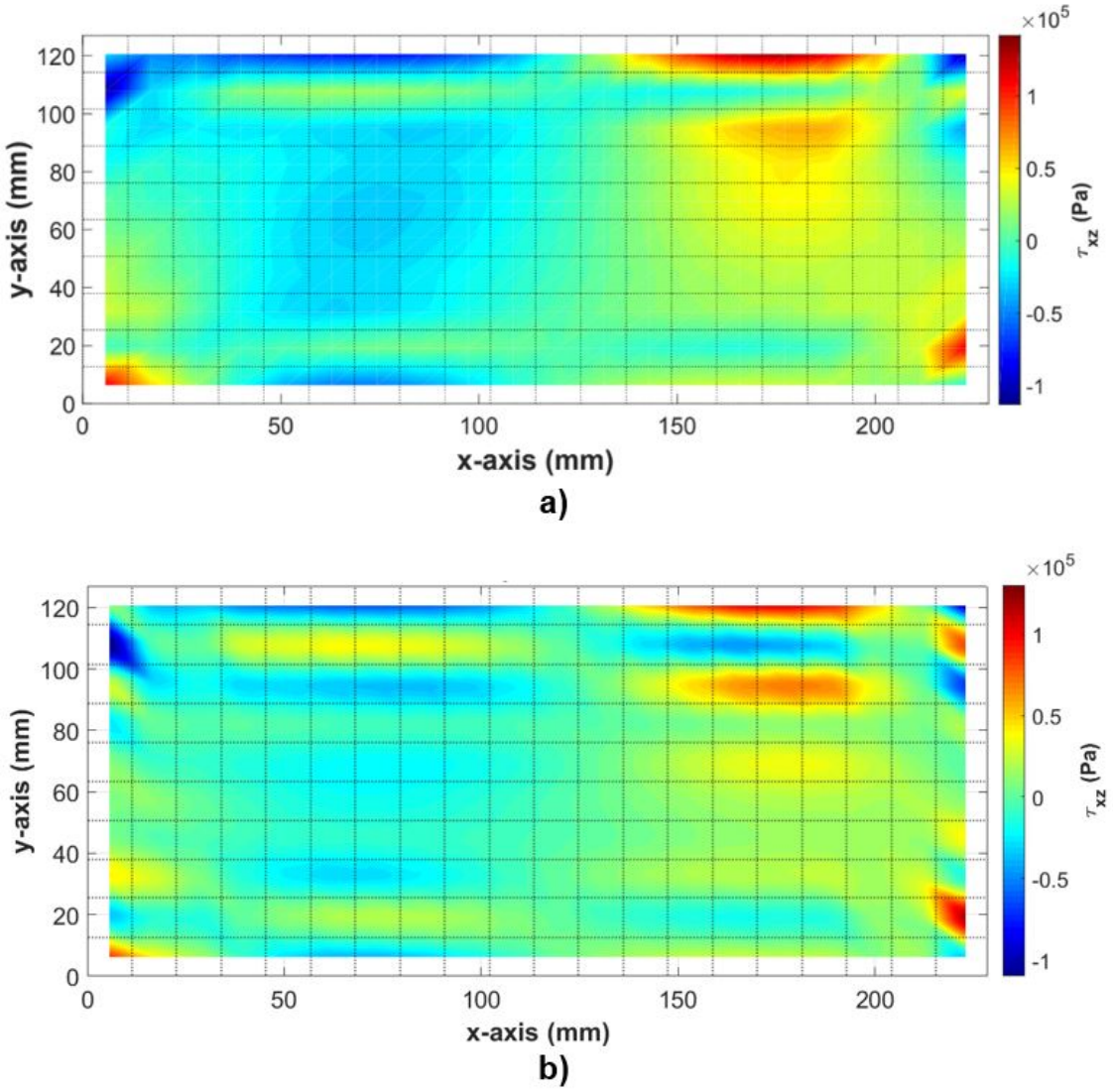

Figure 4.16: Transverse shear stress field σ_{xx} at midplane for a) in-house post-buckled plate model b) Abaqus post-buckled plate model

4.4.3 Dynamic Analysis and Snap-through Modeling

The previous section created and validated the post-buckled laminated composite plate model. This section considers dynamic analysis of this model to investigate snap-through responses. Dynamic analyses on the post-buckled plate model were required to compare

results with the snap-through boundary, ultimately to validate the Abaqus model. Forcing amplitude and frequency were chosen from the HFP map in Figure 4.10 to be applied to the model. Dynamic loads were applied as uniform pressures with a sinusoidal amplitude through time at the chosen forcing frequency. Nonlinear dynamic implicit analyses were implemented and automatic time incrementation was utilized within Abaqus during the dynamic step. A detailed description of creating a dynamic analysis of a post-buckled composite plate is provided in Chapter 3 Section 3.3.4.

To reduce the amount of modeling required, only a portion of the snap-through boundary shown in Figure 4.10 was investigated using Abaqus. The portion of the HFP space analyzed in this work was the left snap-through boundary at around 80 Hz forcing frequency, where single-well responses transition to chaotic and periodic snap-through responses. This included creating Abaqus models for dynamic loading at 7g 60-90Hz, 6g 60-90Hz, 5g 60-80Hz, 4g 70-85Hz, 3g 70-90Hz, 2g 80-90Hz, and 1g 80-90Hz. Although loading is reported in acceleration g's, loading in Abaqus was applied as alternating uniform pressure loads in MPa. The appropriate equivalent pressure loading input into Abaqus is calculated based on plate thickness and density, provided by:

$$q = density \times thickness \times gravity \times g's \tag{4.1}$$

Due to the high computational expense of the dynamic simulations, running many models can become exceptionally time consuming. To overcome this, simulations were run for 1.5 seconds of dynamic analysis. Note that although 1.5 seconds seems breif, this represents over 100 forcing cycles of snap-through responses. If the response type (i.e. single-well, chaotic snap-through, periodic snap-through) was not clear, longer simulation times were implemented to provide more time history data to analyze. The desired outputs of these models primarily consisted of displacement, velocity, and time data, as the snap-through response types can be determined based on identifying dynamic displacement patterns or using phase projections (discussed in Chapter 2 Section 2.2).

4.4.4 Dynamic Analysis and Snap-through Boundary Results

Starting with a 7g forcing amplitude, several dynamic models were created implementing forcing frequencies from 60Hz to 90Hz to the post-buckled plate. Based on the HFP map the 60Hz model is expected to exhibit a single-well response, while the 70Hz and 80Hz models are predicted to experience periodic snap-through at these specific excitation frequencies. Finally, a 90Hz model was created and should result in chaotic snap-through behaviors.

The response types observed from these Abaqus models were compared with the response types reported in the HFP map from Figure 4.10 to determine the validity of the Abaqus models. It is expected that the response types should match. For example, at the loading 4g-60Hz the HFP map reports a single-well response. Thus, at this same loading the Abaqus model should yield a single-well response as well as validation. The Abaqus models matched the expected responses.

The 7g-60Hz model is expected to exhibit a single-well response based on the HFP map. This prediction is verified from the Abaqus results as the mid node displacement is plotted. Figure 4.17a shows that the mid node does not experience large displacements during excitation and there is no snap-through. This is characteristic of the singe-well response. Additionally, a phase projection is plotted using the mid node velocity versus displacement and appears as a small elliptical shape.

The response switches from single-well to periodic snap-through when the forcing frequency is increased to 70Hz. The periodic snap-through (p-snap) response consists of large dynamic displacements as shown in Figure 4.18. It is also noted that with the increase in displacement magnitudes, the phase projection grows. As the snap-through is very periodic the projection appears as a single elliptical slightly less orderly compared to the single-well response.

As the forcing frequency is increased further to 90Hz, the response shifts from periodic to chaotic snap-through (c-snap). Similar to p-snap, the c-snap response exhibits large deformations accompanied by dynamic snap-through, however, the response is less predictable.

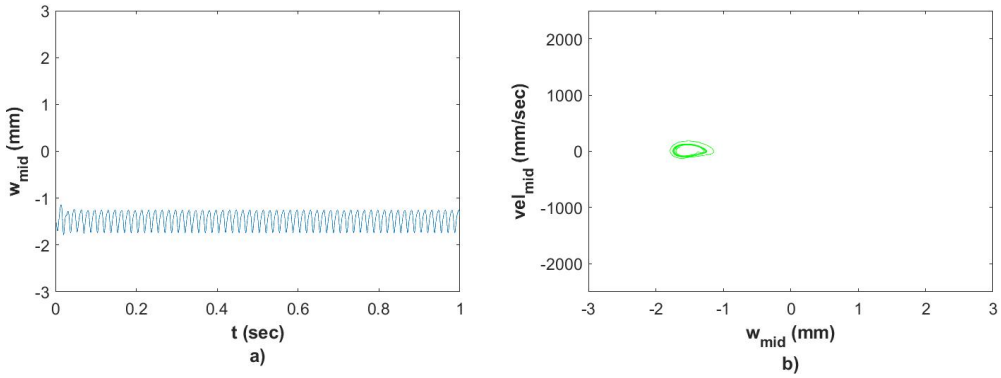

Figure 4.17: Responses for post-buckled plate dynamically excited at 7g-60Hz a) single-well displacement response b) single-well velocity vs. displacement phase projection

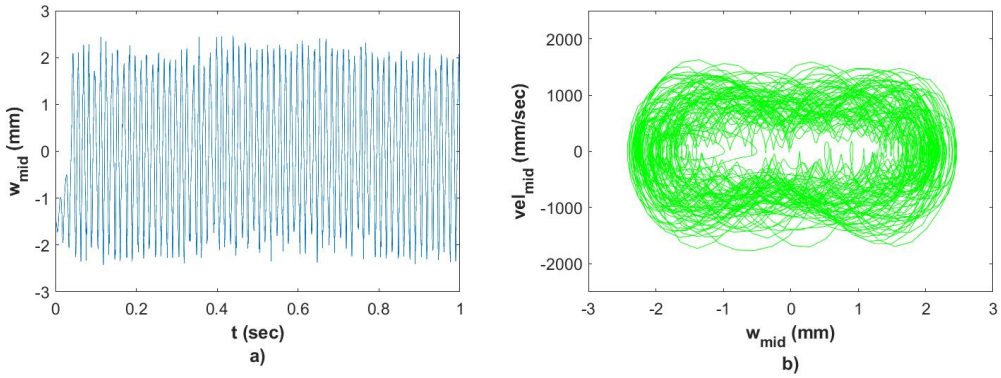

Figure 4.18: Responses for post-buckled plate dynamically excited at 7g-70Hz a) p-snap displacement response b) p-snap velocity vs. displacement phase projection

The response for 7g-90Hz excitation is provided by Figure 4.19. The displacement shifts from a positive displaced configuration to a negative displaced configuration in a frenzied manner. The c-snap phase projection shown by Figure 4.19b portrays an elliptical shape, with two internal orbits as the plate oscillates from one potential configuration to the other. This phase projection is the most chaotic in comparison to the p-snap and single-well responses.

The responses presented for 7g 60-90Hz matched the predicted responses from the HFP map developed by previous work. Simulations at 1g through 6g were also created and

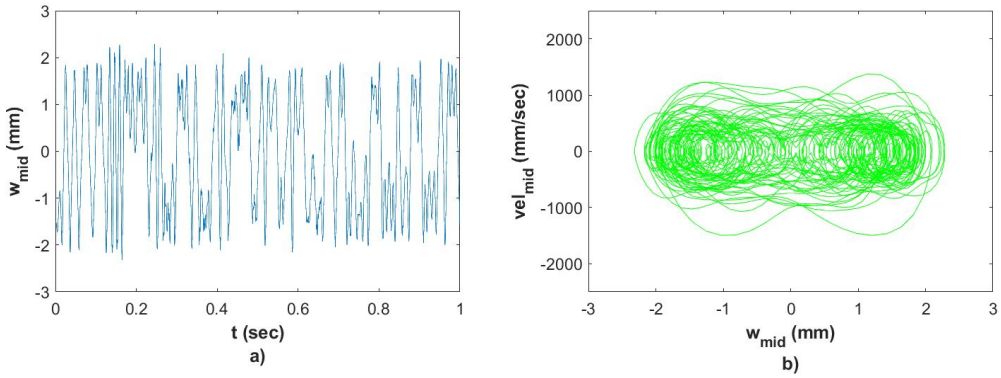

Figure 4.19: Responses for post-buckled plate dynamically excited at 7g-90Hz a) c-snap displacement response b) c-snap velocity vs. displacement phase projection

analyzed to determine the snap-through response types to be compared with the HFP map results. These responses will not be provided here however all response types were found to match the responses expected based on previous work, effectively validating the dynamic Abaqus model.

Transient Dynamic Responses

In Kim's previous work, it was found that at certain forcing parameters the model exhibited transient snap-through responses [5]. These same phenomena were found from the Abaqus model results. At 7g loading around 90Hz, previous work found that transitions between c-snap and p-snap behaviors were observed. Specifically, the in-house model started with c-snap and switched to p-snap at around 0.7 seconds into the simulation. This same occurrence was noted with the Abaqus model results, however this occurred at 80Hz excitation, where c-snap transitioned into p-snap at around 0.5 seconds into the model. Figure 4.20 shows the displacement over time for the Abaqus model to illustrate. The displacement begins with c-snap, where snap-through is irregular, then switches to p-snap where snap-through is nearly periodic. This is very similar to the results reported by Kim and is worth noting.

A similar manifestation was reported by Kim at the 6g loading case at the interface of

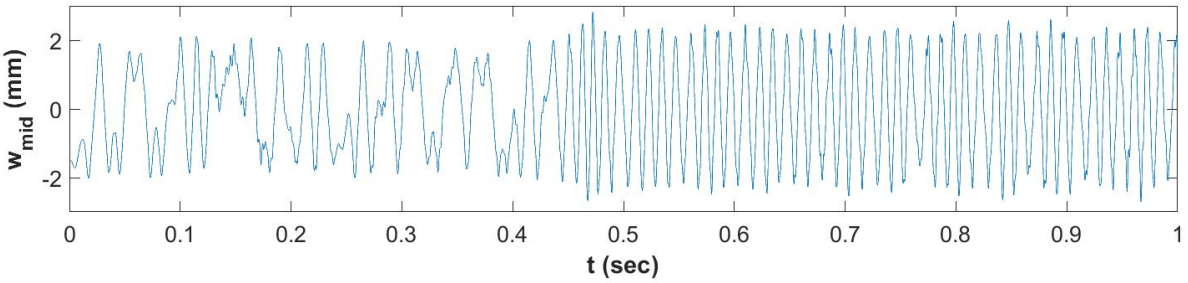

Figure 4.20: Displacement response for post-buckled plate dynamically excited at 7g-80Hz. Response begins with c-snap and switches to p-snap at around 0.5 seconds.

80Hz forcing frequency. The Abaqus model displayed this transition between c-snap and p-snap responses again at 6g-80Hz loading. The in-house and Abaqus models both exhibited these specific details in transient response types at identical frequency and amplitude ranges, augmenting confidence in both models.

4.4.5 Snap-through Analysis Discussion

Numerous dynamic simulations in Abaqus were analyzed along the left snap-through boundary within the HFP map to validate the Abaqus model. The snap-through response types for each Abaqus simulation were compared with the HFP map predicted response. All Abaqus models successfully matched the expected response types. The Abaqus simulations that were analyzed are provided in Figure 4.21. From this figure it is clear that all Abaqus simulations yielded snap-through responses which matched the responses expected from the HFP map created from a previous in-house numerical model. This section serves as validation to this model which is highly valuable as snap-through is a difficult problem to explore.

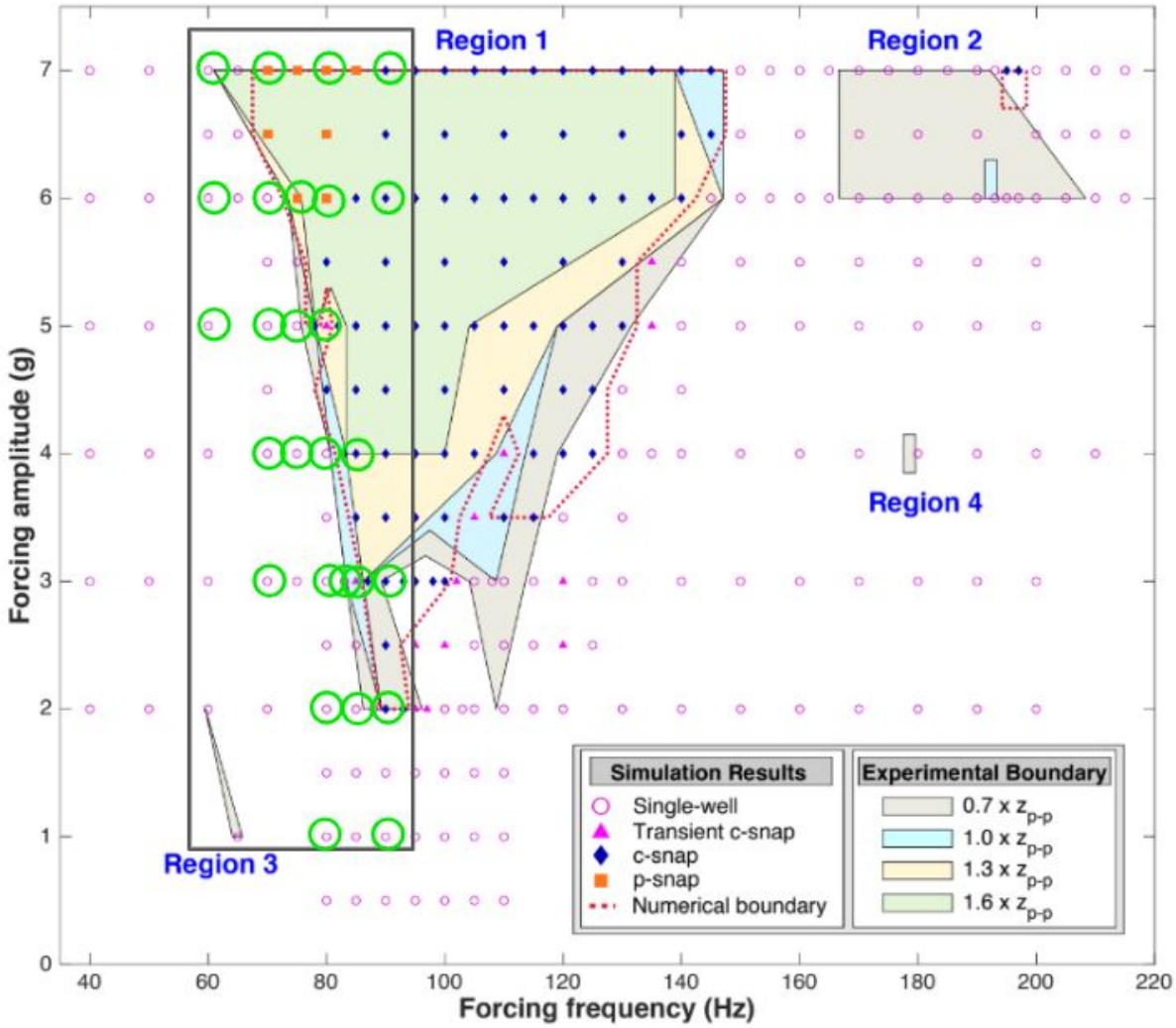

Figure 4.21: Abaqus simulations plotted with the HFP map. Green circle markers depict Abaqus simulations that matched the expected response type. All Abaqus results aligned to the predicted HFP map response.

4.5 Chapter Conclusion

This chapter validated several Abaqus plate models. To begin, a parametric plate study was performed that compared displacement results from both Abaqus and analytical calculations. This explored the theory behind modeling plates in Abaqus and validated the isotropic thin

plate model. Next, a cylindrical bending problem was investigated for a laminated composite plate. Again, the Abaqus results were compared with analytical results. This validated the composite plate model using static analysis before advancing to dynamic analysis. Finally, the snap-through boundary from previous work is used to validate the Abaqus dynamic model. With successful composite plate modelling from this chapter, the next chapter will advance the understanding of snap-through by investigating static and dynamic analyses of this phenomenon.

Chapter 5

STRESS FIELD CHARACTERIZATION AND EXPLORATION OF STATIC REDUCTION

5.1 Chapter Overview

Previous work primarily focused on characterizing the harmonic forcing parameter boundaries for dynamic snap-through responses of a laminated composite plate undergoing harmonic loading. As aforementioned in Chapter 4, the Abaqus dynamic finite element results for this model matched very closely to the experimental data. This shows that the model is accurate, however, the dynamic model is slow and even seconds of simulation results require hours of computation time. Thus, this chapter will investigate the hypothesis that static models can be used to capture the stresses seen during extreme dynamic behaviors like snap-through. This extension of work will compare the dynamic snap-through responses with static responses using Abaqus modeling.

To the author's knowledge, not much work has been done to determine to the extent at which static stresses deviate from dynamic stresses for snap-through. This chapter will explore how displacement and stresses compare for dynamic and static responses of snap-through of a laminated composite plate under harmonic loading. To address this, identical post-buckled composite plate models will be analyzed using two different analysis types in Abaqus: (1) a static analysis and (2) a dynamic implicit analysis. In both analyses, the post-buckled plate will be subjected to a transverse uniform pressure loading to cause snap-through. This chapter will focus on periodic snap-through results, as previous work has shown that periodic snap-through is attributed with higher stresses, deeming it as a "worst case" response when compared to chaotic snap-through or single-well responses. After performing both static and dynamic analyses, the resulting stress and displacement magnitudes

will be compared to characterize the different stress magnitudes given static versus dynamic analyses. The stresses within the plate spatially and temporally can become very complex, therefore, the primary stresses of interest which will be analyzed most thoroughly are in-plane axial and transverse shear stresses, σ_{xx} and τ_{xz} respectively.

5.2 Static Snap-through Modeling

In order to compare static snap-through to dynamic snap-through responses, first static snap-through finite element models of the composite plate were created. The static snap-through model is a finite element model of a post-buckled plate to which static, transverse pressure loading sufficient to induce buckling is applied. Creating the static snap-through model involved two distinct steps: (1) creating a post-buckled plate by applying axial loading (2) inducing static snap-through to the post-buckled plate by applying a transverse load sufficient to induce transverse buckling. The general modeling process of creating a static snap-through plate model has been discussed thoroughly in Chapter 3, Section 3.3.5. However, further details and plate dimensions will be provided here in this section.

The structure of interest is a laminated composite plate with the same material properties and ply layup as the composite plate modeled in Chapter 4 (see Chapter 4 Section 4.3.1. for material properties). The plate length and width dimensions were 228.6 x 127.0 mm. These plate dimensions are similar to the dimensions from Chapter 4 for the snap-through boundary study. The dimensions are slightly altered for this example in order to simplify the model to a symmetrically-buckled plate. In Chapter 4, the post-buckled plate model was buckled asymmetrically as a non-uniform shell edge load was applied, buckling the plate to a higher buckled rise on one free edge compared to the other free edge. This was done to match with experimental results, which were imperfect. This chapter will focus on a plate that is buckled with a uniform shell edge load, creating a symmetrically buckled plate. Beginning with a flat plate, the Abaqus plate model was then buckled using a uniform edge load of 0.86 N/mm along the right edge of the plate. A more detailed process for creating a buckled plate in Abaqus is provided in Chapter 3 Section 3.3.3. After buckling, the buckled rise of the

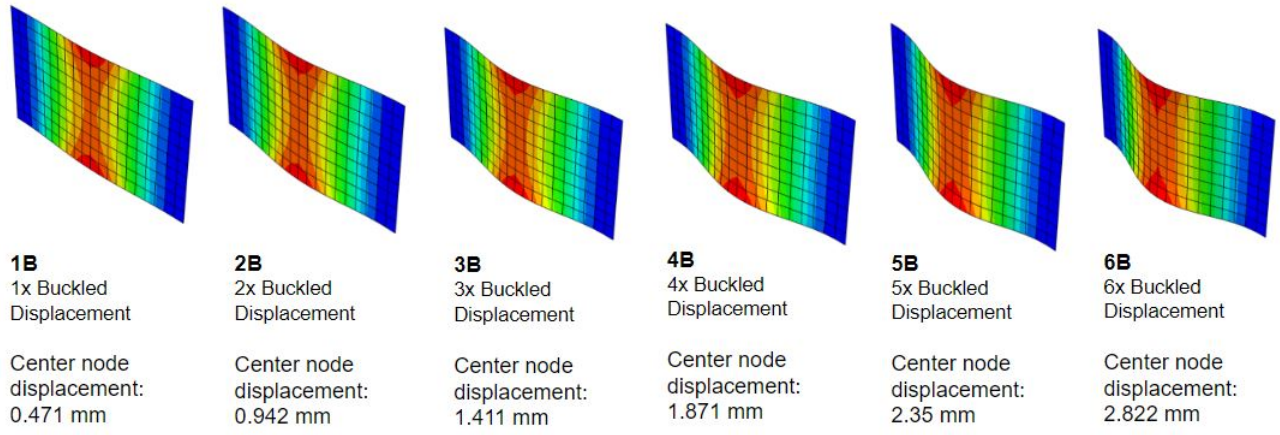

Figure 5.1: Buckled rises with equivalent given names and center node displacements

midnode of this plate was 0.471 mm. To observe the effect of buckled rise depth on stress results, five additional post-buckled plate models were created with deeper buckled rises. These five additional models were created by further buckling the plate to two times this buckled rise, then three times this buckled rise, then four, and so on. In total, six different buckled rise models were created. To eliminate confusion throughout this chapter, we will refer the first buckled rise of 0.471 mm as 1B, then the plate with two times the buckled rise (a rise of 0.942 mm) as 2B, and so on. Figure 5.1 illustrates the buckled rises with their equivalent given names which will be used throughout this chapter.

Each plate with a unique buckled rise is considered to be an individual structure. After developing all six different buckled structures, the plates were subjected to transverse, uniform pressure loading to initiate snap-through. This process consists of clamping two plate edges and then applying a static, transverse pressure load to the plate surface that is sufficient to cause transverse buckling. This static snap-through analysis involves applying a uniform pressure load to the top surface of each 1B-6B plate, forcing the plates to deflect from a positive to a negative deflection (snap-through). A demonstration of the typical static snap-through behavior is shown in Figure 5.2.

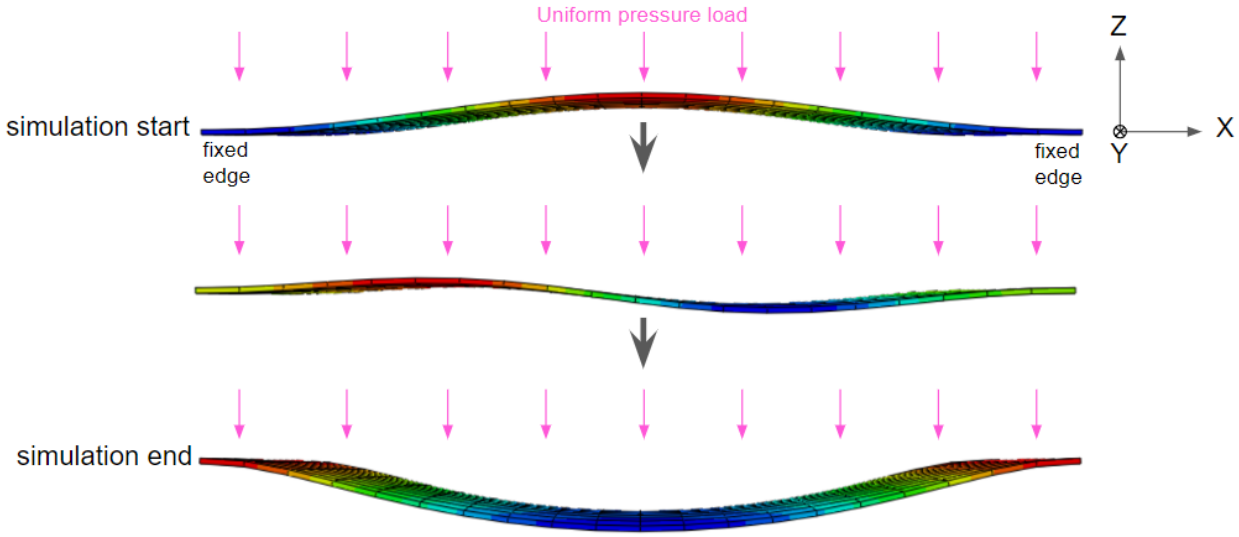

Figure 5.2: Displacement example of 3B buckled plate undergoing snap-through from uniform pressure loading during a static analysis

5.3 Static Snap-through Results

5.3.1 Static Analysis Force and Displacement

Results were analyzed after performing the static snap-through analyses on all six structures from the previous section. Later the static simulation results will be compared with the dynamic simulation results. First, the static force-displacement plots were created from Abaqus output using the applied pressure load versus the displacement at the plate midspan (midnode). The midnode location is provided in Figure 5.3. The force-displacement plots provide information regarding the static snap-through behavior of the plates and validate that the captured response is correct. It is expected that the force-displacement curve is mostly symmetric about the x-axis. Figure 5.4 provides the force-displacement curve for the 1B buckled structure. Applied pressure loading is reported in MPa, displacements are reported in mm. The figure shows that at point one (at the start of the simulation), the center node displacement of 1B is shown as 0.47 mm, because no displacement from the

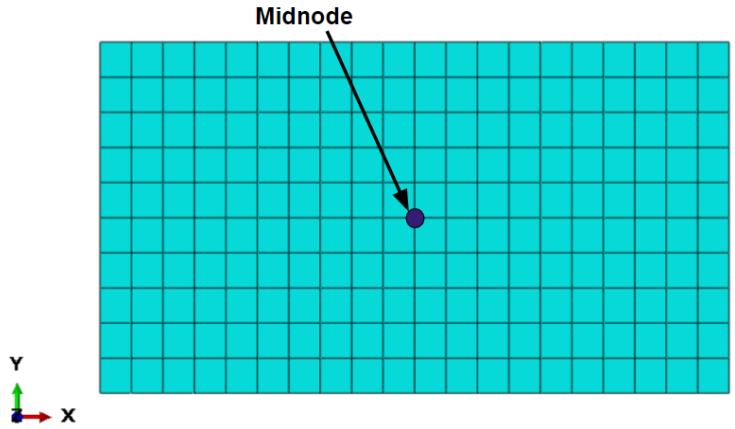

Figure 5.3: Midnode location on Abaqus plate model.

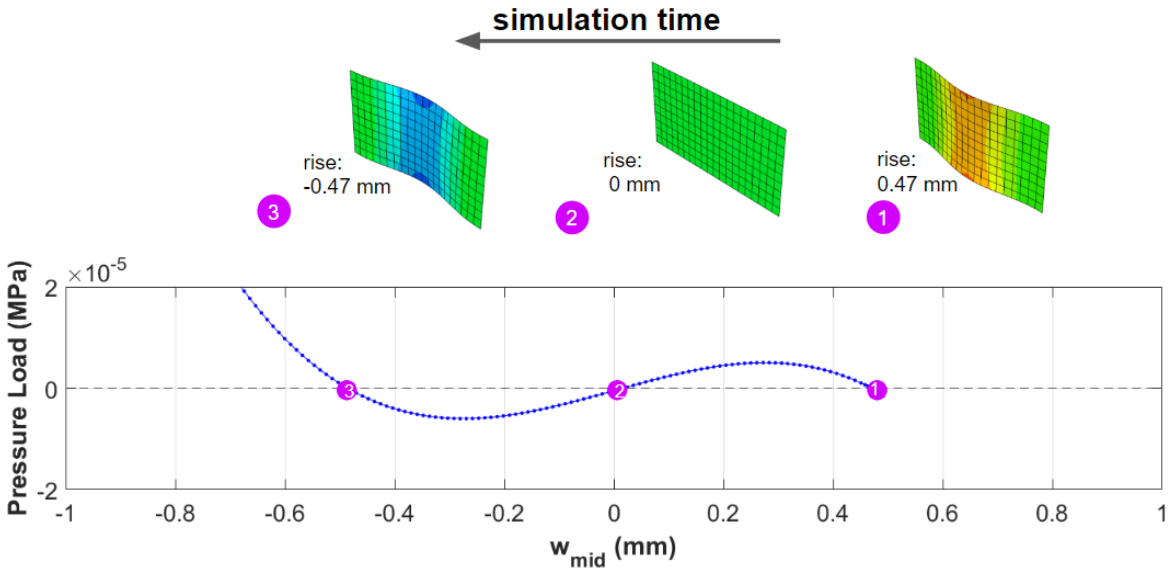

Figure 5.4: 1B force-displacement curve with displacement measured at the plate midnode. 1-3 markings report plate configurations at specified locations along the curve.

initial configuration has occurred yet. Midway through snap-through (point 2), the plate displacement is 0 mm as the structure is forced back to a flat position from its initial buckled rise. Next, as the loading changes the plate is forced to a displacement of -0.47 mm (point 3). Note that at point 2 in Figure 5.4 the plate's configuration appears completely flat. This is possible for post-buckled plates with small buckled rises, as is the case for this figure. For deeper buckled rises, the plate configuration at $w_{mid} = 0$ mm may not appear symmetric and flat and instead may appear as an asymmetric shape similar to the plate in Figure 5.2.

Further analyzing the force-displacement plot in Figure 5.4, the curve reaches the x-axis at three instances which are denoted as 1-3 points in the plot. The unloaded starting point is marked by point 1. As the analysis progresses, the load is scaled by a single parameter, and is shown to increase up to a local maximum while displacement decreases. As the applied load is continually scaled, the load begins to decrease and crosses 0 MPa at a 0 mm displacement. This point is marked as point 2 in Figure 5.4, where the plate is relatively flat (due to a shallow buckled rise). Following this the load decreases, until hitting a local minimum, then it begins to increase with decreasing displacement. Finally, the curve crosses the x-axis again at point 3 with a displacement around -0.47 mm and the plate assumes a configuration that is the mirror image of its initial shape. This pattern is seen with all structures, 1B-6B. Figure 5.5 shows the force-displacement curves for all six structures with varying buckled rises. As the buckled rise deepens, a greater applied pressure load is required to achieve snap-through. With increasing buckled rise, the force-displacement curves develop sharper transitions from local maximum to local minimums.

5.3.2 Axial Stress

The stresses within the plate both spatially and temporally can become very complex to analyze when dealing with hundreds of increments throughout a simulation. For this reason, the primary stresses that will be analyzed in this chapter are axial and shear stresses. This section will focus on axial stress results for static snap-through. Stresses will be analyzed at the midplane of the composite plates. It would be increasingly time consuming to analyze

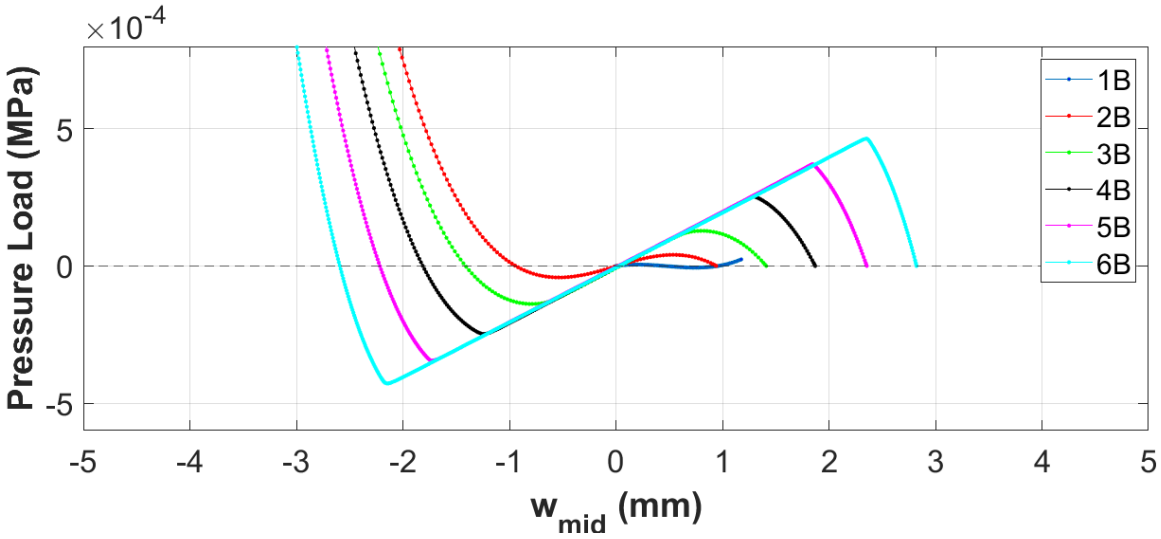

Figure 5.5: Force-displacement curves for varying buckled rises 1B-6B

the stress time history at every single point along the plate midplane. Therefore, to begin, the maximum in-plane axial stress σ_{xx} values along the plate midplane were plotted in a contour plot. Figure 5.6 displays the contour plots for static snap-through of the 5B structure containing the maximum tensile and compressive axial stresses found throughout the simulation. Note that Figure 5.6 applies to the 5B structure. For the remainder of

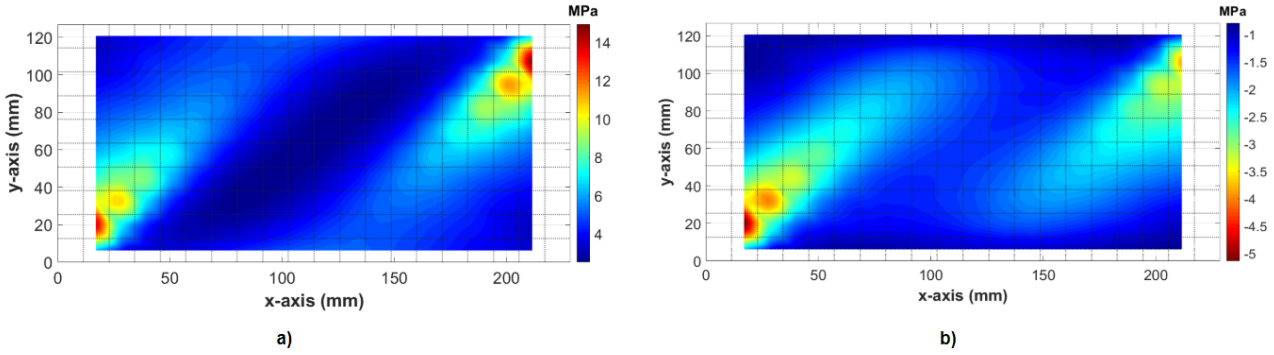

Figure 5.6: Maximum tensile (a) and compressive (b) in-plane axial stresses σ_{xx} at plate midplane for static snap-through of 5B structure

this chapter, the 5B structure is of focus to simplify the presented results and discussion as the other buckled rise levels behaved similarly. From the figure, the contours show that maximum in-plane axial stress values occur near the plate edges. Additionally, the stresses are larger near opposite corners. This is associated to the composite layup, where the fiber direction is oriented 45 degrees from the x-axis. These contour results are important for a later section, where these static results will be compared with dynamic results.

Above, contour plots of maximum stress values were generated for axial stress. Although these plots provide a general idea of where maximum stresses are found on the plate midplane, the contour results do not show information of points at each increment in the simulation. Analyzing these axial stresses through many simulation increments at every point on the plate would be rather time consuming. Thus, axial stress σ_{xx} was analyzed only at the midnode of the plate. This location was chosen simply for comparison purposes; the stress history at midnode of the plate will also be analyzed for the dynamic simulations as well, then the static and dynamic simulation results will be compared. To start, the center node axial stresses were extracted from Abaqus, then plotted over increments throughout the entire simulation. For all buckled rises, the in-plane axial stress σ_{xx} at the center node decreased and then remained relatively constant until increasing again after the plate had snapped through. Figure 5.7 portrays the trend of axial stress throughout the static simulations for each of the six structures. It is shown that the axial stress σ_{xx} follows the same trend with increasing depth of buckled rise. With a deeper rise, the maximum axial stress during snap-through increases. Because results follow a similar trend for all plate buckled rise depths, stresses for only the 5B plate will be analyzed for the remainder of this chapter.

5.3.3 Shear Stress

The previous section examined in-plane axial stress σ_{xx} for static snap-through. Here, transverse shear stress τ_{xz} is analyzed. The shear stress will later be compared with dynamic results. Again, due to the complexity of analyzing stresses both spatially and temporally, the shear stresses were first analyzed by creating contour plots of the maximum stress values

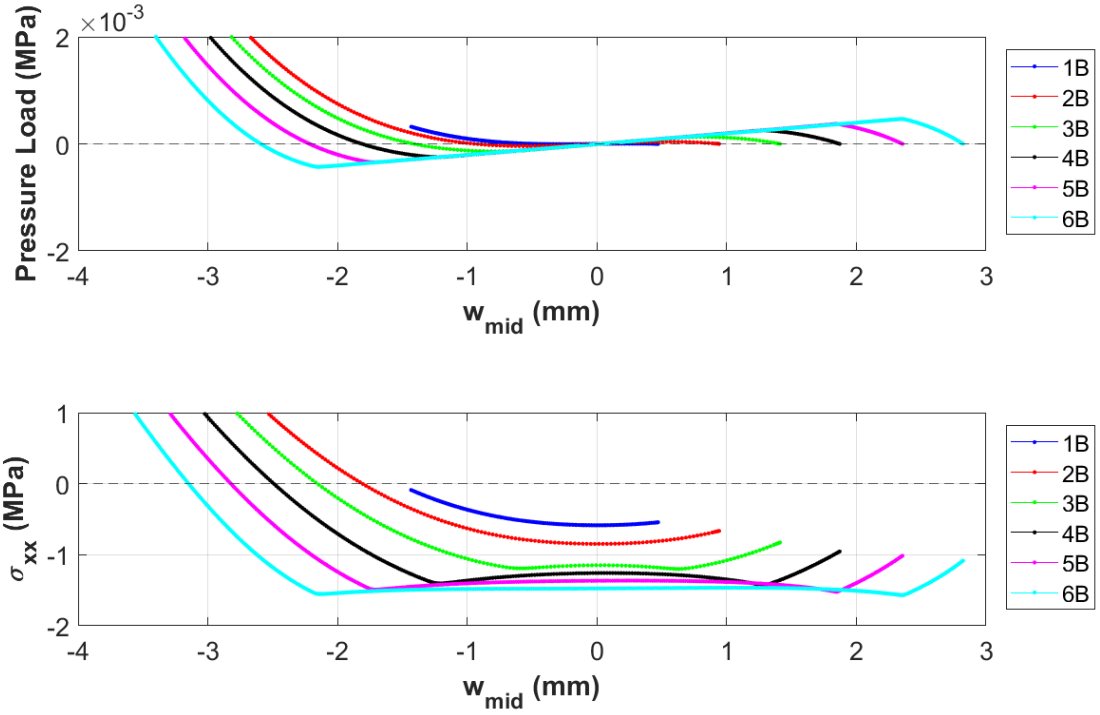

Figure 5.7: Force-displacement curves and center node axial stresses for varying buckled rises 1B-6B

from all stress histories. Figure 5.8 provides this contour plot for the 5B plate for static snap-through. The figure shows that maximum transverse shear stresses are found along the plate edges.

Next, the transverse shear stresses were analyzed at four different locations on the plate to provide further information on the stress response over all increments of the simulation rather than providing only maximum values. Figure 5.9 shows the shear stress values throughout the static simulation at different locations on the plate midplane for the 5B structure. Although the shear stresses appear to be unpredictable, these stress trends are found in all varying buckled rise depths when comparing the 5B model to the other static models. These static shear stress plots will be utilized later in this chapter to compare with dynamic shear stress trends.

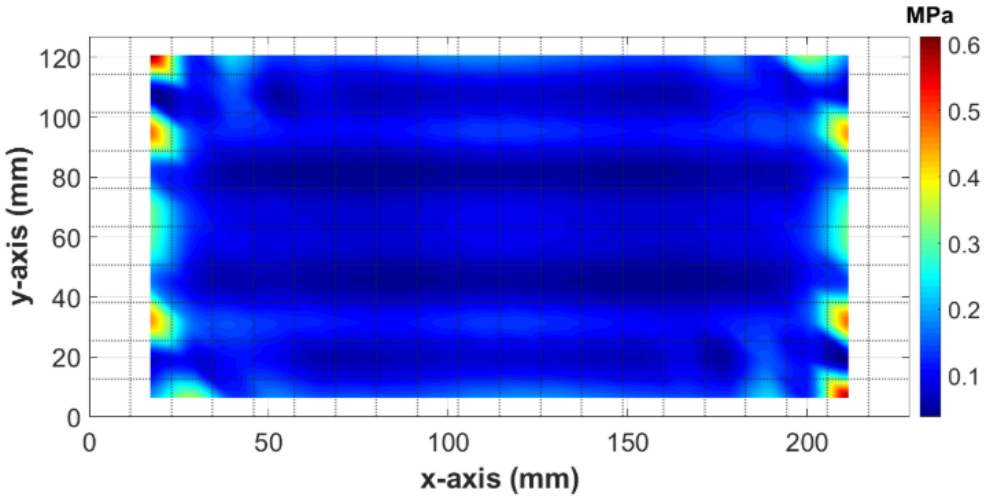

Figure 5.8: Maximum transverse shear stresses τ_{xz} at plate midplane for static snap-through of 5B structure

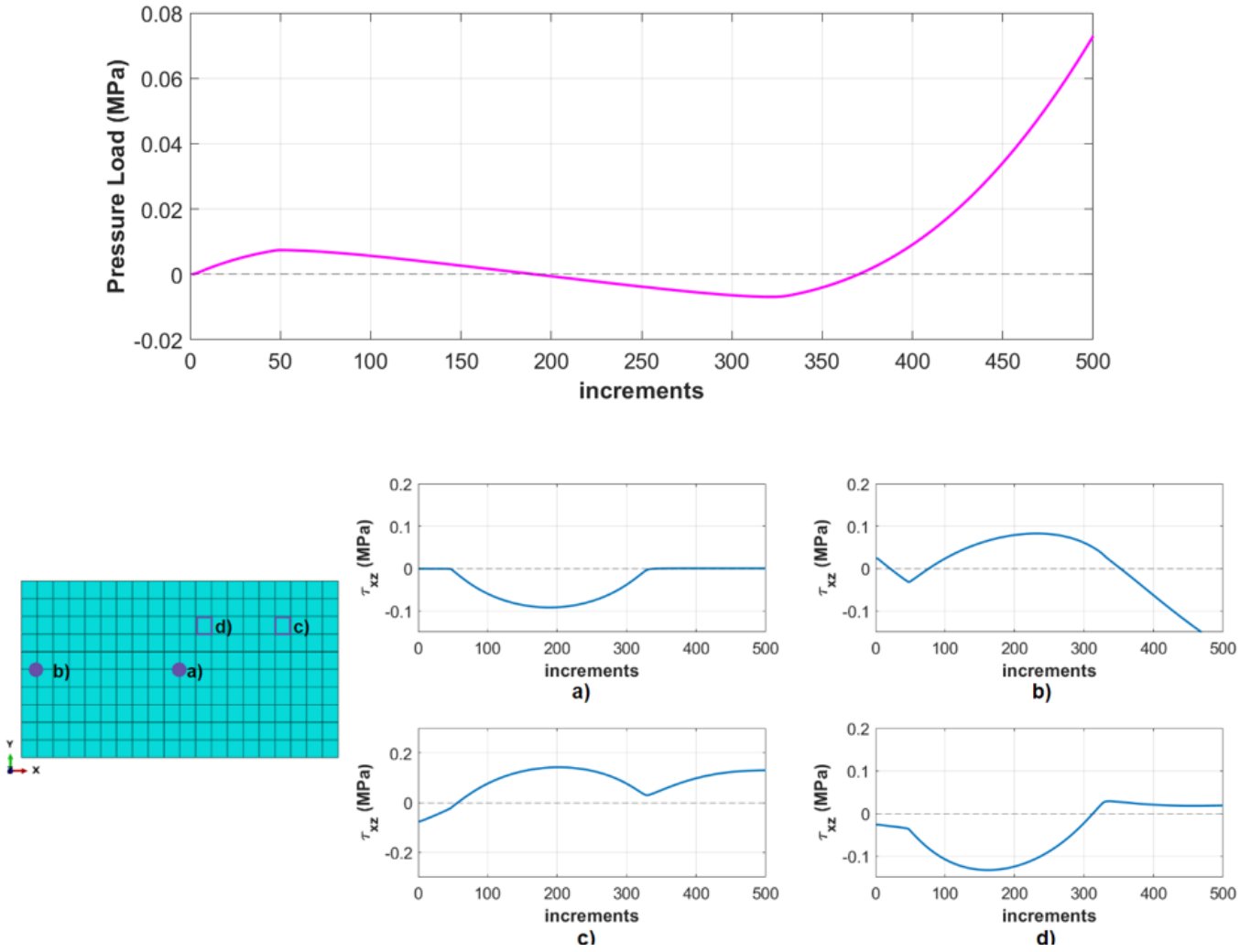

Figure 5.9: Transverse shear stresses at different locations (both nodes and elements) along the 5B plate throughout increments of static snap-through simulation

5.4 Dynamic Snap-through Modeling

5.4.1 Introduction and Modeling

The previous sections discussed modeling and analyzing static snap-through models in Abaqus. This section focuses on creating and analyzing dynamic snap-through models. As previously discussed, the nonlinear dynamics of buckled plates is complicated and previously it was not

expected that the static stresses are useful in a general sense. However, the hypothesis of this chapter is that static snap-through models may predict dynamic snap-through models' stress responses particularly well. This section will focus on the case of dynamic periodic snap-through because in previous studies, periodic snap-through has been attributed to high stresses and is seen as a "worst case" response. To begin investigating the hypothesis of this chapter, the dynamic equivalent of the static snap-through models from the previous section were produced. Identical to the static analysis structures, the same buckled rise models were used as initial structures prior to the dynamic analysis step. For detail on the steps associated with creating these initial buckled plate models, refer to Chapter 3 Section 3.3.3.

Beginning with the six buckled rise structures 1B-6B, dynamic analyses were performed in Abaqus. It is recommended to use a direct-integration, implicit dynamic analysis for nonlinear problems [10]. Automatic time incrementation was utilized within Abaqus within the dynamic step. High forcing amplitudes were transversely applied to achieve periodic snap-through responses. As mentioned in the previous paragraph, periodic snap-through is of interest as it is shown to exhibit larger deformations and stress amplitudes than chaotic snap-through behavior [6]. Throughout all dynamic simulations, the plates boundary conditions were clamped-clamped and free-free, identical to the static models. The detailed modeling process for creating dynamic snap-through models is provided in Chapter 3 Section 3.3.4.

This work will report only on the dynamic responses of 4B and 5B structures for simplification as all results for the different buckled rise depths were similar. Periodic snap-through (p-snap) behavior for 4B and 5B structures was found at high amplitude forcing frequencies of around 120Hz and 130Hz, respectively. To start, a forcing amplitude of 18g (g-force) for 4B produced p-snap responses. However, a higher forcing amplitude of 32g was required for 5B to reach p-snap behavior attributable to the deeper buckled rise. These forcing parameters (amplitude and frequency) were found with ease using similar forcing parameters provided by the snap-through boundary map discussed in Chapter 4 Section 4.4. Starting with these amplitudes, amplitude magnitudes were increased in dynamic analysis to determine the influence of forcing amplitudes on stress parameters, which will be discussed in a

later section of this chapter.

5.5 Dynamic Snap-through Results

5.5.1 Dynamic Analysis Displacements

Periodic snap-through of the 4B structure was found at 120Hz excitation, with a forcing amplitude of 18g. Likewise, periodic snap-through of the 5B structure is identified at a forcing frequency of 130Hz, and a 32g amplitude. As shown in Figure 5.10, the 5B structure reaches a slightly higher alternating displacement of around 3.7 mm compared to the 4B structure, only reaching around 3.2 mm, during dynamic excitation at these forcing parameters. This is anticipated, as 5B has a deeper initial buckled rise than 4B, and requires greater forcing parameters to achieve p-snap. With increasing buckled rise, higher amplitude displacement responses are expected, which is captured here.

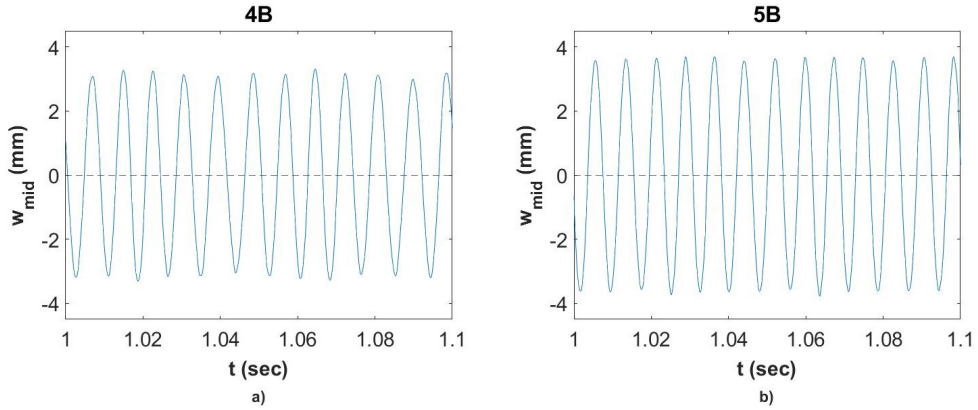

Figure 5.10: Center node displacements for a) 4B structure, 120Hz-18g forcing, b) 5B structure, 130Hz-32g forcing

In addition to these results, p-snap was explored further for the 5B buckled rise, with simulations at 130Hz for 32g, 40g, 48g, 56g, 64g, 72g, 80g, and 88g forcing amplitudes. Figure 5.11 shows that with increasing forcing amplitudes, the alternating maximum displacements do not vary greatly. In the case of 5B, the maximum magnitude of the displacements reaches

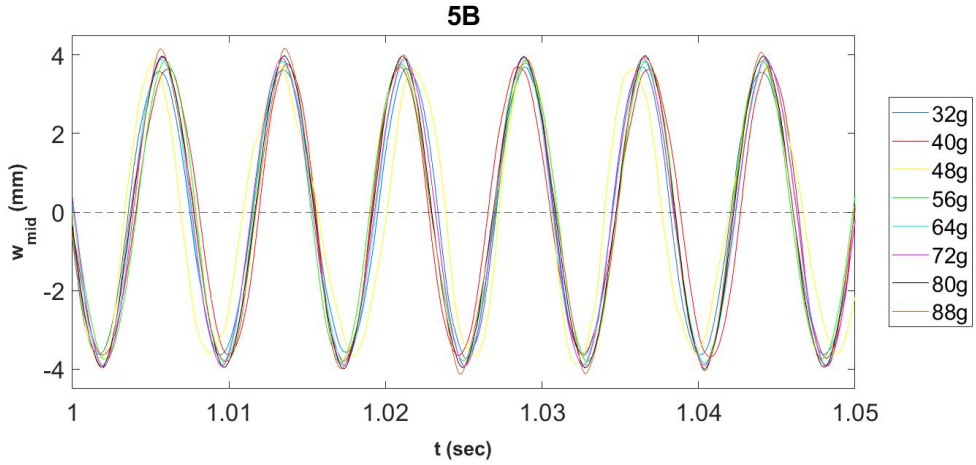

Figure 5.11: Center node displacements for 5B structure, subjected to 130Hz forcing frequency, with varying forcing amplitudes 32g-88g

around 4.0 mm. This is significant as doubling the forcing amplitude from 32g to 64g does not appear to alter the displacement magnitudes to any considerable amount.

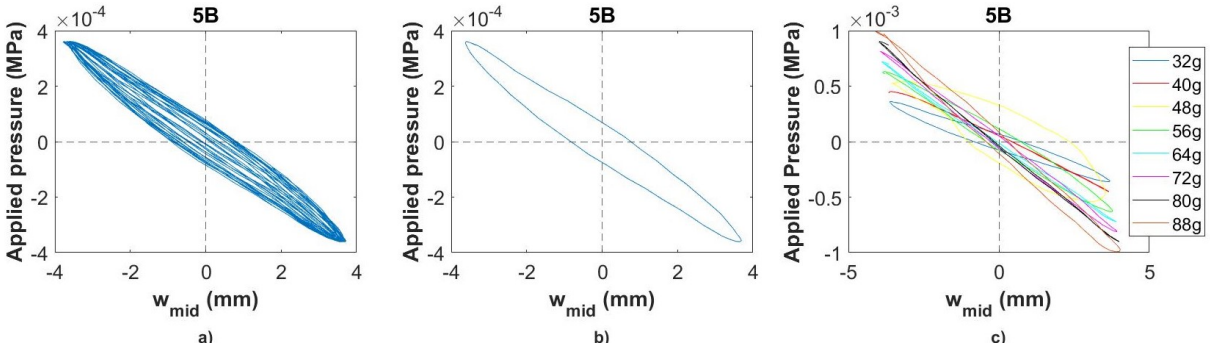

Figure 5.12: Force-displacement results for 5B structure for a) many cycles, 130Hz-32g, b) one cycle, 130Hz-32g, c) one cycle, 130Hz-(32g-88g).

Force-displacement plots of single cycles extracted from the dynamic simulations are provided in Figure 5.12. Given dynamic excitation, the force-displacement plots appear as stretched ellipses with points of maximum displacement occurring at locations of maximum loading magnitude. Figure 5.12a displays the force-displacement curve for many cycles of

dynamic snap-through. As shown, the force displacement relationship over multiple cycles varies slightly, however, tends to follow a similar projected path given the periodic snap-through behavior. Figure 5.12c illustrates the force-displacement relationship with increasing forcing amplitude. As forcing amplitude increases, the ellipse is stretched to greater applied pressure magnitudes, yet the maximum displacement magnitudes do not increase significantly despite the increase in applied pressure. For all dynamic results, the applied loading is 180° out of phase with displacement responses; at the maximum positive load, the maximum negative displacement is reached. From Figure 5.12c, the force-displacement curve for 130Hz-48g appears to develop a wider ellipse shape when compared to the other forcing amplitude results. This is attributed to a greater phase shift at this forcing amplitude, the phase shift is slightly greater than 180°. This is not surprising, as snap-through is sensitive to forcing parameters.

5.5.2 Axial Stress

In a later section, the in-plane axial stresses σ_{xx} for static and dynamic analyses will be compared. Axial stresses were already discussed for static snap-through in a previous section. Thus, this section will introduce analyzing axial stress results for dynamic analyses. Similar to with static analysis, contours plots of the maximum axial stress values throughout the entire dynamic analysis were created. An example of the axial stress contour plots for the 5B structure are provided by Figure 5.13.

As with the static snap-through contours, the dynamic contours provide an idea of maximum stresses seen throughout the simulation, but do not show a history over time of stress results. Therefore, axial stresses at the midnode along the plate midplane were analyzed for both 4B and 5B structures under dynamic loading. Here, only the 5B structure will be discussed as results were very similar for 4B. Figure 5.14 portrays the dynamic response for the 5B structure undergoing periodic snap-through loading. Maximum tensile stresses are found at peaks of maximum displacements throughout the dynamic simulation. Compression stresses are relatively small, reaching a maximum of around -0.7 MPa. Note that

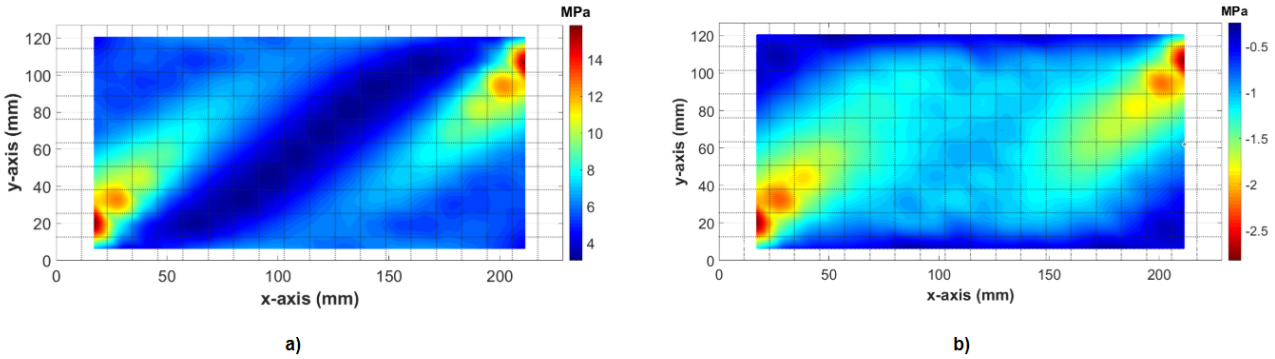

Figure 5.13: Maximum tensile (a) and compressive (b) in-plane axial stresses σ_{xx} at plate midplane for dynamic snap-through of 5B structure subjected to 32g-130Hz forcing

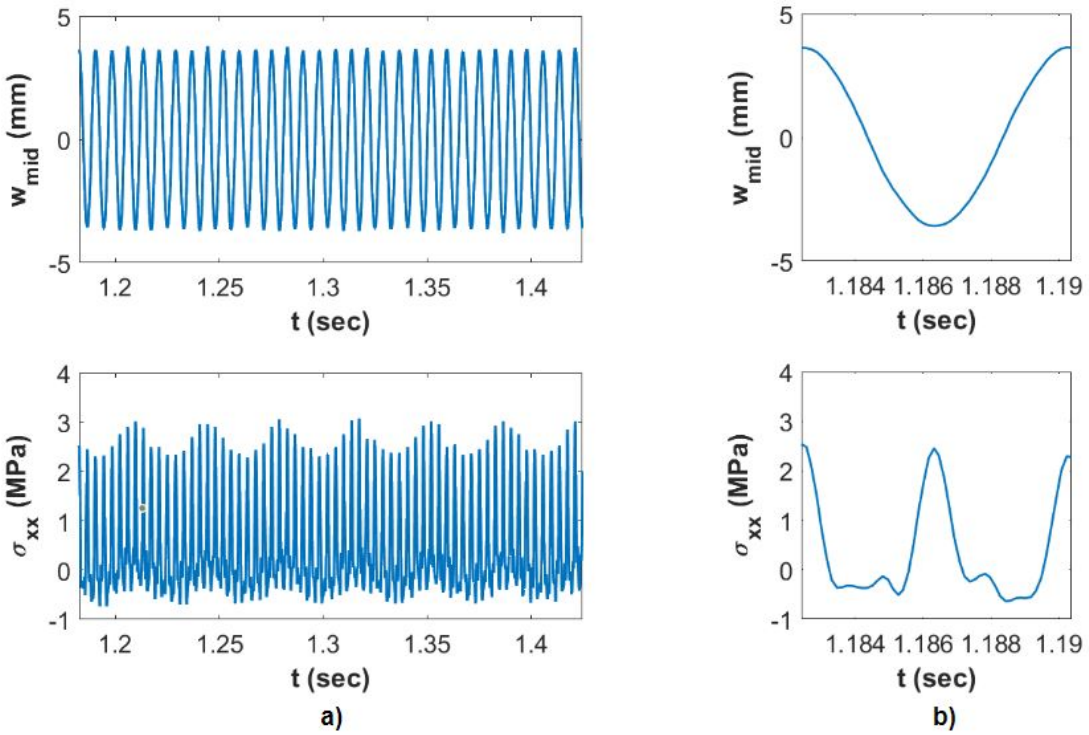

Figure 5.14: Midnode displacements and axial stress at the mid node for 5B structure, subjected to 32g-130Hz forcing for a) many snap-through cycles, b) single cycle

Figure 5.14a provides the midnode displacements and axial stresses over time for many snap-through cycles of the dynamic analysis. Likewise, Figure 5.14b provides these same results but only for a single snap-through cycle. Because the static snap-through response discussed in previous sections only consists of a single cycle, only one dynamic snap-through cycle will be compared with the static results in a later section.

5.5.3 Shear Stress

Transverse shear stress τ_{xz} for dynamic snap-through will also be compared with static snap-through results. Thus, shear stress will be discussed in this section for dynamic snap-through. Similar to with axial stress from the previous section, transverse shear stress τ_{xz} was analyzed using a contour plot of the maximum magnitude of shear stresses over the entire dynamic simulation. Figure 5.15 provides the shear contour plot for dynamic snap-through. The figure shows that the largest shear magnitudes are found along the plate's fixed edges.

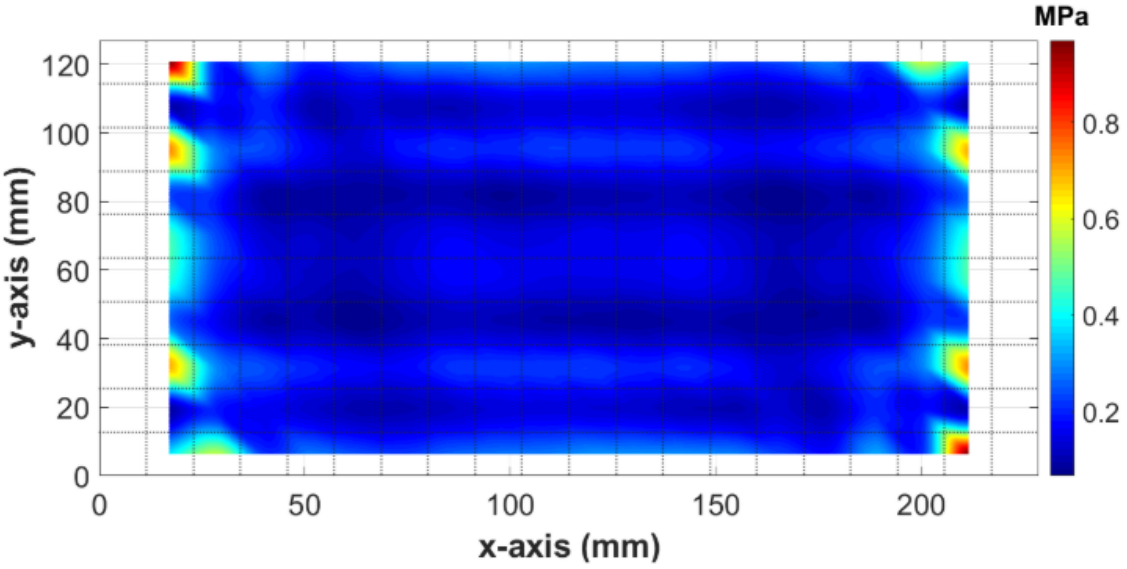

Figure 5.15: Maximum transverse shear stresses τ_{xz} at plate midplane for dynamic snap-through of 5B structure subjected to 32g-130Hz forcing

In addition to shear contour pltos, transverse shear stresses were evaluated at four different locations along the midplane of the plate. These locations were chosen as identical locations that were analyzed in a previous section for static snap-through (see back to Figure 5.9 for locations). As an example, the shear stress found at one of these locations (the midnode) will be discussed in this section. Figure 5.16 displays the shear stress τ_{xz} through-

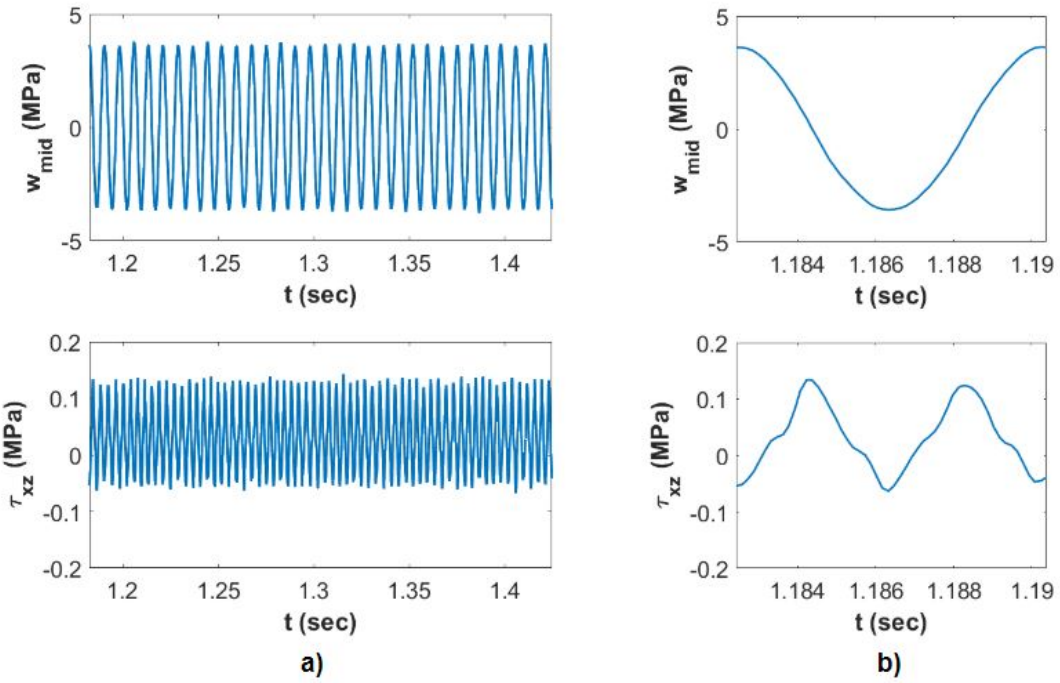

Figure 5.16: Midnode displacements and transverse shear stress at the midplane for 5B structure, dynamic analysis subjected to 32g-130Hz for a) many snap-through cycles, b) single cycle

out time at the midnode. Figure 5.16b reports the transverse shear stress at the midnode for a single snap-through cycle, where the shear oscillates between -0.06 MPa to 1.18 MPa. Along with the shear at the midnode, transverse shear stress was also analyzed at three other locations within the plate. Locations were chosen to match the same locations which static shear stresses were explored in order to compare trends between dynamic and static responses, discussed later. In addition, shear stresses were explored with increasing forcing

amplitude and these results will be discussed in a later section.

5.6 Comparison of Stresses Under Static and Dynamic Response

The previous sections of this chapter discuss static and dynamic snap-through results separately. This section will compare these stress results to investigate to what extent the dynamic stress results deviate from the static stress results. To explore the relationship between static and dynamic stress results for the 5B structure, axial and transverse shear stresses will be compared using contour plots and at single points along the plate midplane.

5.6.1 Axial Stress

To start, in-plane axial stress σ_{xx} of static and dynamic snap-through are compared using contour plots. As in the previous sections of this chapter, these contour plots contain the maximum stress values found during the simulation. The maximum compressive stresses throughout the static and dynamic plates were first compared. These contours are provided in Figure 5.17. The figure shows that the dynamic simulation at 32g-130Hz produced a

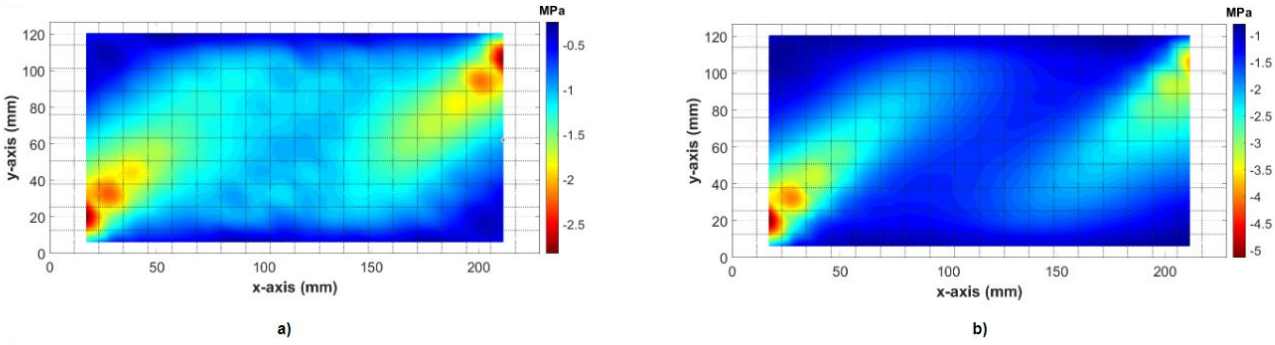

Figure 5.17: Maximum compressive axial stresses throughout entire time history for a) 5B 32g-130Hz dynamic contour, b) 5B static contour

contour which does not reach the maximum compressive stresses that the static simulation

experiences. Over the majority of the plate, the static and dynamic contours show similar trends in shading and the expected locations for the maximum stresses remain similar, however, the actual maximum stress values slightly deviate. The plate undergoing dynamic loading reaches maximum compressive stresses of around -2.5 MPa, whereas the static copy of this plate reaches higher compressive stresses of around -5 MPa. After increasing forcing amplitude, the dynamic compressive axial stresses remained to be over-predicted by the static results, creating what seems to be a compressive stress "fuse" for dynamic snap-through. Despite this over-prediction, the contours appear similar when comparing locations of maximum and minimum stress values.

Next, the maximum tensile stresses found throughout the time history where plotted on a contour for both dynamic and static analyses. From Figure 5.18 the tensile stresses for

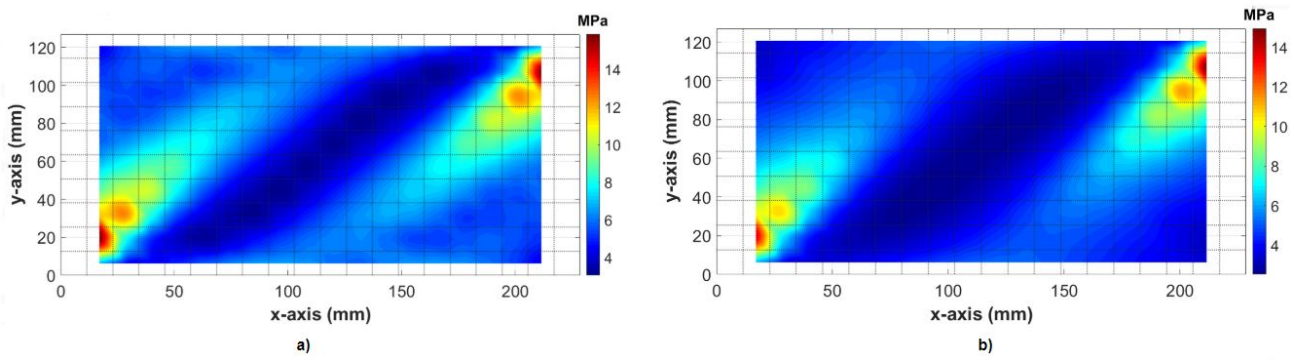

Figure 5.18: Maximum tensile axial stresses throughout entire time history for a) 5B 32g-130Hz dynamic contour, b) 5B static contour

both static and dynamic simulations match closely. Dynamic results shown are attributed to 32g-130Hz loading, however, at the increased loading amplitude of 88g, the dynamic contour results continued to match the static contour very similarly. From these contour plots, it is shown that the dynamic simulations do not result in much greater maximum stress values than the static simulations, where in both cases maximum tensile stress values are located

at the plate's fixed ends.

The axial stress contour plots show promising results which suggest the dynamic analysis results may not deviate far from the static analysis results. This hypothesis is further investigated by also comparing the axial stresses at specific points through simulation increments of each analysis type (both static and dynamic). To illustrate, in-plane axial stresses σ_{xx} at the midnode of the plate midplane are compared through simulation time for both dynamic and static snap-through. Static simulations are solved using arc length method which uses increments of arc length. Likewise, dynamic simulations are solved using time increments rather than increments of arc length. It is worth noting that because these two increment types are different, stress histories compared in this section use "increment" as the x-axis rather than the typical variable "time". Comparing the in-plane axial stress σ_{xx} at the mid node of the plate for both static and dynamic simulations reveals that the dynamic stress follows the static stress rather closely.

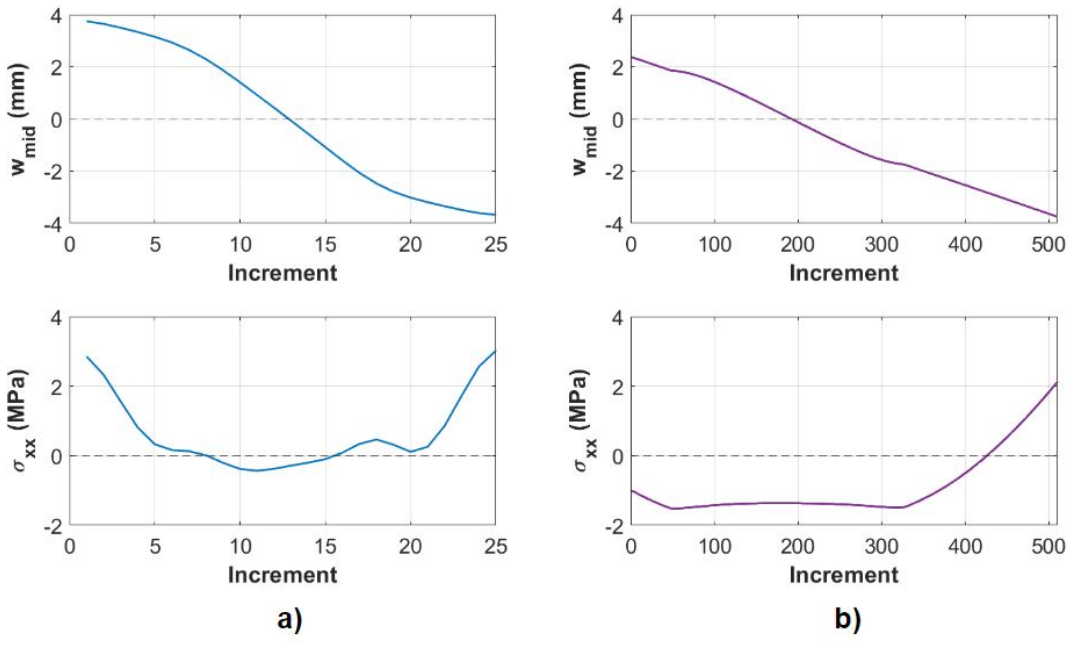

Figure 5.19: Center node displacements and axial stress at the mid node for 5B structure, a) dynamic analysis at 32g-130Hz harmonic loading, b) static analysis

Figure 5.19 displays comparisons between one dynamic snap-through cycle and the static snap-through cycle for the 5B structure. The increment quantities provided in this figure vary as increments used in dynamic analysis are associated with time, while the increments used in static analysis are associated to arc length. Maximum tension is found at the maximum and minimum displacement values, occurring when the plate's buckled rise is at its maximum. As the plate snaps through and reaches a relatively flat, asymmetric configuration, the axial stress decreases, reaching the compression regime. As the plate begins to bend into a maximum displacement, the axial stress increases into points of maximum tension stress. This trend is recognized for both dynamic and static results. At points where the dynamic displacement values surpass the static displacements, the dynamic axial stresses slightly exceed the static stresses. The static stress values are shown to exceed the dynamic stress values during the compression region. Repeated dynamic simulations with increasing forcing amplitude proved that these observations remain valid, and increasing forcing amplitude did not significantly increase the compression or tension values.

5.6.2 Shear Stress

The results provided so far portray the efficacy of using a static analysis to predict the dynamic analysis stress results. To verify that the static analysis may be used to predict the dynamic analysis results more fully, transverse shear stress τ_{xz} for both analysis types is also compared. Again, contour plots were generated from the maximum shear stress values extracted from the analyses. Figure 5.20 provides the maximum shear stress contour plots for both static and dynamic snap-through. The contour plots for shear stress τ_{xz} for both dynamic and static analyses are provided in Figure 5.20. Maximum magnitudes of shear stress are located along the fixed edges of the plates. A grid-like pattern is seen within the mid region of the plates for both dynamic and static analysis, most likely attributed to the plate dimensions. Overall both the dynamic and static analyses provide very similar shear stress results. Again, when undergoing dynamic analysis, the plate appears to see slightly higher shear stresses. However, these stresses do not greatly vary from the static analysis

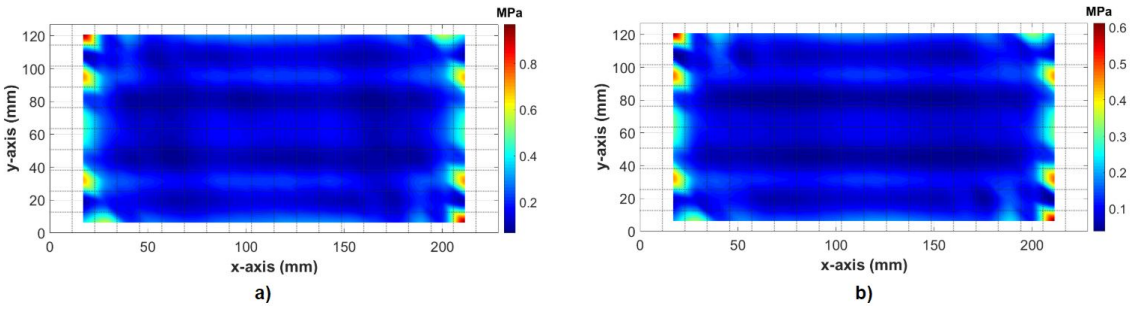

Figure 5.20: Maximum magnitudes of transverse shear stresses throughout entire time history for a) 5B 32g-130Hz loading dynamic analysis, b) static analysis

and are within the same order of magnitude.

In addition to reviewing the contour plots, transverse shear stress τ_{xz} was explored for both static and dynamic snap-through responses by examining the stress histories at single points through simulation time. Shear stresses were analyzed at different locations along the plate midplane. Locations were chosen along both the plate mid region and plate edges to provide data which is mostly representative of the plate. The shear at the midnode was

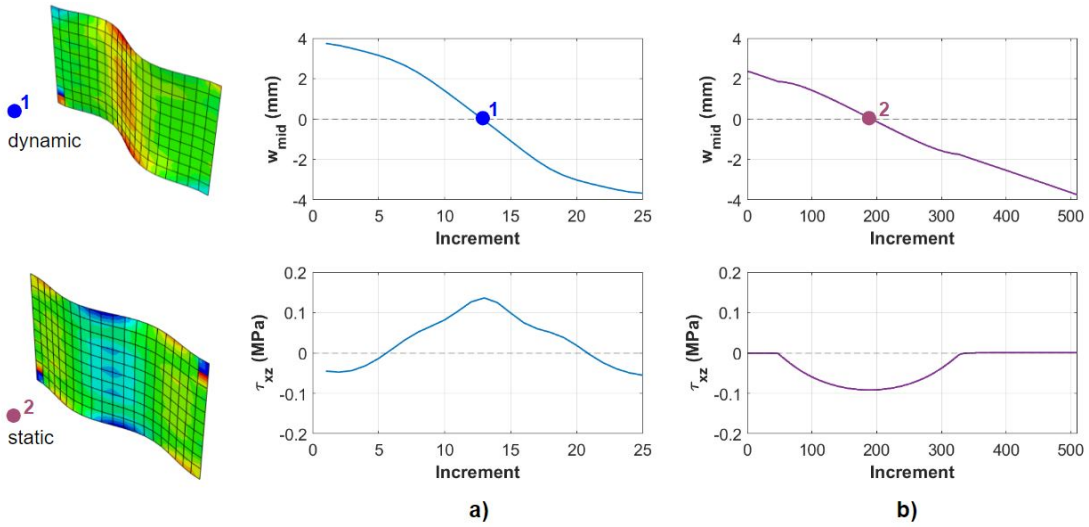

Figure 5.21: Midnode displacements and transverse shear stress τ_{xz} at the midplane for 5B structure, a) dynamic analysis at 32g-130Hz harmonic loading, b) static analysis

first analyzed for 32g-130Hz dynamic excitation. As shown in Figure 5.21, the magnitude of the dynamic shear stress slightly exceeds the static shear stress magnitude. However, both shear stresses follow a similar trend where shear remains relatively constant and comes to a maximum peak at around the time the plate passes a flat configuration where no displacement is observed. The amplitudes of shear stress between the dynamic and static analyses differ in sign; the dynamic shear stress reached a maximum positive peak while the static shear stress reached a maximum with a negative peak value. This is simply attributed to the direction at which the plate snapped through, shown in the left of Figure 5.21.

The shear stress at other three other locations were analyzed, however, only one additional location will be discussed here for simplicity purposes. Results from location (d) (see back to Figure 5.9 for location on plate) are displayed in Figure 5.22. Again, the shear stress

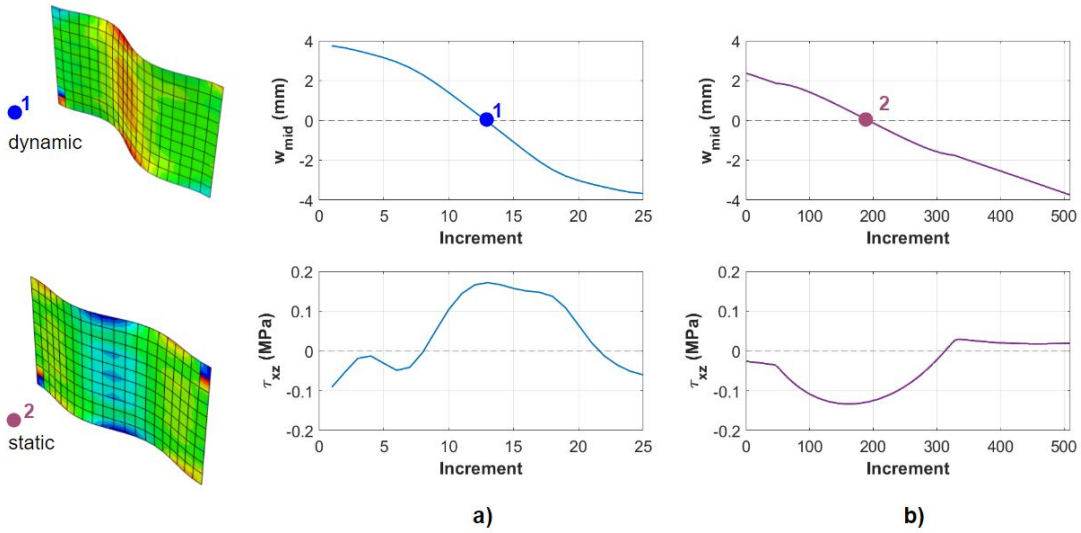

Figure 5.22: Midnode displacements and location (d) shear stress for 5B structure, a) dynamic analysis at 32g-130Hz harmonic loading, b) static analysis

results for location (d) appear positive for dynamic and negative for static analyses. This is identical to the results previously shown for the midnode and is attributed to the snap-through direction and plate configuration. At first glance the transverse shear results for

dynamic and static do not appear to be aligned, however, this is attributed to the difference in sign caused by the snap-through direction. From Figure 5.22, the maximum magnitude of shear stress at location (d) for both static and dynamic analyses both occur at points where the midnode returns to 0 mm deflection.

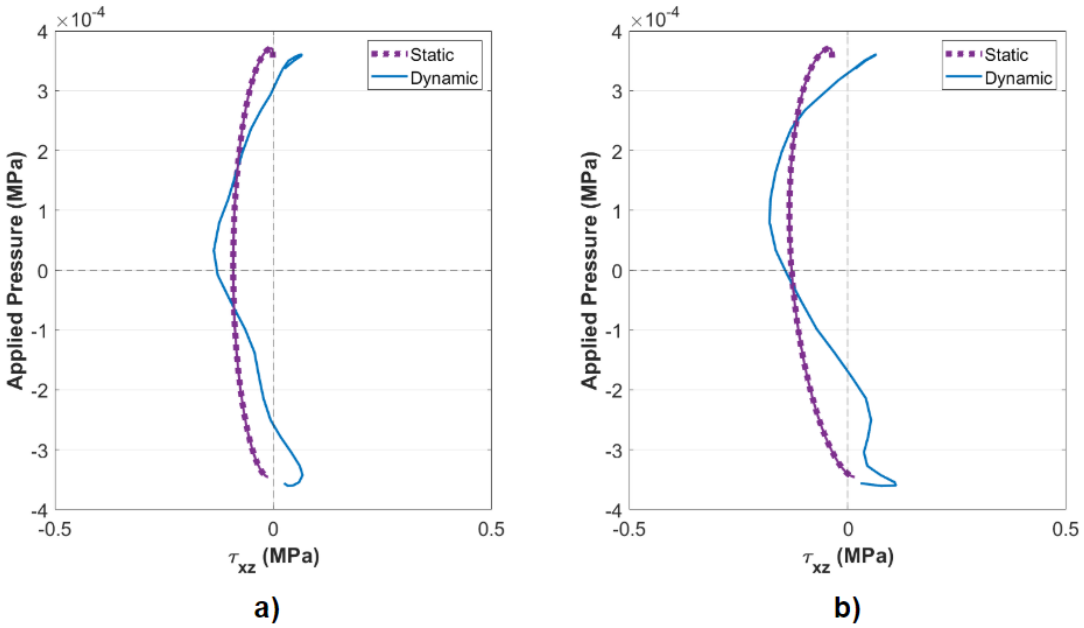

Figure 5.23: Applied loading versus transverse shear stress for 32g-130Hz dynamic loading and static loading, a) at the mid node b) at location (d)

To further analyze the shear stress results the shear stresses for static and dynamic analyses were plotted against the applied pressure load. Figure 5.23 portrays this result. Note that the sign of shear stress was flipped for the dynamic result to match the static result for comparison purposes. Figure 5.23 shows maximum values of shear stresses for both static and dynamic analyses occur when the applied pressure loading is either zero or at a maximum amplitude. At both the mid node and location (d) the plots for static and dynamic shear stress match closely with the exception of dynamic shear stress reaching slightly larger magnitudes at peaks. These figures imply the transverse shear stresses from dynamic snap-through may be estimated using static analysis, however, exact stress values

will vary slightly.

5.6.3 Effects of Increasing Forcing Amplitude

Throughout this chapter it is shown that at 32g-130Hz forcing amplitude, the static and dynamic stress results generally are within agreement. The forcing amplitude used in the dynamic analyses was increased in order to determine whether this trend remains true for large amplitude loading. Forcing amplitude was ranged between 32g-88g with a consistent excitation frequency of 130Hz. This short section will discuss the effects of increasing dynamic forcing amplitude on comparing static and dynamic snap-through results.

Increasing forcing amplitude in dynamic analysis did not appear to greatly alter results; dynamic analyses continued to match closely to static analysis stress results. This was observed using contour plots and again looking at individual points through time for both simulation types. To begin, stress contour plots were generated for axial and shear stresses for all forcing amplitudes explored within this section. However, these contours will not be provided here as they are so similar to the contour plots for 32g loading discussed in the previous section. These additional contour plots may be found in Appendix B. Since the contour plots for increased forcing amplitude still match closely to the static stress contour plots, it can be noted that the static analysis still remains to be a satisfactory tool to predict dynamic responses.

Individual points along the plate midplane were also analyzed at different dynamic forcing amplitudes. As with the contour plots, these stress results showed that even with larger forcing amplitudes, the dynamic snap-through stresses continued to match the static snap-through stresses closely. To illustrate, Figure 5.24 portrays the effects of increasing forcing amplitude on axial stress σ_{xx} at the plate mid node.

Figure 5.24a verifies that at increased forcing amplitude, the dynamic response does not alter greatly. Comparing forcing at 32g and 88g shows that with over twice the load amplitude, the displacement and internal axial stresses at the center node do not increase to any significant extent. The response for dynamic loading at 48g varies the most from all

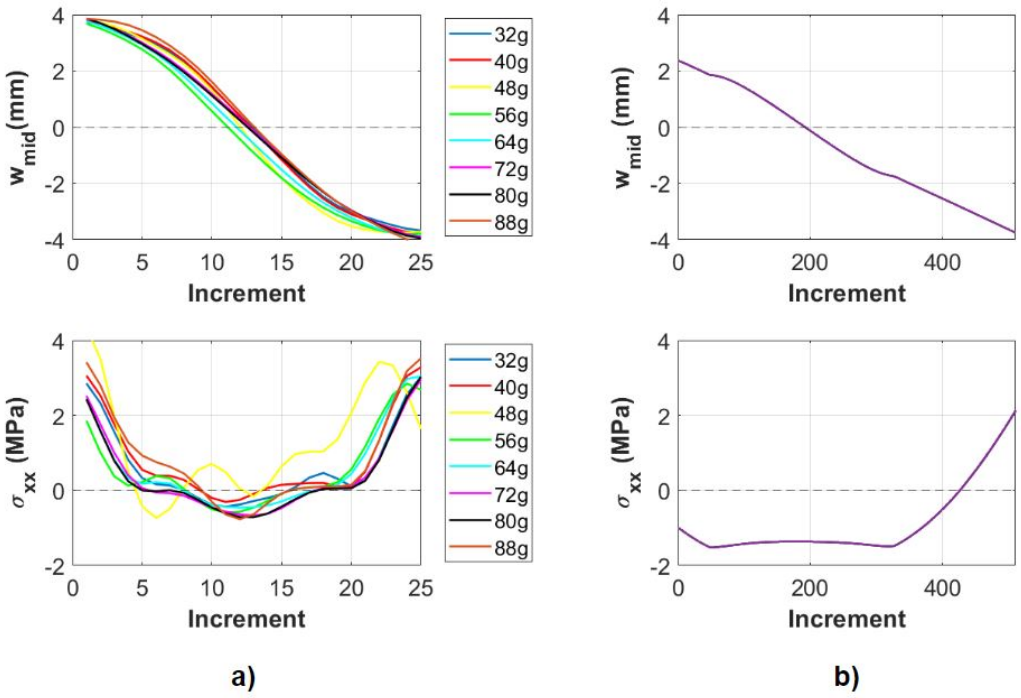

Figure 5.24: Center node displacements and axial stress for 5B structure with varying amplitudes, a) 32g-88g loading dynamic analysis, b) static analysis

dynamic responses, however, this is due to the maximum displacement being slightly out of phase with the harmonic loading.

Figure 5.25 illustrates the effects of increased forcing amplitude on transverse shear stress. Note that in Figure 5.25a, the shear stresses for 40g and 64g loading experience peaks of negative stress, matching the static response, while the remaining forcing amplitude results reach peaks of positive stress. This is identical to what is discussed in the previous section, where the difference in signs is attributed to the direction of snap-through. Thus, the sign of the maximum peak in shear stress is not of interest; it is the shape of the graph and magnitude of the peak that should be analyzed. From this figure, the shear stress magnitudes experienced dynamically by the plate all are relatively equivalent regardless of forcing amplitude.

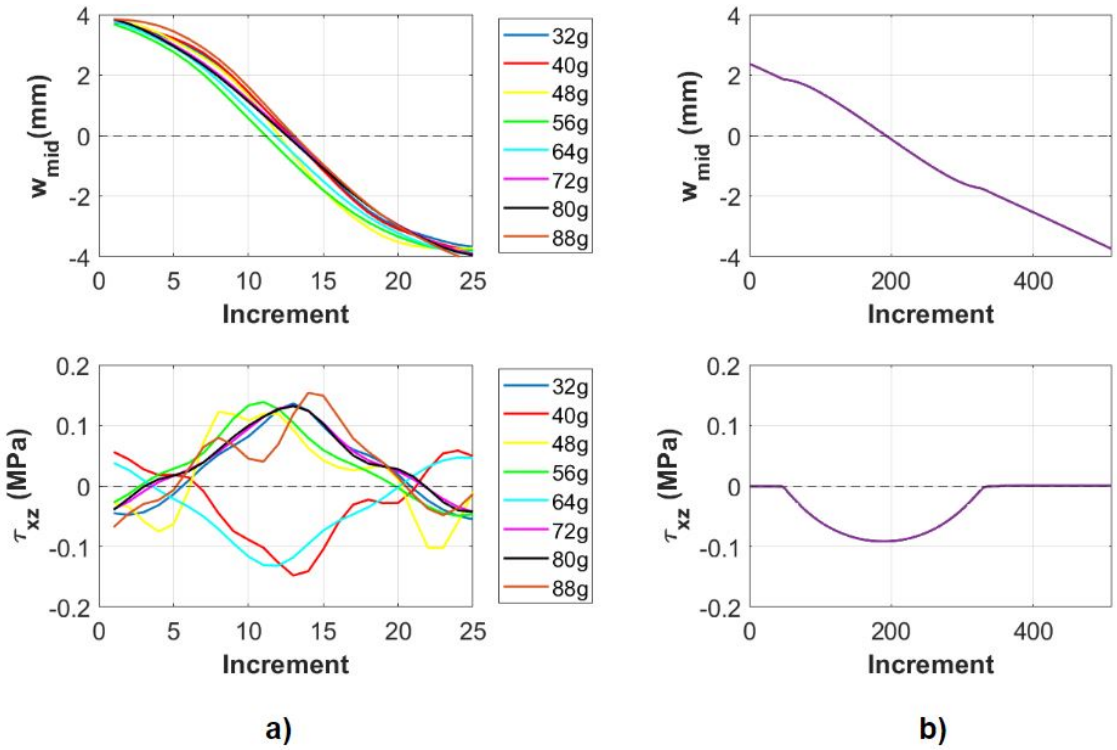

Figure 5.25: Midnode displacements and transverse shear stress for 5B structure with varying amplitudes, a) 32g-88g loading dynamic analysis, b) static analysis

5.7 Chapter Conclusion

It is evident that dynamic and static analyses yield different results. In the case of a composite panel undergoing snap-through, it was found that this difference in results is not as significant as previously expected. Analyzing axial and transverse shear stresses along the plate midplane suggested that the stresses experienced during dynamic snap-through did not vary greatly from the equivalent static snap-through analysis. Additionally, the effects of increasing forcing amplitude verified that with larger dynamic loading, this conclusion still holds true.

Despite the apparent efficacy of using static analysis to predict dynamic analysis responses, there are some limitations to this study. Firstly, although the stresses in the case

of dynamic analyses generally matched the static analysis stresses, the static analysis can not predict exactly what stress magnitudes will be reached. The static analysis may only be used as a tool to predict what order of magnitude of stresses to expect. Additionally, more work exploring this may be required, as only the axial stress σ_{xx} and the shear stress τ_{xz} were studied along the plate midplane. In reality, all stress components must be explored and at every location along the plate thickness which was not explored fully here due to the high spatial complexity involved. Limitations aside, the static analysis of snap-through proves to be a useful predictor in estimating dynamic responses.

Chapter 6

FATIGUE FRAMEWORK

6.1 Chapter Overview

The previous chapters of this thesis explored the snap-through behavior of post-buckled laminated composite plates. Throughout this work stress fields were analyzed and compared for both dynamic and static analyses. One concern of snap-through is that large deformations may induce high stresses, possibly decreasing fatigue life [6]. This chapter will investigate fatigue life characterization specific to multi-directional composite laminates undergoing periodic snap-through. Specifically, periodic snap-through will be observed for fatigue life as it results in the largest deformations and highest snap-through rate. This deems it as a "worst case" response when compared to single-well and chaotic snap-through.

Although there are several methods to characterizing fatigue life, this chapter focuses on the constant fatigue life (CFL) diagram method discussed by Kawai and Koizumi [4]. The CFL diagram method involves decomposing stress responses into components of alternating stress and mean stress and using these components to define fatigue life. Stress results from composite panels undergoing dynamic snap-through will be analyzed and a fatigue life will be mapped to every point along the plate using the CFL diagram method and previous experimental data provided by Kawai and Koizumi. The primary purpose of this chapter is to advance the understanding of fatigue characterization for snap-through of composite plates by investigating the use of CFL diagrams on finite element model results. Additionally, the results of this chapter will help determine what plate dimensions and material properties are required to induce a short fatigue life for future experimental testing on plate snap-through and fatigue.

6.2 Fatigue Characterization

6.2.1 Introduction and Modeling

In this section, plate finite element models with varying plate thicknesses are created using Abaqus. The models will be used to determine fatigue life using the CFL diagram method. To begin, previous work by Kawai [4] involved creating CFL diagrams through experimental testing of composite materials. Each CFL diagram is specific to a material and mode of failure. In this section, we will focus on the composite material T800H/3631 composed of Toray carbon fibers as this is the material which was used to create the CFL diagrams. Specific material properties for this composite material were not provided in the previous work, so properties will be approximated from another study which reported properties for the same composite material [13]. The material properties used in modeling are provided in Table 6.1 and the material density was modeled as 1.64 $\frac{g}{cm^3}$.

Table 6.1: T800H/3631 Material Properties

Property	Value	units
E1	165	GPa
E2	11.2	GPa
v12	0.041	
G12	6.53	GPa

All plates were modeled with a width of 127 mm and a length of 228.6 mm, identical to the geometric dimensions of plates modeled in previous chapter within this work. Plate thicknesses were varied from 2 mm to 8 mm at 1 mm increments in order to determine the influence of plate thickness on fatigue life. Plates were modeled with a $[45/90/-45/0]_{2S}$ laminate symmetric, quasi-isotropic layup of T800H/3631 to match the layup used in the CFL diagram explored in this fatigue study. Similar to the boundary conditions of other plates

modeled throughout this thesis, the 127 mm wide plate edges were modeled as completely fixed and the 228.6 mm long plate edges were modeled as completely free. Prior to any dynamic modeling, each plate was axially buckled to a buckled rise of 2.5 mm. The axial loads to achieve a buckled rise of 2.5 mm varied per plate depending on plate thickness (thicker plates required larger axial loads). Like Chapter 5, but unlike Chapter 4, these buckled plate results are for initially flat plates that are symmetrically buckled. Chapter 3 Section 3.3.3 provides the detailed approach on creating buckled laminated composite plates in Abaqus.

After the buckled plate models were created, dynamic analysis performed to find periodic snap-through responses. Periodic snap-through responses were desired for this study because it was previously observed that periodic snap-through yields larger deformations and higher resultant stresses than chaotic snap-through or single-well dynamic behaviors [6]. These higher stresses may induce a reduced fatigue life. Forcing parameters required to produce periodic snap-through vary with plate geometry. Therefore, different forcing amplitudes and frequencies were required for the dynamic analyses for each different plate because the plate thicknesses varied from 2 mm to 8 mm. In order to find the required snap-through loads for each plate thickness, a nonlinear static snap-through analysis was performed in Abaqus for each different plate. The detailed process for creating a static snap-through analysis model is provided in Chapter 3 Section 3.3.5. The static snap-through analysis for each plate yielded the static uniform pressure load required for each plate to snap-through. These static snap-through loads are higher than the loads required for dynamic snap-through, however, they provide a good judgement on the dynamic snap-through load amplitude that will result in dynamic periodic snap-through. Figure 6.1a displays the static and dynamic snap-through loads required to achieve periodic snap-through for the varying plate thicknesses.

After determining the forcing amplitude required for snap-through, the forcing frequency must be determined. Based on previous work, periodic snap-through for composite plates may be found around a dynamic forcing frequency value of around 80-90% of the first mode frequency. Thus, a frequency analysis was performed in Abaqus on each plate to determine

the first mode frequency. Figure 6.1b shows the mode 1 frequencies for each plate model. Additionally, the figure shows the forcing frequency that was used to produce periodic snap-through in dynamic analysis for each model.

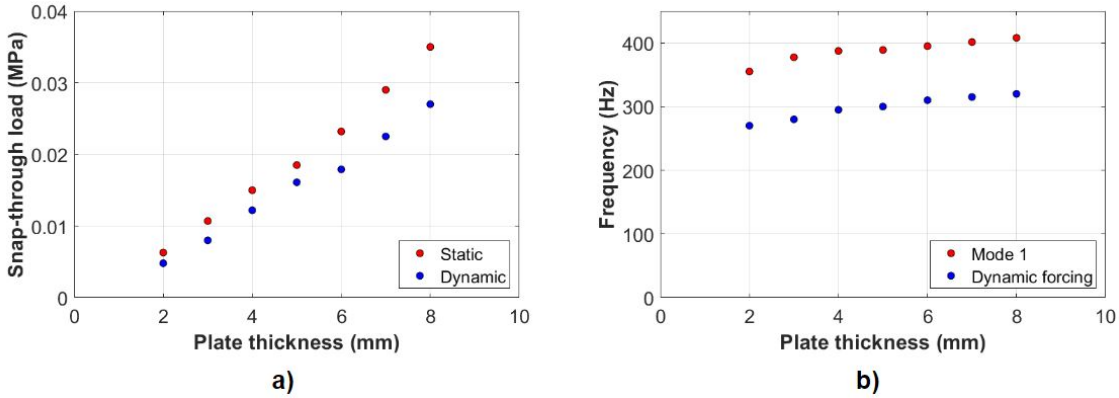

Figure 6.1: a) Required periodic snap-through loading for static and dynamic analyses with varying plate thickness, b) Mode 1 frequencies and periodic snap-through forcing frequencies for varying plate thickness

Table 6.2: Harmonic Forcing Parameters

Thickness (mm)	**Amplitude (MPa / g's)**	**Frequency (Hz)**
2	0.0048 / 150	270
3	0.008 / 165	280
4	0.0122 / 190	295
5	0.0161 / 200	300
6	0.0179 / 185	310
7	0.0225 / 200	315
8	0.027 / 210	320

After determining the approximate required forcing amplitudes and frequencies for dynamic snap-through analysis of each different plate, nonlinear dynamic implicit analyses were

used in modeling dynamic snap-through. Loading is applied as a uniform pressure load with an amplitude which varies harmonically. Each plate is given a different forcing amplitude and frequency because the thickness of each plate is different. The dynamic forcing parameters for each plate used in each dynamic analysis are provided in Table 6.2. From Table 6.2, the forcing amplitudes are provided in g's. The appropriate equivalent pressure loading can be calculated in MPa or Pa based on plate thickness and density, provided by Equation 4.1 from Chapter 4. Nonlinear dynamic implicit analyses were implemented and automatic time incrementation was utilized within Abaqus during the dynamic step. The dynamic models of each plate and loading were run until dynamic responses stabilized to an obvious periodic snap-through response. Chapter 3 Section 3.3.4 discusses the detailed process for creating a dynamic snap-through analysis model.

6.3 Fatigue Mapping

6.3.1 The CFL Diagram and Stress Analysis

Each dynamic snap-through model yielded displacement and stress results that will be analyzed within this section. Axial stresses σ_{xx} are of interest because the CFL diagrams provided from work by Kawai and Koizumi [4] were created from fatigue tests focused on mode one failure. An illustration of mode one failure is portrayed in Figure 2.7 from Chapter 2. As shown in the figure, mode one failure consists of tension or axial loading. Prior research was limited to producing a CFL diagram only for axial failure of the composite material focused on in this chapter [4]. Therefore, fatigue life will only be analyzed for mode one failure and only axial stresses σ_{xx} will need to be examined in this chapter. However, it should be noted that future work should analyze the fatigue life for both axial and shear failure modes after additional CFL diagrams become available.

Figure 6.2 depicts a recreation of the CFL diagram from Kawai and Koizumi [4] specific to the composite material and laminate layup explored in this work. The CFL diagram appears as a plot of alternating and mean stress created from experimental fatigue data. To

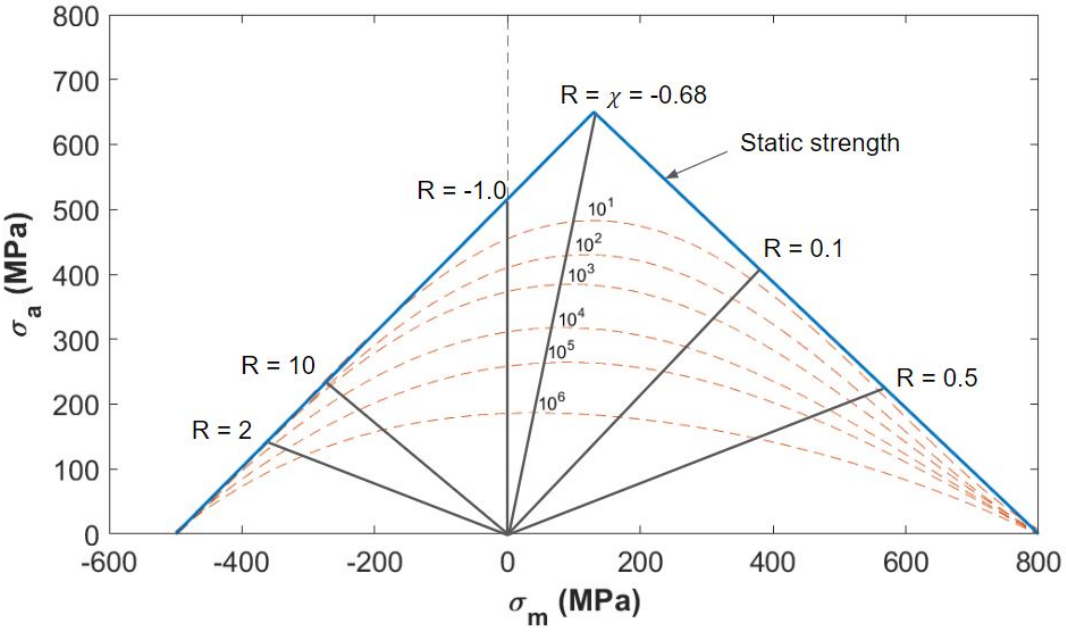

Figure 6.2: CFL diagram for $[45/90/-45/0]_{2S}$ laminate, mode one failure, recreated from [4]

create the diagram, constant amplitude fatigue tests on coupon specimens were performed with different stress ratios (ratios of maximum and minimum fatigue stresses) [4]. The outer bounds of the plot are determined by the static strength of the material. As observed in Figure 6.2, the inner portion of the plot consists of a nesting of dotted bell-shaped curves, each labeled with the number of cycles to failure. The variable "R" is found within the plot and this symbolizes stress ratio, described as the ratio of minimum fatigue stress to maximum fatigue stress. The specific stress ratio shown as χ on the plot is the ratio of compressive strength to tensile strength.

Stress results from dynamic simulations may be analyzed and applied to the CFL diagram displayed in Figure 6.2. The dynamic models with varying plate thickness discussed within this chapter were subjected to harmonic forcing, resulting in oscillating stress time histories. These stress histories are of importance when using the CFL diagram. An example of one of these time histories for axial stress σ_{xx} at a point along the plate surface is provided by

Figure 6.3. Alternating and mean stress along with stress ratio may be calculated from stress

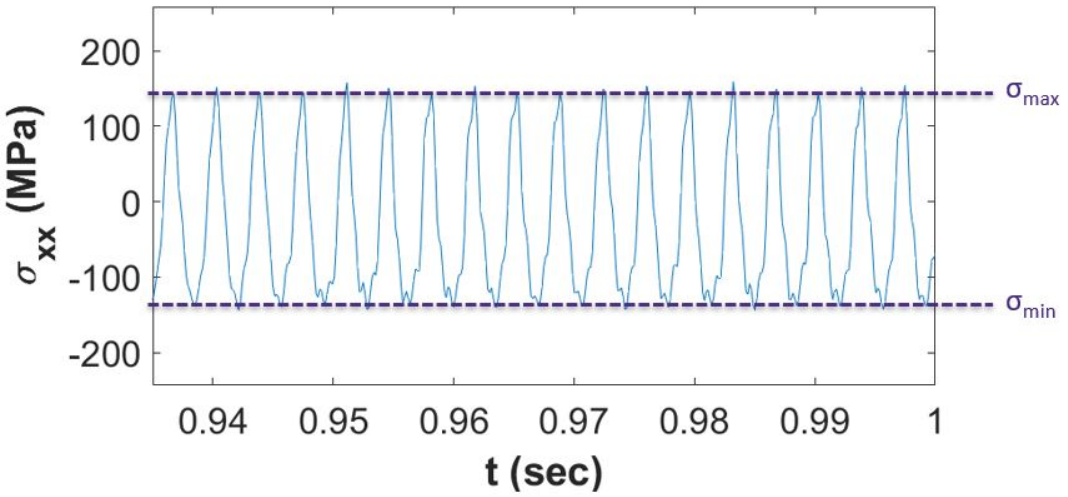

Figure 6.3: Axial stress σ_{xx} history for arbitrary point along surface of 3mm thick plate from 165g-280Hz dynamic loading

histories such as the one provided in Figure 6.3 from Equation 6.1.

$$\sigma_a = \frac{\sigma_{max} - \sigma_{min}}{2}, \qquad \sigma_m = \frac{\sigma_{max} + \sigma_{min}}{2}, \qquad R = \frac{\sigma_{max}}{\sigma_{min}} \tag{6.1}$$

After finding the values of alternating and mean stress for a single location along the plate surface, these two values are used to plot a point on the CFL diagram. The location of the point on the diagram determines fatigue life. The stress history provided in Figure 6.3 only is associated to a single point on the plate, however, this method can be applied to all locations just as easily, characterizing the fatigue life of every single point along the plate. This idea of determining fatigue life to the full spatial resolution of the structure will be explored in the following section.

6.3.2 Assigning Fatigue Life

Stress histories are recovered at every location along a plate following a dynamic analysis of harmonic forcing. These stress histories are separated into alternating and mean stress

components. In Chapter 5, contour plots of maximum stress values from stress history results were created. The contour plots provided information on stress at every point along the plate surface. This idea of providing full spatial resolution of stress results may be applied to this fatigue study as well. For instance, alternating and mean stress values can be calculated from the saved stress histories at every location along each plate. This would result in a different alternating and mean stress being attributed to every location. To

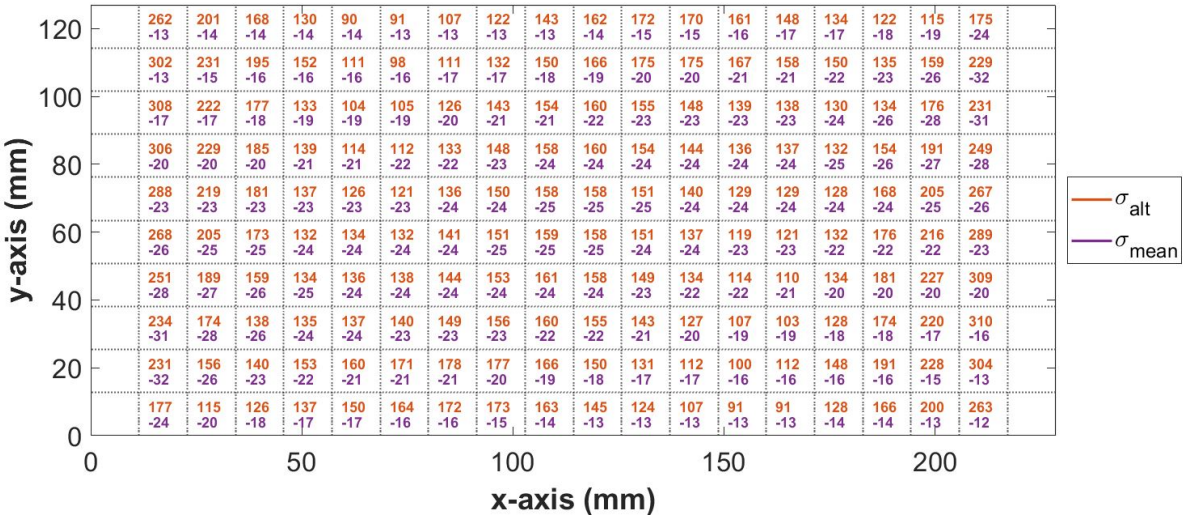

Figure 6.4: Alternating and mean stress per element for 3mm thick plate with 165g-280Hz dynamic loading

illustrate, Figure 6.4 provides a plot consisting of alternating and mean stresses assigned to every element centroid of the plate mesh.

Each element on the plate is attributed to a point on the CFL diagram using the alternating and mean stresses calculated from Equation 6.1. Plotting all the alternating and mean stresses from Figure 6.4 on the CFL diagram yields the plot portrayed in Figure 6.5. Shown in Figure 6.5, each element's failure is depicted by a red point. this figure reveals that the majority of the elements on the plate surface will not fail over 10^6 cycles. However, some points lie above the dotted bell-shaped curve marking the boundary for 10^5 cycles. All points remain close to the zero line of mean stress. This implies that the mean stress is

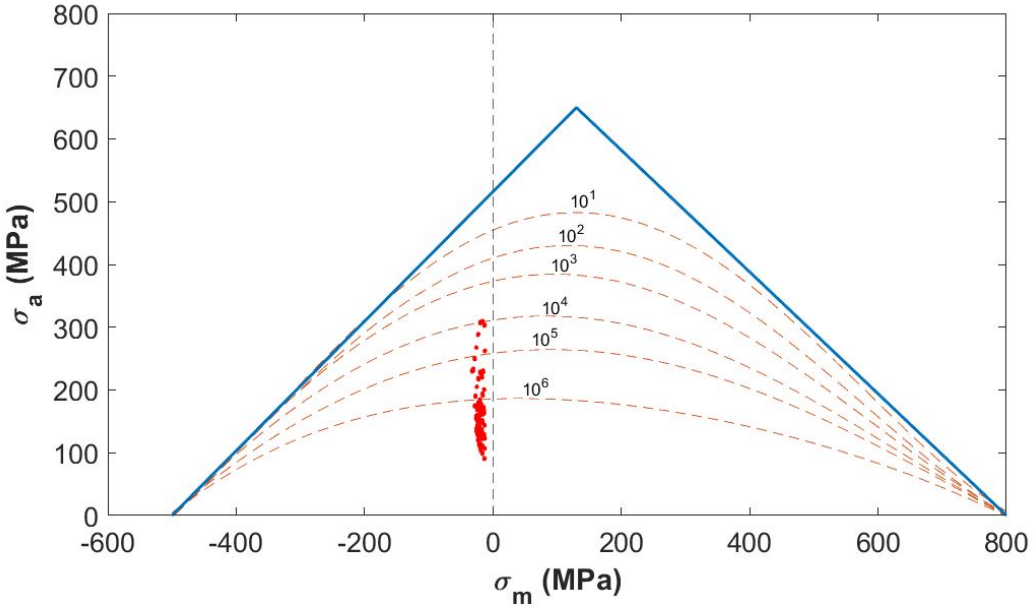

Figure 6.5: CFL diagram with stress results for 3mm thick plate with 165g-280Hz dynamic loading

not the limiting factor in fatigue life and the fatigue life is most dominated by alternating stresses for this plate model.

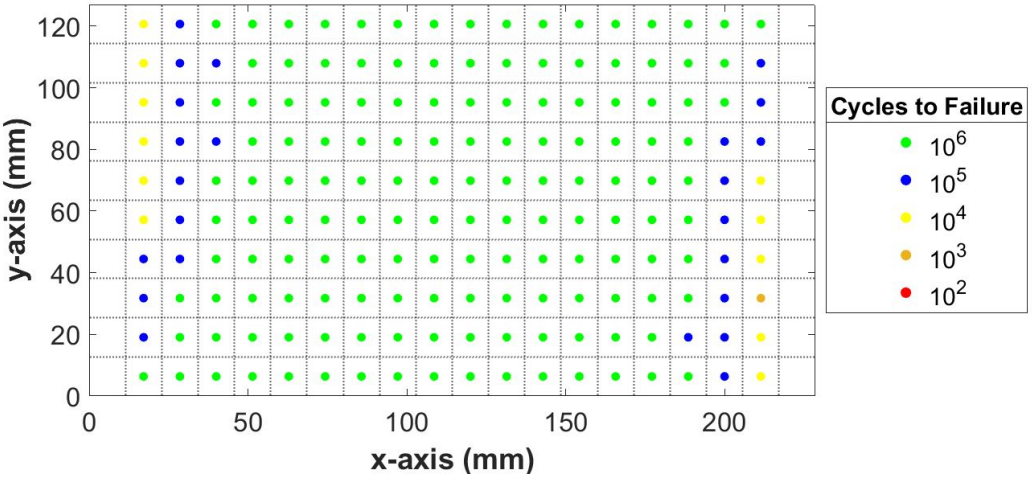

Figure 6.6: Fatigue life plot results for 3mm thick plate with 165g-280Hz dynamic loading

Reading points from the CFL diagram allows for the ability to characterize fatigue life for every point. Figure 6.6 depicts the fatigue life plot for every element along the plate surface of the 3mm thick plate. As shown, fatigue is likely to happen earlier near the plate edges which are fixed during dynamic loading. This is expected, as viewing Figure 6.4 shows the plate ends are also the locations of maximum alternating stresses the plate experiences. The large alternating stresses are a concern of plates undergoing snap-through and has previously been discussed in work by Kim and Wiebe [6]. Their work investigated the possibility of great increases in alternating stresses for post-buckled plates when compared to flat plates under similar dynamic loading, which may significantly reduce fatigue life. Although flat plates will not be discussed here, large alternating stresses associated with post-buckled plates are noticeable and should be noted.

6.3.3 Effects of Increasing Plate Thickness

As aforementioned, several post-buckled plate models were created with varying plate thicknesses from 2 mm to 8 mm. Using the forcing parameters previously listed in Section 6.2.1 Table 6.2, periodic snap-through was found for each plate model. The dynamic simulations for each plate possessed axial stress σ_{xx} histories which were separated into alternating and mean stresses using the same method as discussed in the previous section. The alternating and mean stresses for each plate were all plotted on the CFL diagram. This plot is provided in Figure 6.7. The figure shows that with increasing plate thickness, decreasing mean stress values are observed. Additionally, larger alternating stresses are reported as plate thickness increases. This increase in alternating stress and decrease in mean stress may lead to low-cycle failure of the composites due to the triangular shape of the failure diagram; as mean stress values move away from the peak of the nested curves, a smaller alternating stress is required to reduce failure life. The general trend of these results suggests that with increasing plate thickness, failure life decreases at certain locations along the plate surface. As done in the previous section, life plots may be created for all different plate thickness models. Figure 6.8 illustrates the life plot for the 5 mm thick plate created from the results

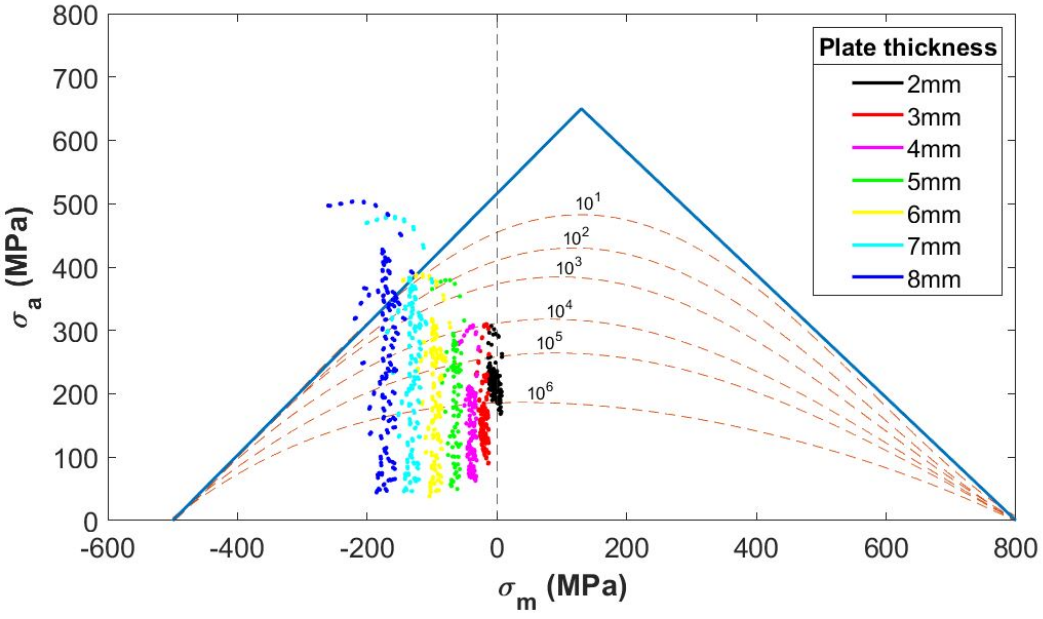

Figure 6.7: CFL diagram with axial stress results for varying plate thicknesses

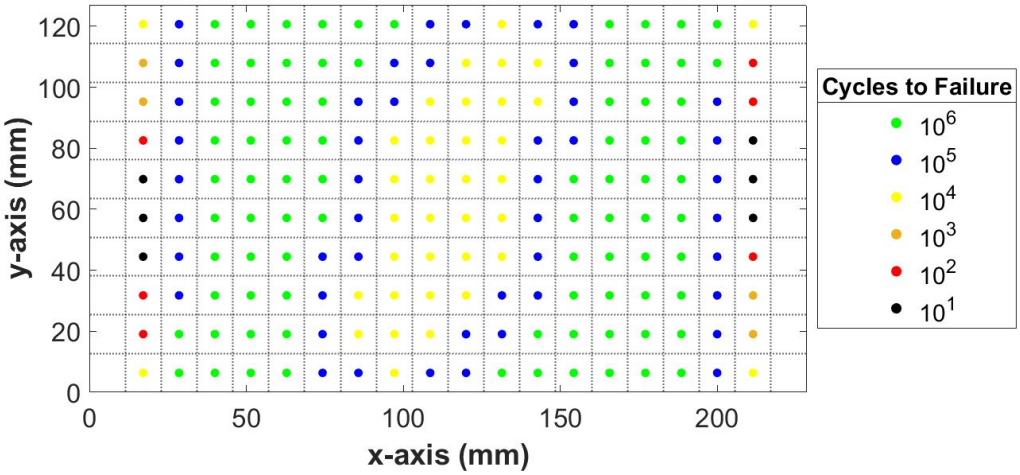

Figure 6.8: Fatigue life plot results for 5mm thick plate with 200g-300Hz dynamic loading

of the CFL plot. By comparing the previous life plot from Figure 6.6 with Figure 6.8, the 5 mm thick plate possesses a significantly reduced life compared to the 3 mm plate. Again, the highest alternating stresses were found on the plate edges resulting in a reduced fatigue

life.

6.4 Chapter Conclusion

This chapter explored using fatigue diagram methods to characterize fatigue life of post-buckled composite plates undergoing dynamic periodic snap-through. By separating axial stresses into alternating and mean stress components, stresses may be plotted on a constant fatigue life (CFL) diagram where fatigue life can be determined. From this method, fatigue life can be characterized at every location along the plate surface, providing valuable information regarding fatigue life relating to snap-through responses.

A study on increasing plate thickness and fatigue life revealed that thicker post-buckled plates possess higher alternating stresses and lower mean stresses at many locations along the plate. This combination reduces the fatigue life significantly. This study of varying plate thickness is valuable in for future experimental work on fatigue and composites during dynamic snap-through. One limitation of this study included the lack of failure modes considered. The CFL diagram used in this chapter provides fatigue predictions for axial loading only. Further studies should explore additional failure modes such as shear failure. Additionally, only one stress component, σ_{xx} was explored in this study as a CFL diagram was only provided for the first mode failure. To fully analyze fatigue life, all stress components should be considered and additional CFL diagrams must be created for alternative loading scenarios aside from axial loading.

Chapter 7

THESIS CONCLUSION

7.1 Summary of Work

This thesis demonstrated several studies attributed to snap-through of post-buckled laminated composite plates using finite element software. First, prior experimental and computational results were used to validate the Abaqus dynamic model used herein. The Abaqus models were able to exhibit single-well, periodic snap-through, and chaotic snap-through responses at the appropriate forcing parameters. This is significant as it offered validation to an in-house finite element code and matched experimental results closely. Understanding the snap-through boundary allows us to better predict the response of post-buckled composite plates undergoing dynamic forcing and the associated stresses.

The first contribution of this work investigated static and dynamic periodic snap-through. As dynamic simulations often are accompanied with large computational expense, exploring the difference between static and dynamic analysis is valuable to determine if static analysis may be used to predict dynamic analysis results. This study found that the static and dynamic analyses for snap-through of post-buckled plates did not vary greatly in regards to axial and shear stresses at the plate midplane. The static analysis of snap-through offered a satisfactory tool for predicting the stresses of the dynamic analysis equivalent. However, although the static and dynamic analyses showed similar trends in stress results, the dynamic shear results are less predictable as magnitudes were slightly higher for the dynamic analysis when compared to the static analysis. This information suggests that static analysis may be used to predict stress trends and relative order of magnitude of stresses, but a dynamic analysis is required for complete accuracy in stress values.

The second contribution of this work included a fatigue study on laminated composites

was explored using constant fatigue life (CFL) diagrams. Several post-buckled composite plate models were created with varying plate thicknesses. Dynamic analyses were performed on the post-buckled laminated composites resulting in periodic snap-through responses. The axial stresses σ_{xx} at the plate surfaces were evaluated and decomposed into alternating and mean stress components. These stress components were plotted on the CFL diagram for each different plate. Using the CFL diagram, a fatigue life is determined at every location along each plate surface. Using this information, plots were created for each plate showing the fatigue life at every point along the plate. Fatigue life was shown to be lower at plate edges where fixed boundaries existed. Additionally, results showed that fatigue life decreased as plate thickness increased due to an increase in alternating stress and a decrease in mean stress. This study provided information which may be used for future experimental work on fatigue life of composites panels and snap-through while also exploring the concept of CFL diagrams for laminated composites.

7.2 Future Work

This work investigated snap-through of post-buckled composite plates using Abaqus/CAE finite element software. The first study of validating the snap-through boundary using Abaqus found that the models successfully matched the expected snap-through behaviors. However, for this study only the left snap-through boundary was verified due to time restrictions of this work as each simulation is very computationally expensive. Ideally, the entire snap-through map should be verified, an effort that may be explored in future experimental work.

Additionally, another portion of this work investigated comparisons between static and dynamic snap-through. Results of both static and dynamic analyses were compared by comparing axial stresses σ_{xx} and shear stresses τ_{xz} at the plate midplane. These stress components were selected as they are representative of the axial stress and shear stress experienced by the plate, however, the remaining stress components should also be explored in future work. Additionally, the stresses were examined only at the plate midplane to reduce the complexity of the analysis. Future work should explore the stress fields along the entire

thickness of the plate.

The fatigue study performed in this work analyzed fatigue life of several post-buckled plates undergoing dynamic periodic snap-through. This work looked at fatigue life characterization through the use of a CFL diagram created from previous work. Although fatigue life was found using this method, results were not complete as only axial stress was analyzed for fatigue. This was due to a lack of CFL diagram for shear failure. Further experimental testing must be performed to create more CFL diagrams for different modes of failure in order to complete this section of the study. Additionally, future experimental work could be performed to test the results found from this work to determine the accuracy of the fatigue results.

BIBLIOGRAPHY

[1] Faycel Beji. Buckling analysis of composite stiffened panels and shells in aerospace structures. 2018.

[2] The Boeing Company. Boeing 787 from the ground up: Composites in the airframe and primary structure.

[3] Robert Jones. *Mechanics of Composite Materials*. Taylor Francis, Inc., 1998.

[4] M. Kawai and M. Koizumi. Nonlinear constant fatigue life diagrams for carbon/epoxy laminates at room temperature. *Composites*, 2007.

[5] Han-Gyu Kim. *Experimental and Numerical Nonlinear Dynamics and Stress Field Analysis of Post-Buckled Composite Plates*. PhD thesis, University of Washington, 2019.

[6] Han-Gyu Kim and Richard Wiebe. Numerical investigation of stress states in buckled laminated composite plates under dynamic loading. *Composite Structures*, 235(111743), 2020.

[7] Laszlo Kollar and George Springer. *Mechanics of Composite Structures*. Cambridge University Press, 2003.

[8] Abaqus Analysis User's Manual. Section 29.6: Shell elements.

[9] Abaqus Analysis User's Manual. Section 6.2.4: Unstable collapse and postbuckling analysis.

[10] Abaqus Analysis User's Manual. Section 6.3.1: Dynamic analysis procedures: overview.

[11] Abubakr Musa and Husain Al-Gahtani. Series-based solution for analysis of simply supported rectangular thin plate with internal rigid supports. *Advances in Civil Engineering*, 2017:1–7, 2017.

[12] A.T. Nettles. Basic mechanics of laminated composite plates. Technical Report NASA-RP-1351, 1994.

[13] Yoji Okabe and Nobuo Takeda. Takeda wave propagation characteristics quantitative evaluation of interlaminar-toughened cfrp composite by ultrasonic. *Composite Materials*, 1999.

[14] Nestor Perez. *Fracture Mechanics*. Springer International Publishing, 2004.

[15] SV Ramani and DP Williams. Notched and unnotched fatigue behavior of angle-ply graphite/epoxy composites. Technical report, 1976.

[16] Feifei Wang and Degang Cui. Congress of the international council of the aeronautical sciences. In *Proceedings of ICAS 2014*, 2014.

Appendix A

ADDITIONAL STRESS FIELD RESULTS FOR POST-BUCKLED PLATE USED IN VALIDATING SNAP-THROUGH BOUNDARY

Additional stress field results are provided in this appendix to provide further validation in Abaqus modeling in Chapter 4 Section 4.3.2. In Chapter 4 an Abaqus post-buckled plate model is created and compared with an in-house model prior to further analysis to validate the models. The stress field comparisons for axial stress σ_{xx} at the top surface of the plate was provided along with the transverse shear stress τ_{xz} at the plate midplane. The remaining stress fields will be provided here in this appendix.

Figure A.1 provides the in-plane axial stress field σ_{xx} results for the in-house and Abaqus plate models evaluated at the bottom surface of the plates. Likewise, Figure A.2 provides the in-plane axial stress σ_{yy} for both models at the top surface of the plates. Figure A.4 provides the figure for transverse shear stress τ_{yz} for both plate models at the midplane.

Looking at all figures in Appendix A, the Abaqus post-buckled plate model stress fields match the in-house model's stress fields very closely. The contour plots all are of close magnitude. Figure A.1 shows that the in-plane axial stress field σ_{xx} for both models. The maximum stress values are found at the plate edges and the mid region. Figure A.2 and Figure A.3 provide the stress fields for σ_{yy} at the top and bottom surfaces of both plates. Both figures suggest the in-house and Abaqus models match closely, where maximum stress values are found at the fixed plate edges and the mid region of the plate. Lastly, Figure A.4 shows that the shear stress field tau_{yz} at the plate midplane match closely for the in-house and Abaqus models. The largest shear stresses are found near the plate edges.

These stress fields were used to confirm the accuracy of the Abaqus model compared

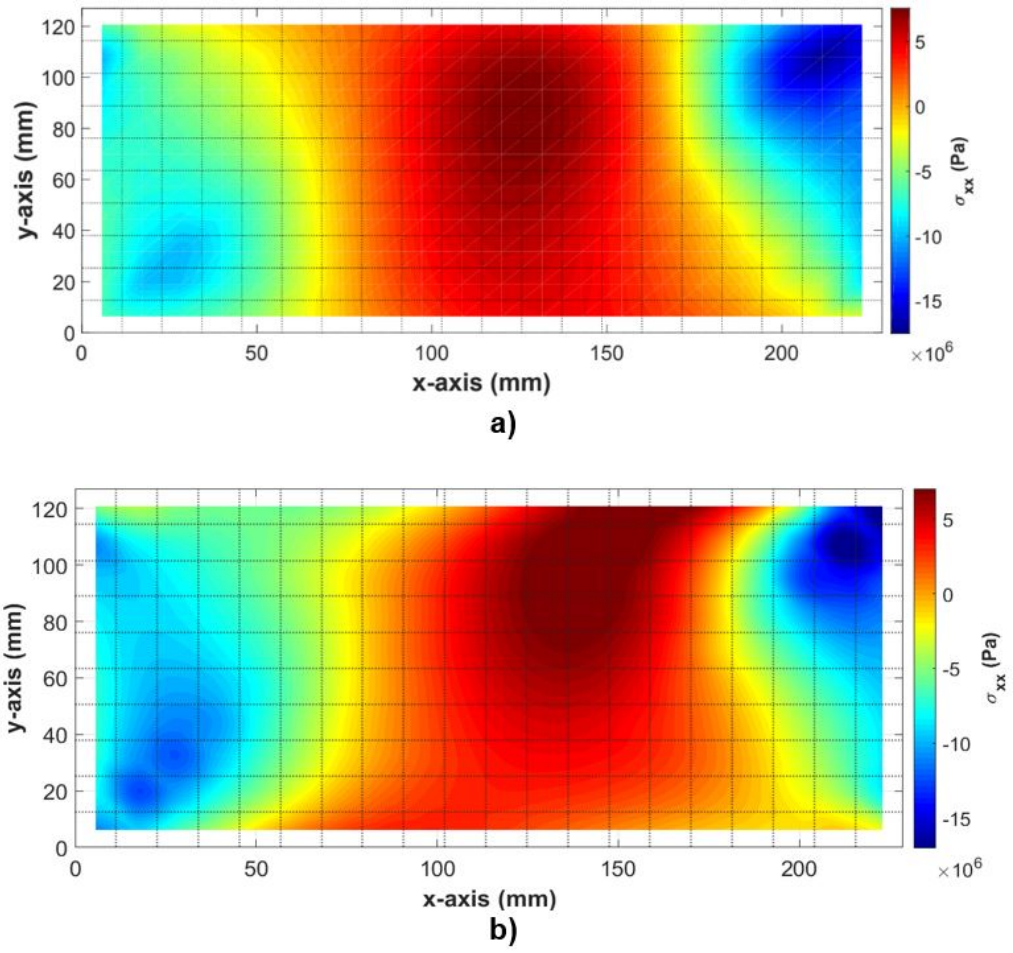

Figure A.1: In-plane axial stress field σ_{xx} at bottom surface (z = -h/2) for a) in-house post-buckled plate model b) Abaqus post-buckled plate model

to the in-house model. The similarities between the stress fields provided in this appendix support the conclusion that the Abaqus post-buckled plate model from Chapter 4 is an accurate recreation of the in-house finite element model.

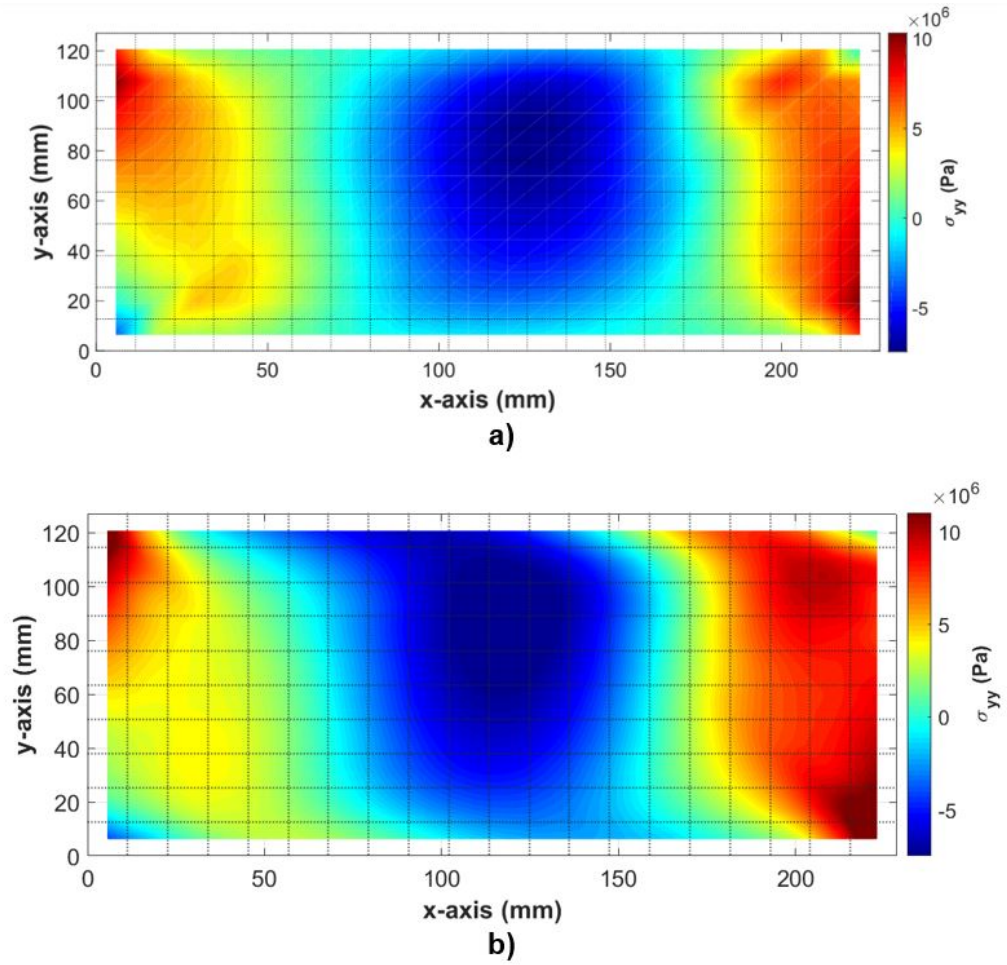

Figure A.2: In-plane axial stress field σ_{yy} at top surface (z = h/2) for a) in-house post-buckled plate model b) Abaqus post-buckled plate model

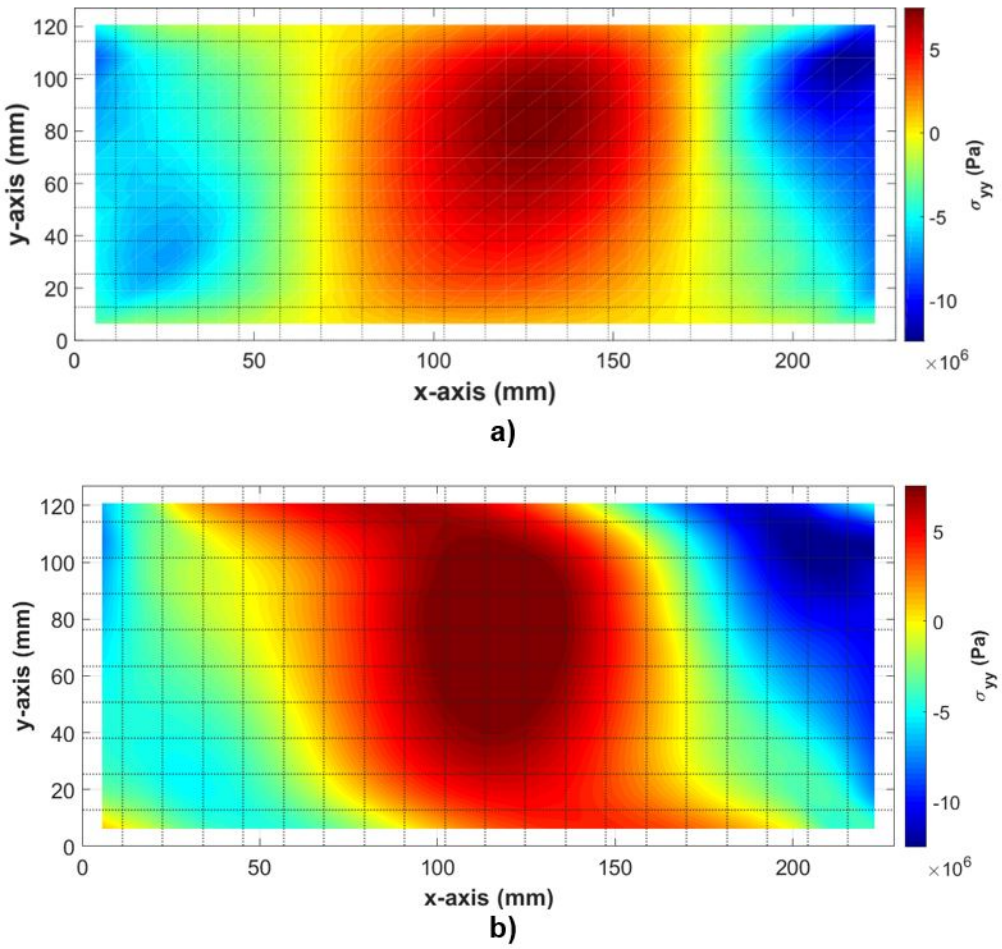

Figure A.3: In-plane axial stress field σ_{yy} at bottom surface (z = -h/2) for a) in-house post-buckled plate model b) Abaqus post-buckled plate model

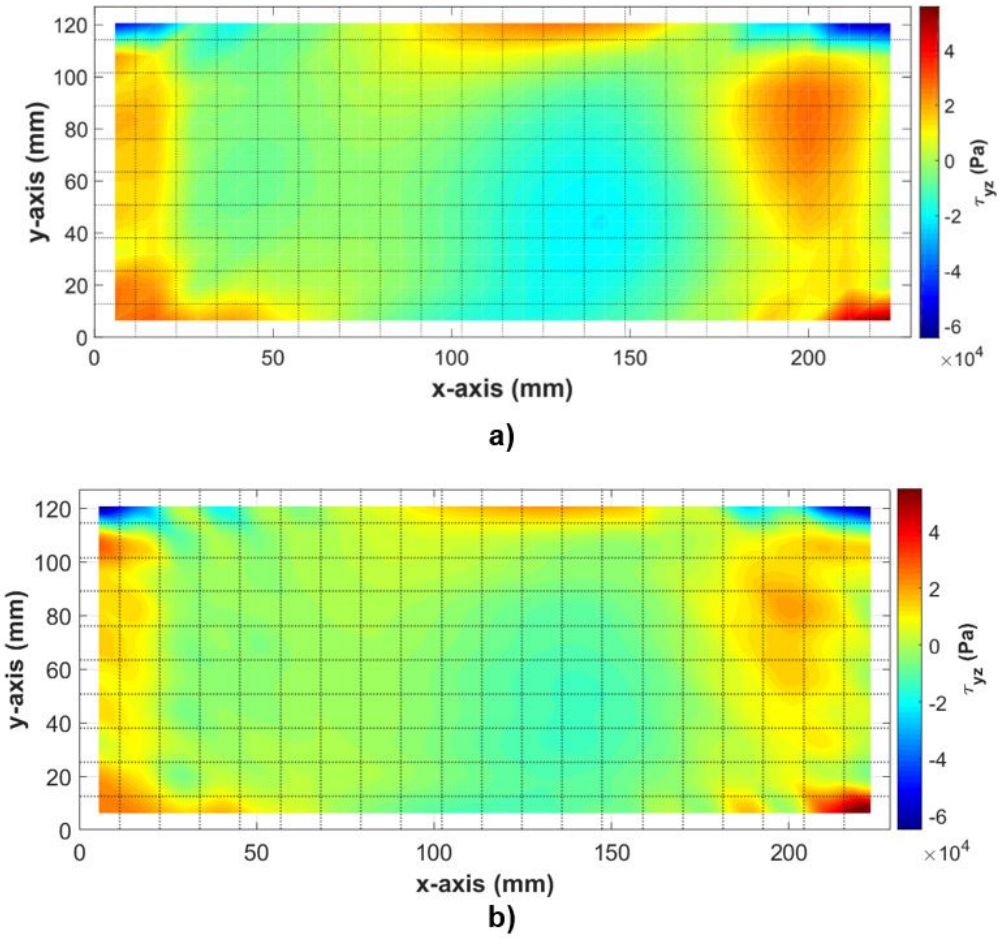

Figure A.4: Transverse shear stress field τ_{yz} at midplane (z = 0) for a) in-house post-buckled plate model b) Abaqus post-buckled plate model

Appendix B

EFFECTS OF INCREASING FORCING AMPLITUDE IN DYNAMIC SNAP-THROUGH: STRESS RESULTS COMPARISON BETWEEN STATIC AND DYNAMIC ANALYSIS

Chapter 5 of this thesis investigated the extent at which dynamic snap-through stress results deviate from static snap-through stresses. The study included increasing the forcing amplitude in dynamic snap-through simulations to determine the effect of increasing amplitude on the stress results. This appendix provides contour plots for results comparing dynamic results to static results for forcing amplitudes 40g, 48g, 56g, 64g, 72g, 80g, and 88g. As in Chapter 5, in-plane axial stress σ_{xx} and transverse shear stress τ_{xz} will be provided here. All stress contour plots are plots of maximum stress values throughout the simulations, evaluated at the plate midplane.

B.1 40g-130Hz dynamic snap-through

Figure B.1 shows the dynamic snap-through axial stress results for 40g-130Hz excitation compared with the static snap-through results. This figure shows that both the maximum tensile and compressive axial stresses between static snap-through and the 40g dynamic snap-through are close in magnitude. In Chapter 5, it was found that at 32g excitation, the dynamic compressive axial stress results were at a lower magnitude when compared to the static results. Again, this is observed even at a higher forcing amplitude of 40g.

Transverse shear stress τ_{xz} contours were also examined for the case of 40g forcing amplitude. Figure B.2 provides the comparison for 40g dynamic snap-through and static snap-through results. The figure shows that shear stresses reach a higher magnitude comparing dynamic snap-through to static. This trend was also seen with the 32g dynamic forcing

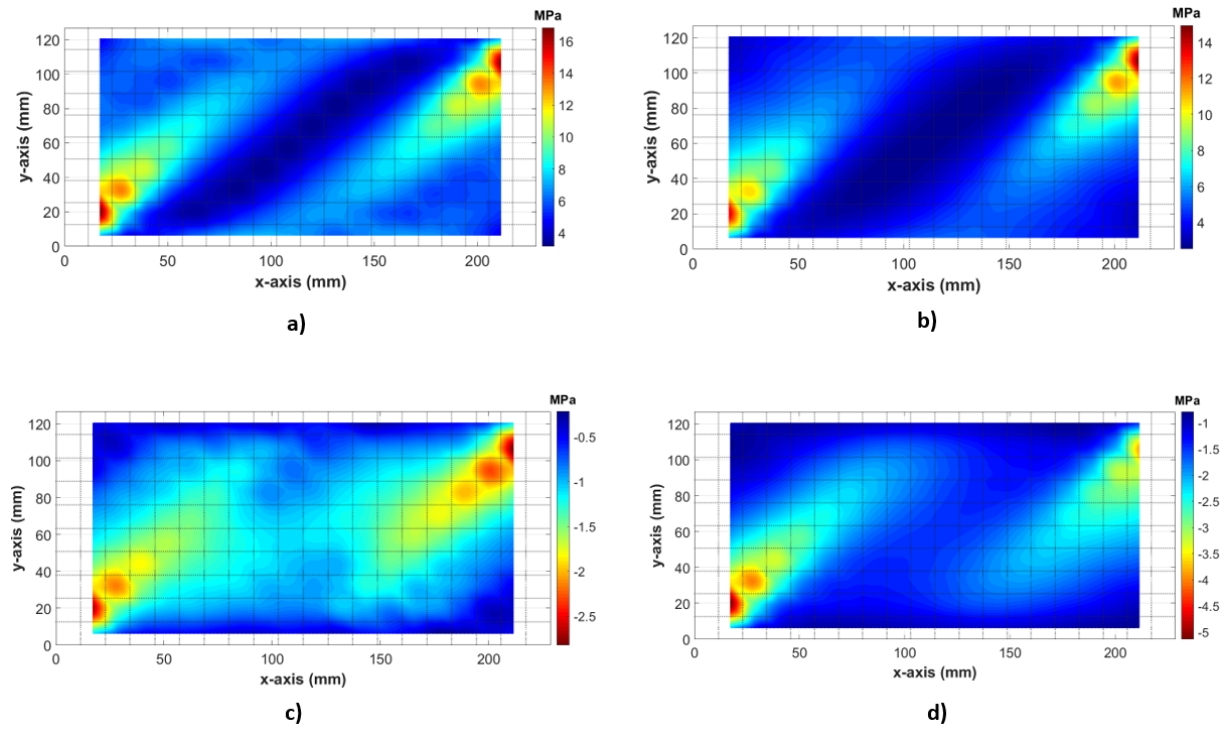

Figure B.1: Maximum in-plane axial stress σ_{xx} at midplane a) tensile, dynamic snap-through 40g-130Hz forcing, b) tensile, static snap-through, c) compressive, dynamic snap-through 40g-130Hz forcing, d) compressive, static snap-through

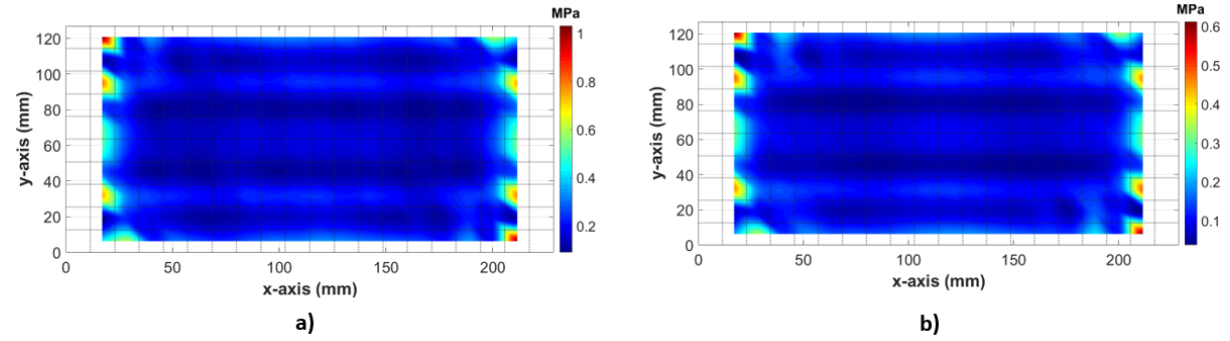

Figure B.2: Maximum magnitude of transverse shear stress τ_{xz} at midplane a) dynamic snap-through 40g-130Hz forcing, b) static snap-through

results provided back in Chapter 5, indicating that increasing forcing amplitude does not cause the dynamic results to deviate further from static results.

B.2 48g-130Hz dynamic snap-through

Increasing the forcing amplitude further to 48g yielded similar stress contour plots as the plots provided above. Here, the in-plane axial stress σ_{xx} and transverse shear stress τ_{xz} contour plots are provided for 48g forcing amplitude. Static results are also provided alongside the dynamic results for comparison purposes. Figure B.3 provides the axial stress results for 48g-130Hz dynamic snap-through compared with the static results. The tensile and compressive axial stresses for 48g appear slightly higher compared to static results, and compared to the results for 40g provided in previously in Figure B.1. However, stress results are still within close range to the static results. Additionally, shown later, when loading is again increased to 56g, this increase in stress results is not seen even though the amplitude is increased.

Figure B.4 provides the maximum transverse shear stresses for 48g dynamic snap-through compared with static snap-through. Again, the stresses evaluated from the 48g dynamic results appear larger than previously seen for 40g loading, however, the results continue to match the static snap-through results closely. The next section in this appendix will show that further increasing the dynamic forcing amplitude does not increase these stresses.

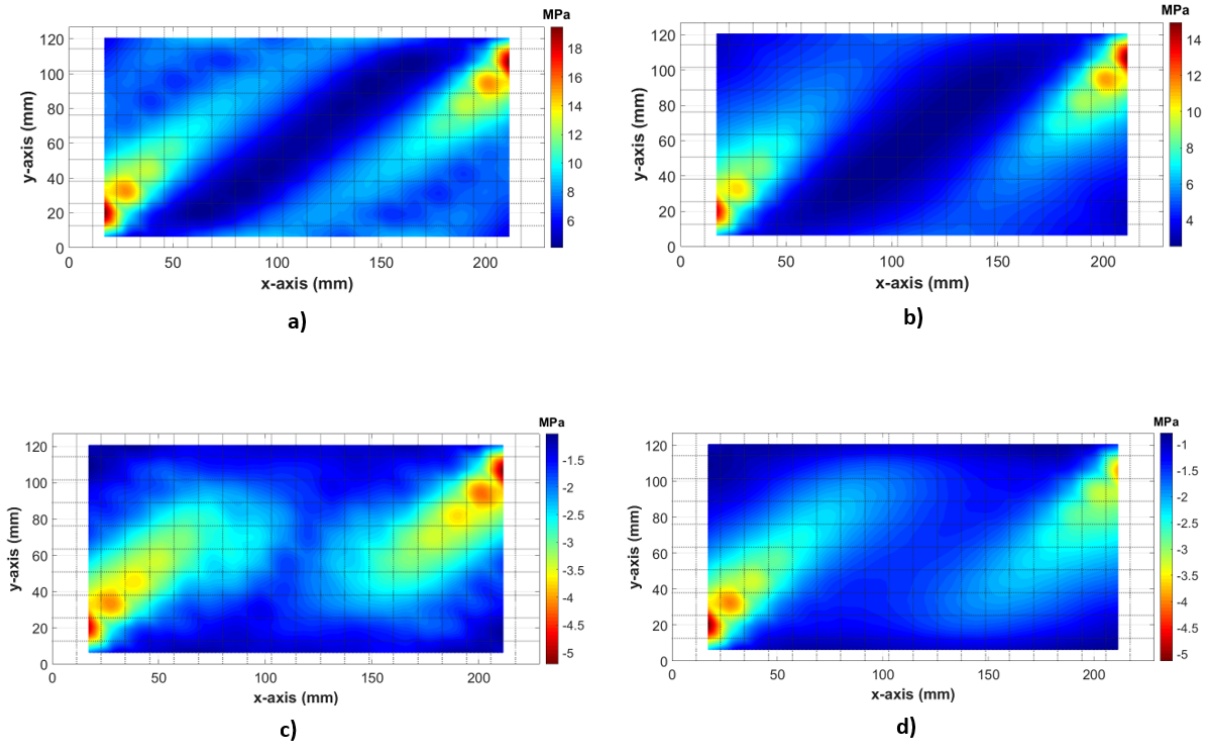

Figure B.3: Maximum in-plane axial stress σ_{xx} at midplane a) tensile, dynamic snap-through 48g-130Hz forcing, b) tensile, static snap-through, c) compressive, dynamic snap-through 48g-130Hz forcing, d) compressive, static snap-through

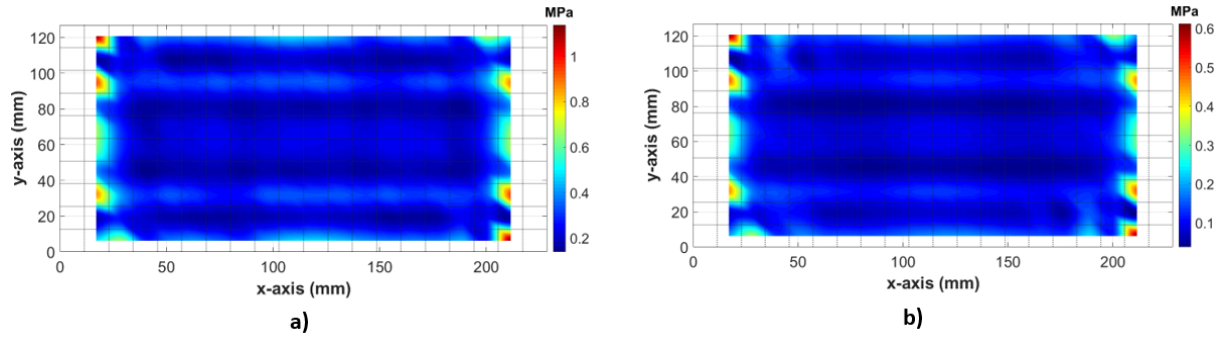

Figure B.4: Maximum magnitude of transverse shear stress τ_{xz} at midplane a) dynamic snap-through 48g-130Hz forcing, b) static snap-through

B.3 56g-130Hz dynamic snap-through

The dynamic forcing amplitude was further increased to 56g to determine the effects of increasing amplitude. Again, in-plane axial and transverse shear stresses are examined against static results. Figure B.5 provides the contour plots for in-plane axial stresses σ_{xx} with 56g dynamic snap-through and static snap-through. The figure shows very similar results

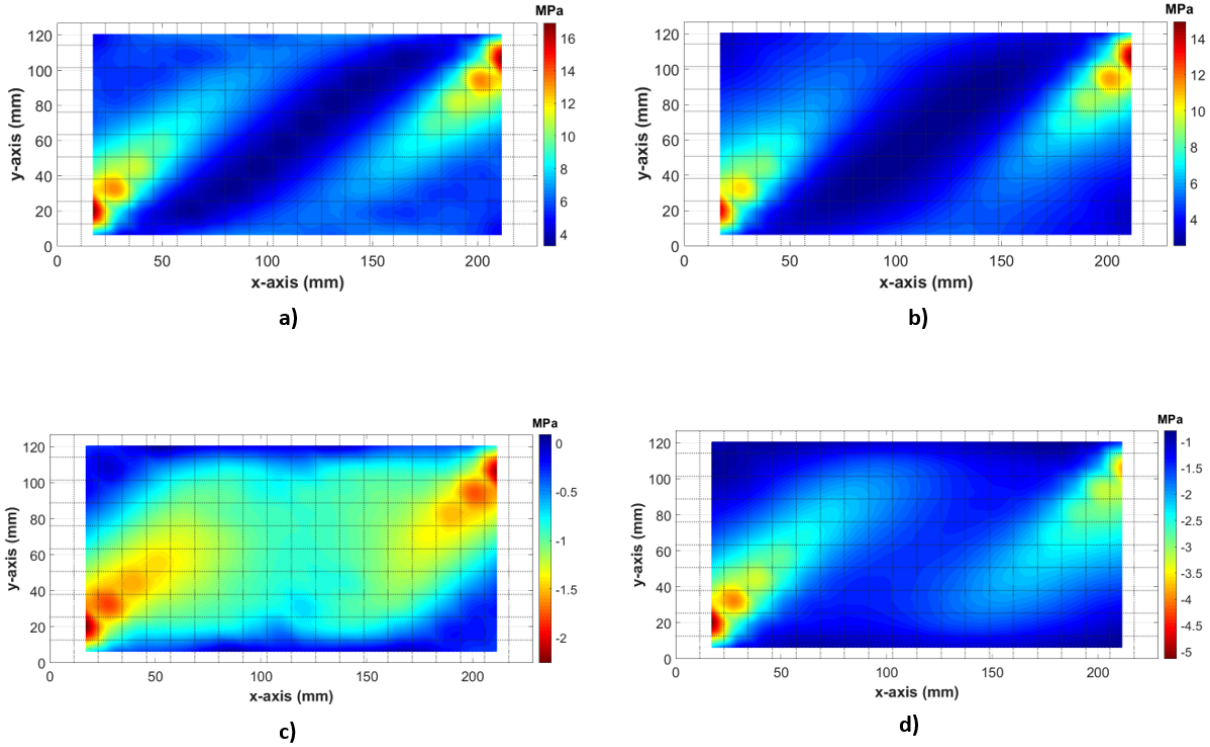

Figure B.5: Maximum in-plane axial stress σ_{xx} at midplane a) tensile, dynamic snap-through 56g-130Hz forcing, b) tensile, static snap-through, c) compressive, dynamic snap-through 56g-130Hz forcing, d) compressive, static snap-through

to the static results. Additionally, comparing the maximum tensile and compressive axial stress contours for 56g forcing from Figure B.5 with 40g forcing from Figure B.1 shows that increasing the amplitude did not significantly change maximum stress results. The same conclusions are observed from examining the transverse shear stress plots provided in Figure

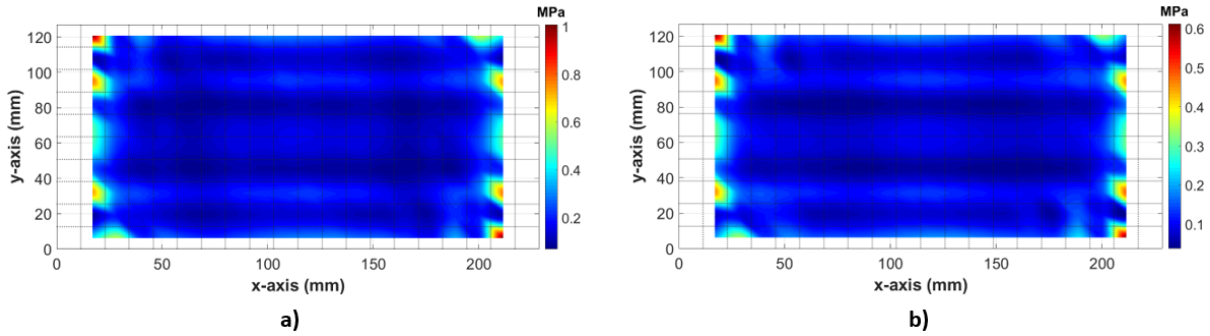

Figure B.6: Maximum magnitude of transverse shear stress τ_{xz} at midplane a) dynamic snap-through 56g-130Hz forcing, b) static snap-through

B.6.

B.4 64g-130Hz dynamic snap-through

Again, the dynamic forcing amplitude was increased to 64g. The in-plane axial stress and transverse shear contour plots were created and compared with static results. Figure B.7 provides the maximum axial stress results for the 64g dynamic snap-through and static snap-through. As with the lower amplitude results from previous appendix sections above, the axial stress results for 64g dynamic forcing do not exceed the static results any significant amount. Additionally, looking at Figure B.7cd, the compressive axial stresses for 64g dynamic snap-through are lower than the static snap-through stresses. This is consistent with what was seen for lower amplitude loadings.

Figure B.8 illustrates the transverse shear stress results for 64g dynamic snap-through and static snap-through. Again, the maximum shear results for both dynamic and static are close in magnitude, indicating that increasing forcing amplitude does not significantly effect the dynamic results.

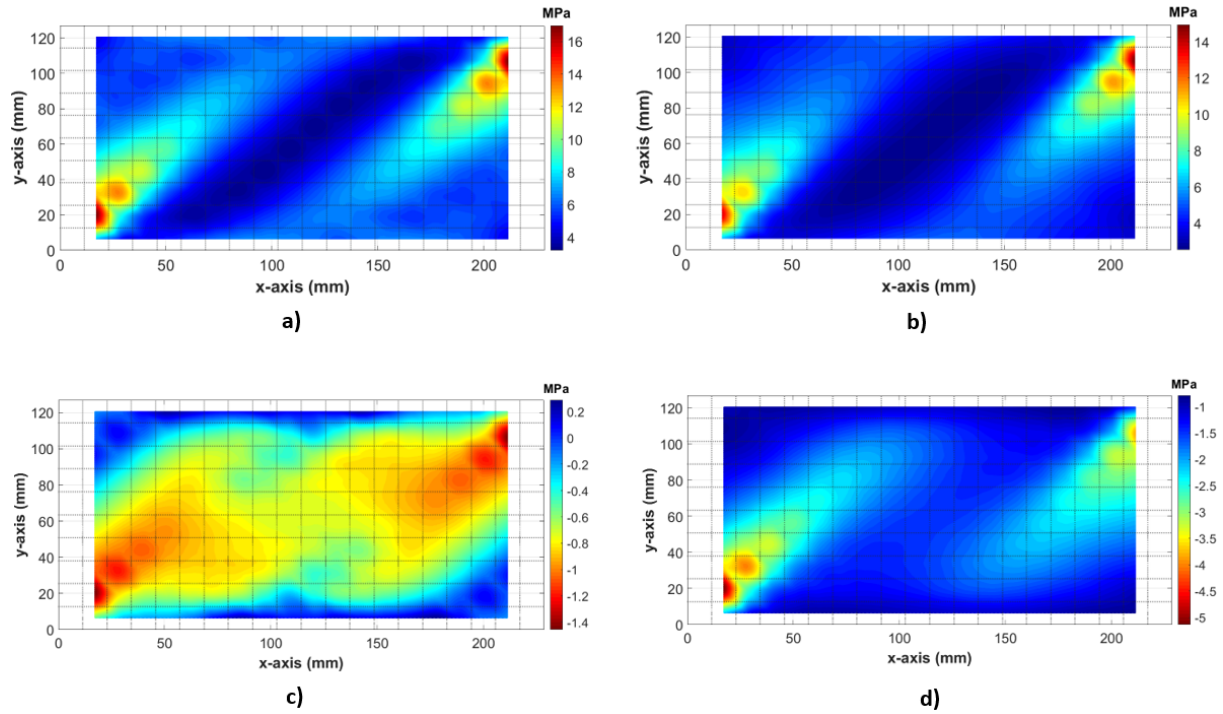

Figure B.7: Maximum in-plane axial stress σ_{xx} at midplane a) tensile, dynamic snap-through 64g-130Hz forcing, b) tensile, static snap-through, c) compressive, dynamic snap-through 64g-130Hz forcing, d) compressive, static snap-through

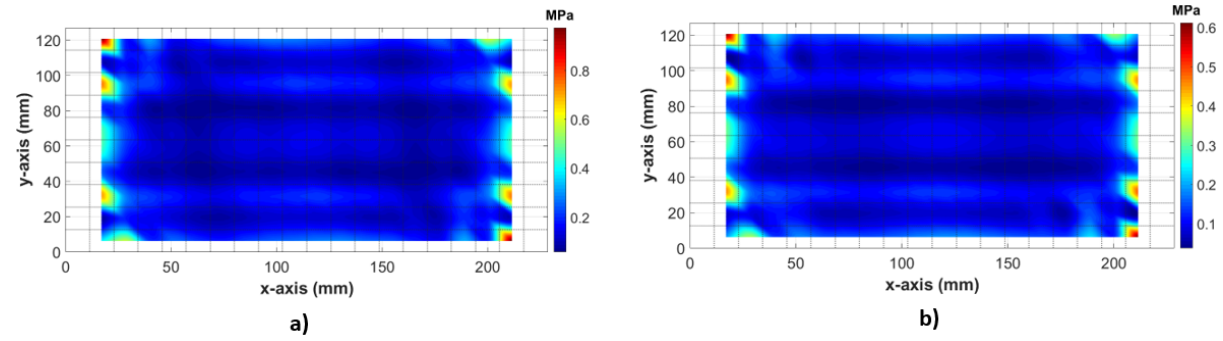

Figure B.8: Maximum magnitude of transverse shear stress τ_{xz} at midplane a) dynamic snap-through 64g-130Hz forcing, b) static snap-through

B.5 72g, 80g, and 88g-130Hz dynamic snap-through

Previous sections of Appendix B displayed and discussed the results for 40g, 48g, 56g, and 64g dynamic snap-through separately. This section of the appendix will discuss 72g, 80g, and

88g dynamic snap-through results together, as all the results were so similar and repeating the discussion for each different forcing amplitude would be rather repetitive.

Figure B.9 and Figure B.10 provide the axial stress σ_{xx} and transverse shear stress τ_{xz} contours for 72g-130Hz dynamic analysis and static analysis. As with previous dynamic results, the 72g results are similar to the static analysis results for both shear and axial stresses. The dynamic tensile in-plane axial stresses shown in Figure B.9a slightly exceed the tensile axial stresses for the static analysis, however, match the contour particularly well. Figure B.9c shows the compressive axial stresses for the dynamic analysis. This stress contour matches the trend of the static contour, however, the dynamic results do not reach the full magnitude of the stati results. This is seen for many of the results regardless of forcing amplitude.

The transverse shear stress τ_{xz} contour plots for 72g excitation are provided by Figure B.10. Again, the dynamic and static results match closely, with the exception of the dynamic results slightly exceeding the static results. Althrough the dynamic results are slightly greater in magnitude, overall the results match closely to the static results. The remaining figures in this section of the appendix provide the dynamic and static stress results for 80g and 88g. Figures B.11 and B.12 provide the in-plane axial stress σ_{xx} and transverse shear stress τ_{xz} for 80g excitation. Likewise, Figures B.13 and B.14 provide the in-plane axial stress σ_{xx} and transverse shear stress B.14 for 88g excitation. These results will not be discussed as they are so similar to the previous results of this appendix section for lower forcing amplitudes.

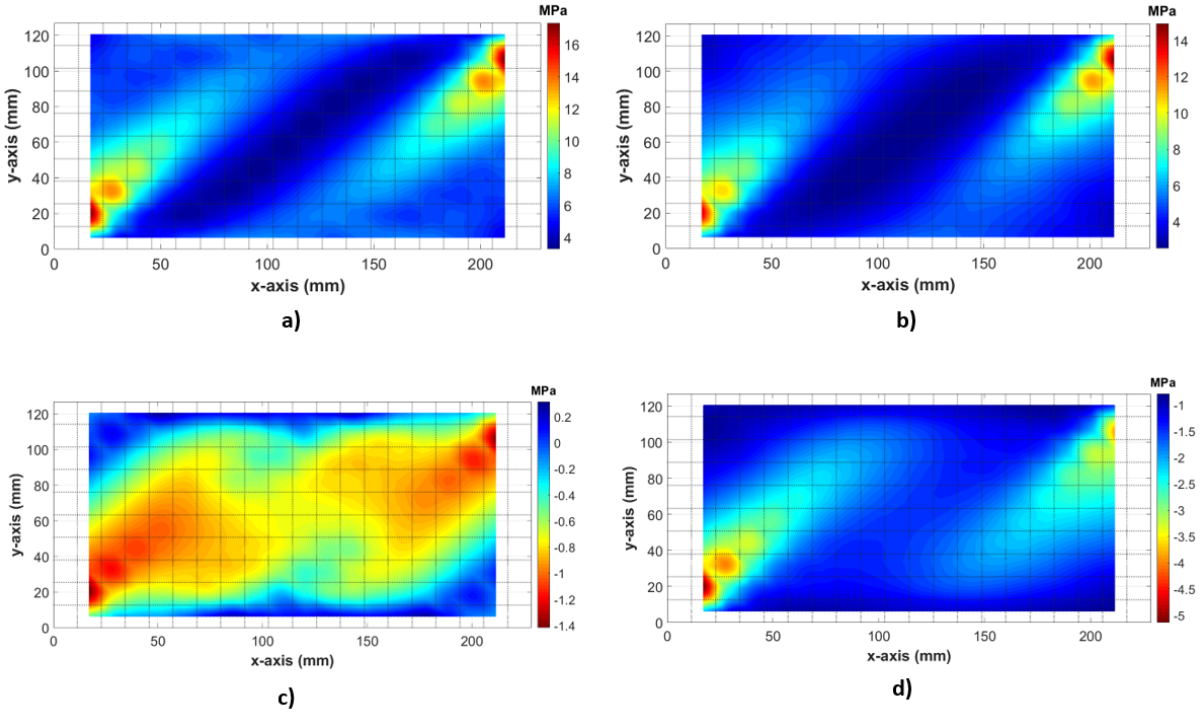

Figure B.9: Maximum in-plane axial stress σ_{xx} at midplane a) tensile, dynamic snap-through 72g-130Hz forcing, b) tensile, static snap-through, c) compressive, dynamic snap-through 72g-130Hz forcing, d) compressive, static snap-through

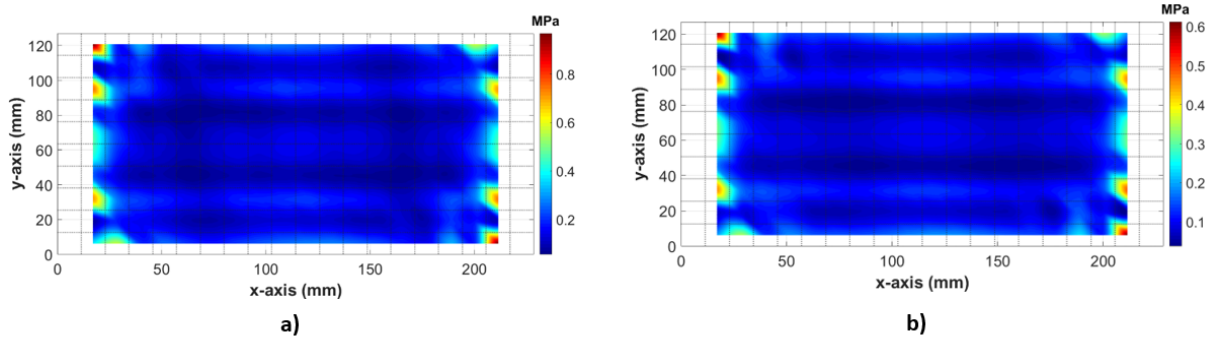

Figure B.10: Maximum magnitude of transverse shear stress τ_{xz} at midplane a) dynamic snap-through 72g-130Hz forcing, b) static snap-through

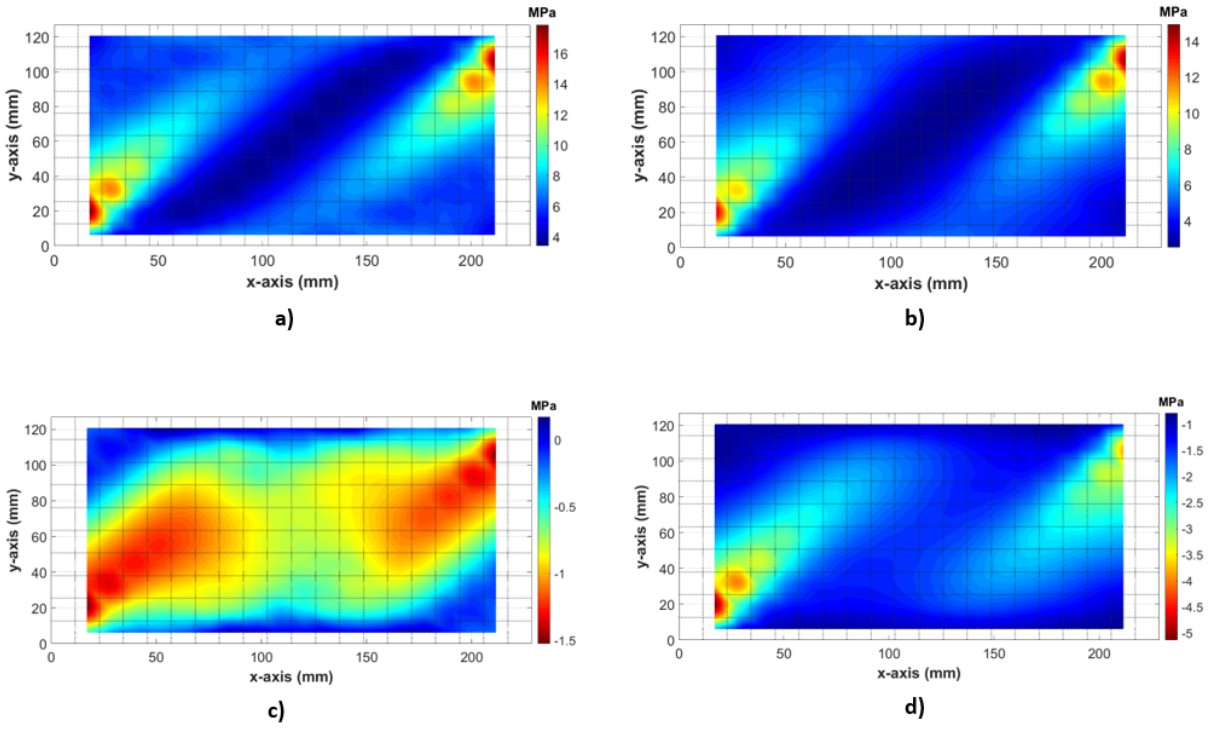

Figure B.11: Maximum in-plane axial stress σ_{xx} at midplane a) tensile, dynamic snap-through 80g-130Hz forcing, b) tensile, static snap-through, c) compressive, dynamic snap-through 80g-130Hz forcing, d) compressive, static snap-through

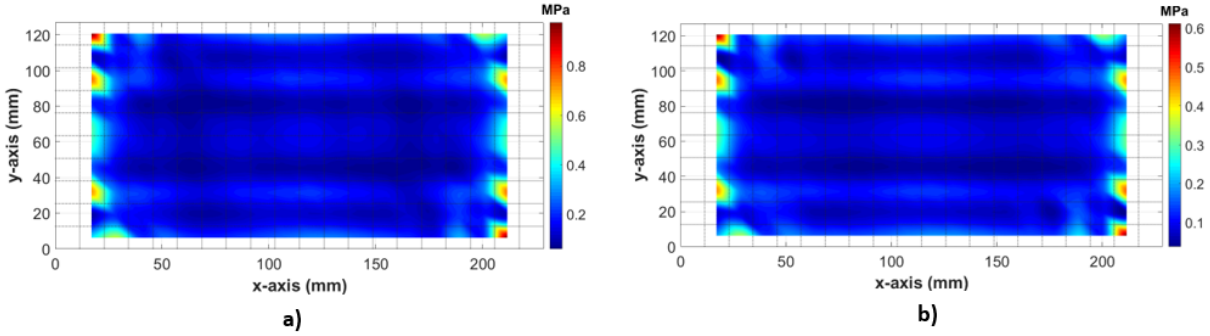

Figure B.12: Maximum magnitude of transverse shear stress τ_{xz} at midplane a) dynamic snap-through 80g-130Hz forcing, b) static snap-through

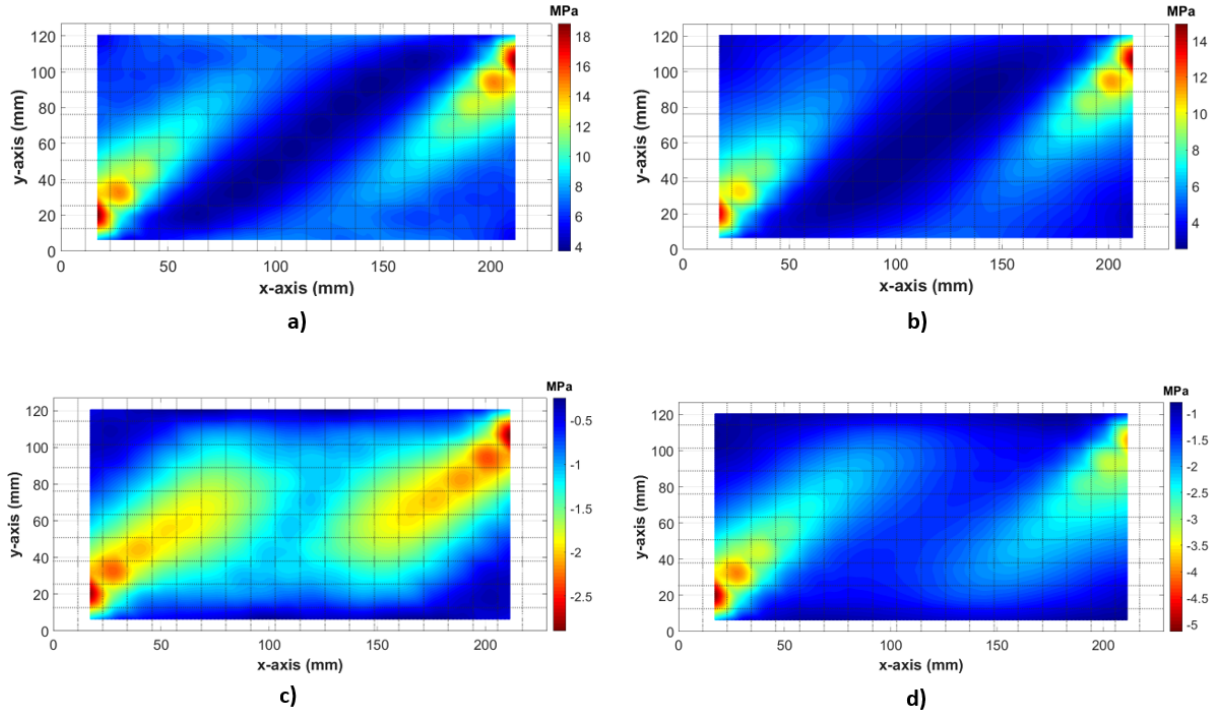

Figure B.13: Maximum in-plane axial stress σ_{xx} at midplane a) tensile, dynamic snap-through 88g-130Hz forcing, b) tensile, static snap-through, c) compressive, dynamic snap-through 88g-130Hz forcing, d) compressive, static snap-through

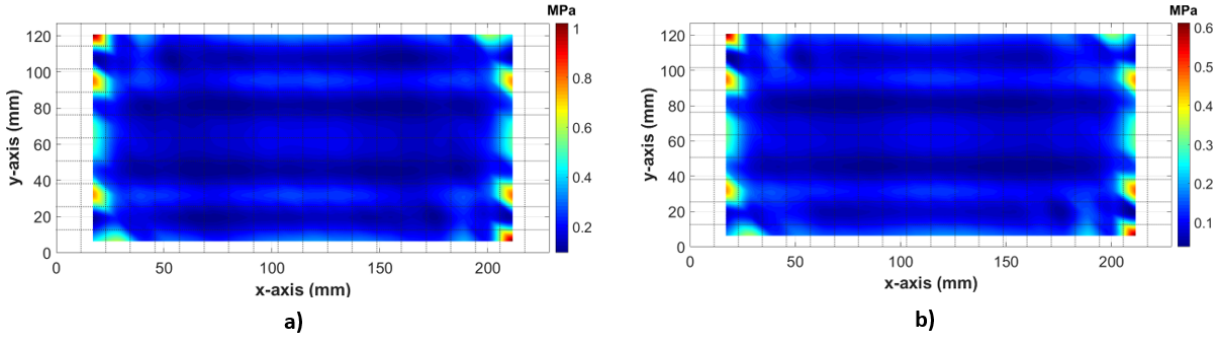

Figure B.14: Maximum magnitude of transverse shear stress τ_{xz} at midplane a) dynamic snap-through 88g-130Hz forcing, b) static snap-through